



VIP report “Use of new broadband echosounder”

Techniques for improved ocean imaging and selectivity in pelagic fisheries

Sascha Fässler¹, Ben Scoulding¹, Dirk Burggraaf¹, Dick de Haan¹, Benoit Quesson², Jeroen van de Sande², Peter Beerens²

¹) IMARES, Haringkade 1, IJmuiden; ²) TNO, Sonar and Acoustics, Oude Waalsdorperweg 63, The Hague

Publication date
9 December 2015
IMARES report
C171/15



European Fisheries Fund: Investment
In sustainable fisheries



Opdrachtgever:

Redersvereniging voor de zeevisserij (RVZ)
Louis Braillelaan 80
2719 EK ZOETERMEER



This report has been produced with financial support of the European Fisheries Fund: Investment in sustainable fisheries.

European Fisheries Fund: Investment in sustainable fisheries



© 2015 IMARES Wageningen UR

IMARES, onderdeel van Stichting DLO.
KvK nr. 09098104,
IMARES BTW nr. NL 8113.83.696.B16.
Code BIC/SWIFT address: RABONL2U
IBAN code: NL 73 RABO 0373599285

De Directie van IMARES is niet aansprakelijk voor gevolgschade, noch voor schade welke voortvloeit uit toepassingen van de resultaten van werkzaamheden of andere gegevens verkregen van IMARES; opdrachtgever vrijwaart IMARES van aanspraken van derden in verband met deze toepassing.

Dit rapport is vervaardigd op verzoek van de opdrachtgever hierboven aangegeven en is zijn eigendom. Niets uit dit rapport mag weergegeven en/of gepubliceerd worden, gefotokopieerd of op enige andere manier gebruikt worden zonder schriftelijke toestemming van de opdrachtgever.

A_4_3_1-V14.2

Contents

Contents.....	3
Summary.....	4
Samenvatting.....	5
1 Introduction.....	6
1.1 Background.....	6
1.2 Assignment.....	7
1.3 Approach.....	8
2 Materials and Methods.....	10
2.1 Data collection.....	10
2.2 Data processing.....	11
2.2.1 Pre-processing.....	12
2.2.1.1 TX-signal reconstruction.....	13
2.2.1.2 RX-signal reconstruction.....	13
2.2.1.3 Matched filtering.....	14
2.2.1.4 Beamforming.....	14
2.2.1.5 Sound intensity level computation.....	14
2.2.2 Imaging.....	15
2.2.2.1 Resampling.....	16
2.2.2.2 Range equalization.....	16
2.2.2.3 Bottom alignment.....	16
2.2.2.4 Normalisation.....	19
2.2.2.5 Bad ping detection.....	19
2.2.2.6 Bad ping interpolation.....	25
2.2.3 School detection.....	25
2.2.4 Transducer calibration.....	29
2.2.5 Frequency spectrum computation.....	31
2.2.6 Classification.....	32
2.2.6.1 Statistical classification.....	32
2.2.6.2 Frequency response classification.....	33
2.2.6.3 Classification merging.....	35
2.3 Backscatter modelling.....	35
2.3.1 Morphological measurements of body components.....	35
2.3.2 Model definition.....	37
3 Results.....	40
3.1 Backscatter modelling.....	40
3.1.1 Model validation and limitation.....	40
3.1.2 Two-dimensional and three-dimensional model comparison.....	42
3.1.3 Model outputs.....	44
3.1.4 Size-class modelling.....	45
3.1.4.1 Herring.....	45
3.1.4.2 Sprat.....	45
3.1.4.3 Boarfish.....	46
3.1.4.4 Horse mackerel.....	46
3.1.4.5 Atlantic mackerel.....	46
3.2 Species classification.....	47
3.2.1 Statistical classification.....	47
3.2.2 Frequency response classification.....	49
3.2.3 Combined classifier.....	53
3.3 Dissemination activities.....	56
4 Conclusions.....	57
5 Recommendations.....	58
6 Quality Assurance.....	60
References.....	61
Justification.....	62
Appendix A: calibration manual.....	63
Appendix B: dissemination & presentations.....	82
Appendix C: echograms of school data (by species and file).....	91

Summary

This project is aimed at improving fishing selectivity and reduce bycatches in pelagic fisheries by using the newest echosounder technology (broadband acoustics) to classify fish species prior to catch operations. It is therefore linked to new EU regulations that entail a discard ban as part of the new Common Fisheries Policy (CFP). At the same time, it has allowed the pelagic sector, represented by the Redersvereniging voor de Zeevisserij (RVZ), to make use of the most recent fisheries acoustic techniques prior to their official market release.

Broadband acoustic techniques make use of so-called chirp pulses and can therefore collect echo strength measurements of fish schools over a wide (broad) frequency range rather than at just a few distinct frequencies (multifrequency approach), which is common in conventional echosounder systems. Consequently, broadband acoustic data has a higher information richness than conventional narrowband (multifrequency) data, and therefore potential to deliver more accurate knowledge on fish identity, size and densities.

A prototype broadband echosounder (type SIMRAD EK80) was installed on an RVZ pelagic freezer-trawler to collect example acoustic data on fish aggregations during several fishing trips targeted at herring, mackerel and horse mackerel. The system used 3 transducers and operated from 45-260 kHz. Software routines were developed to read the raw acoustic data stored by the echosounder, process the signals, produce cleaned images, detect fish schools, and eventually classify the different species. Two classification approaches were applied in combination to utilise the improved resolution and frequency diversity of the broadband data: the first approach aimed to identify species based on statistical features contained in the data (e.g. school size, shape, echo intensity distribution, school density, time signals); the second approach focussed on analysis of the enhanced frequency spectrum available, which differs between different types and shapes of fish species.

Average classification scores for allocation of schools to the correct highest-scoring species class, based on iterative resampling procedures, was between 95-100% in both approaches. Combining the two approaches is especially valuable as it can make use of the advantages unique to both individual approaches. Based on the available datasets, the combined classification approach resulted in an average correct school species classification performance of 100%.

The project lays the basis for use of the broadband technique during standard pelagic fishing operations and demonstrated the potential of it to classify different fish species. The developments made in the project allow using these results to further develop real-time classification tools in the future to practically implement the advantages of the technique with respect to improved fishing selectivity onboard pelagic trawlers.

To improve robustness and further develop the classification algorithm it is important to have access to as much (representative) data as possible. Given the promising results of the method used so far, it is recommended to continue collecting acoustic broadband data together with as much complementary metadata as possible (e.g. weather and biology), for the fish species used so far but also on additional species. These broadband data can also be used to evaluate the classification performances in terms of fish size and mixed schools. The use of more than just the 3 frequency channels used in this project will deliver even more elaborate data to improve species (and size) classification.

Samenvatting

Dit project is gericht op het verbeteren van de visserij selectiviteit en vermindering van bijvangst in pelagische visserij. Door het gebruik van de nieuwste echolood technologie (breedband akoestiek) zullen vissoorten voordat ze in de vangst terechtkomen, kunnen worden geclassificeerd. Het project is daarom gekoppeld aan nieuwe EU-regelgeving die een verbod op het teruggooien van ongewenste bijvangst oplegt als onderdeel van het nieuwe Gemeenschappelijk Visserijbeleid (GVB). Tegelijkertijd heeft de pelagische sector, vertegenwoordigd door de Redersvereniging voor de Zeevisserij (RVZ), gebruik kunnen maken van de meest recente visserij akoestische technieken voordat de apparatuur officieel op de markt komt.

Breedband akoestische technieken maken gebruik van zogenaamde chirp pulsen en kunnen daardoor echosterkte metingen van vis scholen verzamelen over een brede frequentieband vergeleken met metingen op individuele frequenties (multifrequentie benadering), wat nu gebruikelijk is bij conventionele echoloden. Hierdoor bevatten akoestische breedband gegevens een hogere informatiedichtheid dan conventionele smalband (multifrequentie) data, en hebben zij dus een hoger potentieel om nauwkeurigere kennis over vis identiteit, grootte en dichtheid te leveren.

Een prototype breedband echolood (type SIMRAD EK80) werd geïnstalleerd op een pelagische diepvriestrawler van de RVZ om akoestische gegevens over vis scholen te verzamelen tijdens meerdere visreizen gericht op haring, makreel en horsmakreel. Het systeem gebruikt drie bestaande transducers en werkt over een frequentieband van 45-260 kHz. Software routines zijn ontwikkeld om de ruwe akoestische gegevens die worden opgeslagen door de echolood in te lezen, de signalen te verwerken, schone afbeeldingen te produceren, vis scholen op te sporen, en uiteindelijk de verschillende vissoorten te classificeren. Een combinatie van twee classificatie benaderingen is toegepast om van de verbeterde resolutie en frequentie diversiteit van de breedband-gegevens gebruik te maken: de eerste aanpak is erop gericht om soorten te identificeren op basis van statistische kenmerken in de gegevens (bijvoorbeeld grootte en vorm van scholen, distributie van echo-intensiteit waarden, school dichtheiden, tijd signalen); de tweede benadering is gericht op de analyse van het verhoogde frequentiespectrum, welke verschilt tussen verschillende vormen en soorten van vis.

De gemiddelde classificatie scores voor het toewijzen van de scholen vis naar de juiste hoogst-scorende soort, gebaseerd op iteratieve herbemonstering procedures, lagen tussen 95-100% in beide classificatie benaderingen. De combinatie van de twee benaderingen is extra waardevol omdat hierbij gebruik kan worden gemaakt van de unieke voordelen van beide individuele benaderingen. Op basis van de beschikbare datasets resulteerde de gecombineerde classificatie aanpak in een gemiddelde juiste soortclassificatie van 100%.

Het project legt de basis voor het gebruik van breedband akoestische technieken in de pelagische visserij en toont het potentieel voor het gebruik voor de classificatie van vissoorten. De ontwikkelingen die in het project gerealiseerd zijn, maken het mogelijk om in de toekomst de resultaten te benutten voor verdere ontwikkeling van real-time classificatie toepassingen. Hierdoor kunnen de voordelen van de techniek met betrekking tot betere selectiviteit praktisch toegepast worden aan boord van pelagische vissersschepen.

Om de robuustheid van de classificatie methode te verbeteren en het classificatie algoritme verder te ontwikkelen, is het belangrijk om zoveel mogelijk (representatieve) data beschikbaar te hebben. Gezien de veelbelovende resultaten van de tot nu toe gebruikte methodiek wordt aanbevolen verdere akoestische breedband data te verzamelen samen met zoveel mogelijk aanvullende gegevens (b.v. weer en biologische data) van vissoorten dusver bekeken en ook van andere soorten. De breedbandgegevens kunnen ook worden gebruikt om de (theoretische) mogelijkheid van vis lengte bepaling en identificatie van gemengde scholen te evalueren. Het benutten van meer dan alleen de drie frequenties die in dit project gebruikt zijn, zal nog meer uitgebreide gegevens leveren om de soort (en lengte) classificatie te verbeteren.

1 Introduction

1.1 Background

Echosounders are important sensors commonly used on pelagic fishing vessels to detect fish schools, qualitatively assess their size and facilitate catch operations. These same instruments can also be used for scientific purposes, to measure fish densities from which stock abundance indices can be derived. For such quantitative applications, calibrated scientific echosounders are used.

Multifrequency acoustic measurements from echosounders have shown potential for remote fish species identification. Through the use of echosounders operating sound pulses simultaneously at different frequencies, fish species may be distinguished from each other using objective, scientifically derived species identification algorithms. These algorithms rely on individual sound reflection properties of different fish species (Figure 1.1a). They evaluate the echo strength measured between different single frequencies and use these distinct frequency signatures to classify fish species. However, these multifrequency techniques take measurements only at the limited number of single frequencies that are available (Figure 1.1b). Due to the variability around the measured echo strength values at these different frequencies and the sometimes minimal differences between species, classification is sometimes difficult and results not usable for species separation in practice.

Broadband acoustic transceivers transmit and receive over a wide frequency band. They make use of so-called chirp pulses that contain a wide frequency band, which is transmitted in every single ping. The benefits of these broadband pulses is double: the echogram resolution and signal to noise ratio is improved by chirp processing (pulse compression) and they can provide echo strength measurements over a wide (broad) frequency range rather than at just a number of distinct frequencies (Figure 1.1c). Consequently, broadband acoustic data has a higher information richness than conventional narrowband (multifrequency) data, and therefore potential to deliver more accurate knowledge on fish identity, size and densities. Furthermore, it will be much easier to describe other features of the ecosystem from such acoustic broadband data, such as plankton layers and hydrographic features, which may be linked to fish aggregations.

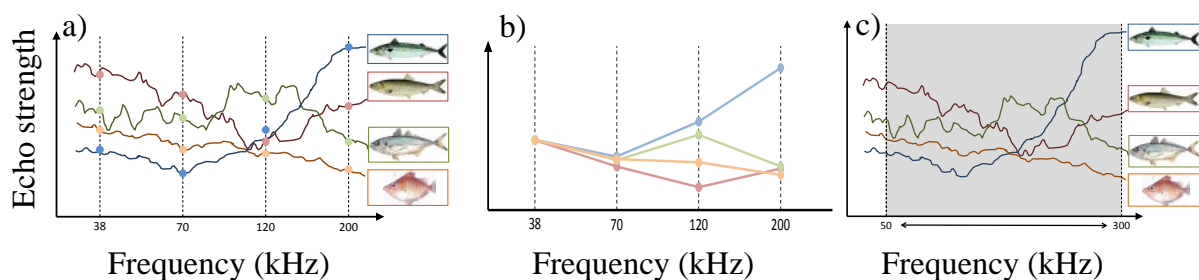


Figure 1.1. Schematic description of frequency-specific identification properties of different fish species. a) Hypothetical echo strength of the fish species (solid lines) and measurements taken at four distinct frequencies (filled circles). b) Corresponding multi-frequency echo characteristics of the fish species. c) Broadband technique covering a wide frequency band (e.g. 50-300 kHz) and measuring echo strengths of the species at essentially 250 individual frequencies.

One of the market leaders of fisheries acoustic equipment (SIMRAD) officially released their new commercial broadband echosounder system, called EK80, in May 2015. Unlike commercial echosounder systems, the EK80 is specifically designed for users in fisheries research and it has a standard data output function for scientific raw data. The system also utilises existing SIMRAD composite transducers currently installed on most pelagic vessels. This project allows the Dutch pelagic sector to make immediate use of the newest and most modern developments for fish species recognition and apply these to improve catch selectivity and reduce discards.

1.2 Assignment

The originally proposed project contained the following specific practical tasks and activities:

WP1: preparation and installation

Three prototype broadband transceivers (WBT's) of the type EK80 will be acquired from the manufacturer Simrad and installed on the RVZ freezer-trawler used for data collection purposes in this project (SCH6). The transceivers are then connected to existing transducers of the 70, 120, and 200 kHz channels. Test of the system will be performed once installed. Care is taken to guarantee that the system is exposed as little as possible to electric and mechanical noise sources and that the installation is in accordance with the manufacturer's requirements. The system is further tested during one day steaming outside the harbour to evaluate its performance at sea.

WP 2: system calibration

No recommended calibration procedures exist for the particular prototype hardware (EK80) used in the project. The operating software is also still under development and a calibration module has not been designed at the start of the project. Generally, echosounder calibration is performed by correctly positioning a metal sphere inside the acoustic beam under the keel of the ship, a few meters below the echosounder transducer. During the calibration, the transmitted and received signal of the echosounder is visualised in the software display to assure proper execution of the calibration, for further analysis, and estimating calibration parameters. The labour-intensive method of lowering and positioning of the sphere is facilitated by the use of tools and procedures developed in similar projects with the RVZ. However, as the system sends out a broadband signal, no single calibration sphere was suitable for the whole frequency band observed. A special calibration routine will therefore have to be developed applying several calibration sphere sizes to cover the bandwidth. Scientists will be present on board to conduct these first-time calibration procedures at the required precision.

WP 3: data collection

Given the novelty of the system and data formats, adequate data collection and storage requirements will have to be assessed and storage facilities acquired to record, transfer, store, and backup the data in the required way. Echosounder settings will have to be set correctly before starting data collection and the system remotely checked during data collection at sea. Assistance will be provided remotely as well if required. Broadband data will be collected from the EK80 prototype system during 4 individual fishing trips directed at 4 target species: herring, mackerel, horse mackerel, and sprat. During EK80 recordings of fish schools, interference caused by other acoustic equipment running simultaneously on board has to be eliminated by switching off such equipment.

WP 4: data analysis

The collected raw broadband acoustic data will be stored in a format specified by the manufacturer to enable processing of the signal with custom code and software. All collected data files will be scanned and evaluated for significant aggregations of the target species. Trawl information will be provided by the vessel operator. Raw broadband data of the identified individual fish school will then be extracted from the data files.

WP 5: demonstrator software development

Software code will be developed to read in data files produced by the EK80 prototype system. The software will produce images, clean data, detect schools, and extract useful parameters for further analysis. Based on the recorded broadband data, existing and new classification techniques are applied and combined to produce and assess classification potential.

WP 6: scatter modelling

Theoretical broadband sound scatter models of the target fish species over the frequency band covered is developed for robustness studies, to assess the theoretical potential of the broadband signal.

All assignments were covered and completed as described except in the following cases:

WP 1: Due to time constraints and short time frames between project approval, hardware delivery, installation, trawler availability, and start of the first data collection trip, the broadband echosounder hardware was first installed on the research vessel R/V Tridens. There it was trialed during a 4 week dedicated acoustic survey. After the survey and completions of satisfactory signal reception and data production tests, the hardware was installed on the freezer-trawler used for data collection.

WP3: As the trawler used for data collection was not available for recording broadband data during a sprat fishing trip, there are only data available on herring, mackerel, and horse mackerel. The settings of the echosounder prototype were also changed for no apparent reason during some trips, resulting in some data not being collected in broadband mode. Additionally, during recordings of fish schools interference was caused by other acoustic equipment running even though it was required to switch these off. This is a tradeoff of data collection during fishing activities as sometimes it was not feasible to switch off other sounders as they are required and a necessity for fishing operations. The disadvantage was the need for more extensive data cleaning procedures afterwards.

WP4: Trawl information at the time of the project was not available at the requested resolution (essentially length-based information per trawl), so conclusions had to be based on the available information which consisted of estimated catch compositions by species.

1.3 Approach

Through collaboration between the pelagic industry and acoustic fisheries scientists this project can improve selectivity in fish capture operations and bycatch reduction by use of a modern commercial broadband echosounder. The project delivers imaging software scripts to read, display and produce the specific information by fish school for subsequent classification and analysis of broadband data. Focus has been on the identification of fish species from the broadband data collected during fishing trips. These identifications are based on collected test data, modelled broadband sound scattering and classification algorithms for the different fish species. The project consisted of data collection periods during different fishery situations. These data and the manufacturer specified prototype data format then formed the basis for the software code developed during the project. A preparation phase consisted of hardware installation, planning and testing which preceded the data collection in the field.

The broadband data collected on fish schools during different fisheries were then used to develop and test different classification methods. Three classification approaches aimed at identifying species are utilized:

1. a statistical classification based on school characteristics (e.g. size, shape, echo intensity distribution, density, or time signals);
2. a classification based on frequency response is used to focus on analysis of the enhanced frequency spectrum of the broadband data, which reveals differences between types of species;
3. As an additional step, both classification approaches are merged to create a combined classifier.

For the execution of the project, the client (Redersvereniging voor de Zeevisserij; RZV) selected IMARES and TNO. IMARES and TNO worked as a consortium, with IMARES being responsible for overall project management, administration and communication, in addition to carrying out its own work packages. The client insisted on working with this consortium based on previous experience and collaboration with members of the RVZ in similar projects. Within the Netherlands, they are the main research institutions in the field of fisheries hydroacoustics and sonar signal processing. IMARES had the responsibility over collection of the raw broadband data. TNO was primarily tasked with and responsible for the development of the software code and part of the subsequent analysis steps. Data analysis and

application of species classification algorithms based on analysis of the wide frequency band pattern and backscatter model predictions was done by IMARES, while TNO concentrated on species classification based on statistical characteristics of the broadband data.

2 Materials and Methods

2.1 Data collection

Acoustic broadband data were collected and recorded during fishing activities on a selected pelagic freezer-trawler (SCH6). The echosounder was a Simrad EK80 prototype version with 3 WBT's connected to composite split-beam transducers with nominal frequencies of 70, 120, and 200 kHz. The system was operated by the EK80 software (version 1.6.0 at project start, 1.7.5 at the end) using recommended settings as described in the developed operating manual (Appendix A). Frequency-modulated (broadband) sound pulses could therefore be generated by the system to send and receive over a wide frequency spectrum spanning a band of 45-260 kHz (Figure 2.1). Broadband data were collected during 3 fisheries in 2014 targeting herring (August), horse mackerel (October), and mackerel (December). A fourth data collection trip was done at the end of 2015 (October) while fishing on horse mackerel. Given the expected data quantities (3 minutes of broadband data recording at the 3 channels used produced 1 GB of data), it was decided to limit recording during the trip to times when fish schools were present and detected by the echosounder.

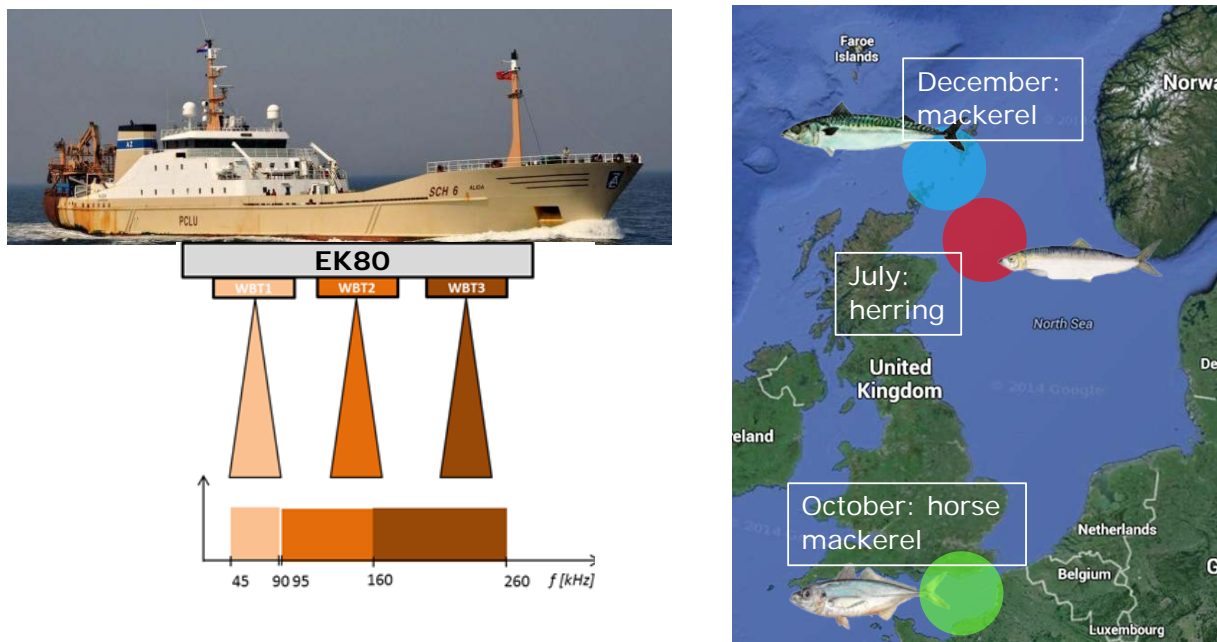


Figure 2.1. Schematic description of the Simrad EK80 broadband echosounder used on a freezer-trawler to cover a 45-260 kHz frequency band (left panel) and collect data during various fisheries (right panel).

During data recording, .raw data files were recorded to an external data storage on board. Once the trawler had returned back to port, the data was transferred to a portable storage device for backup and further analysis on shore. Recommended settings were chosen as to maximise classification potential from the data by utilising frequency modulated information from the full bandwidth available. Apart from the frequency bandwidth characteristics, pulse duration and power settings were chosen identical to narrowband echosounders according to the manufacturer's recommendation. A so-called fast ramping was chosen, whereby an amplitude window is applied on the transmitted pulse: the first few cycles of the transmit signal are used to ramp up the signal amplitude from 0 to 1 (where 1 corresponds to the maximum desired amplitude) and the last few cycles are used to ramp down the amplitude from 1 to 0 (Figure 2.2). The advantage of a fast ramping is that the transmitted pulse contains more energy, which increases the signal to noise ratio. Therefore the use of a broadband signal in combination with fast ramping will significantly increase the signal to noise ratio in the outer edges of the frequency band. This

will result in a longer effective pulse duration and a wider effective frequency bandwidth to increase available bandwidth and range resolution.

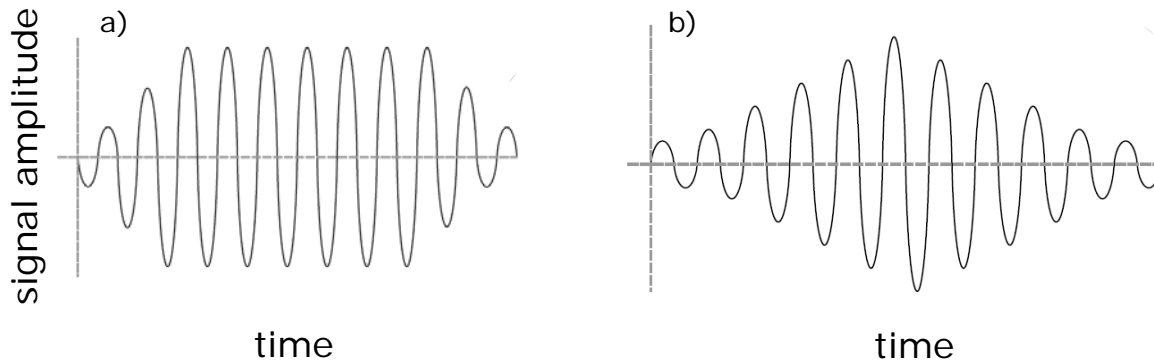


Figure 2.2. Schematic description of the ramping amplitude of a broadband signal. (a) shows a fast ramping situation where the signal amplitude of the pulse is increased from 0 V to maximum level using only two cycles. At the end of the pulse, another two cycles are used to reduce the output level. With slow ramping (b) the output level is increased from 0 V to maximum level using the first half of the pulse duration. The second half of the pulse is then used to reduce the output level.

2.2 Data processing

All data that were recorded during the fishing trips went through the developed processing chain (Figure 2.3). The global processing chain was designed to have a recorded file containing raw data from the EK80 as input. These raw data contained measurements of acoustic pressure in the time domain, and eventually the data processing steps delivered a set of individual detected schools on echograms for further classification to give estimated species type and confidence level as output.

Here, the term fish school is defined as a cluster of fish that is physically disconnected from other clusters in its near vicinity. The term school and cluster may be used interchangeably, both carrying the same meaning. This may differ from a fisherman's definition whereby a school may describe the total amount of fish in a certain area that can be caught in a single haul, irrespective of any existing physical disconnections between school-parts.

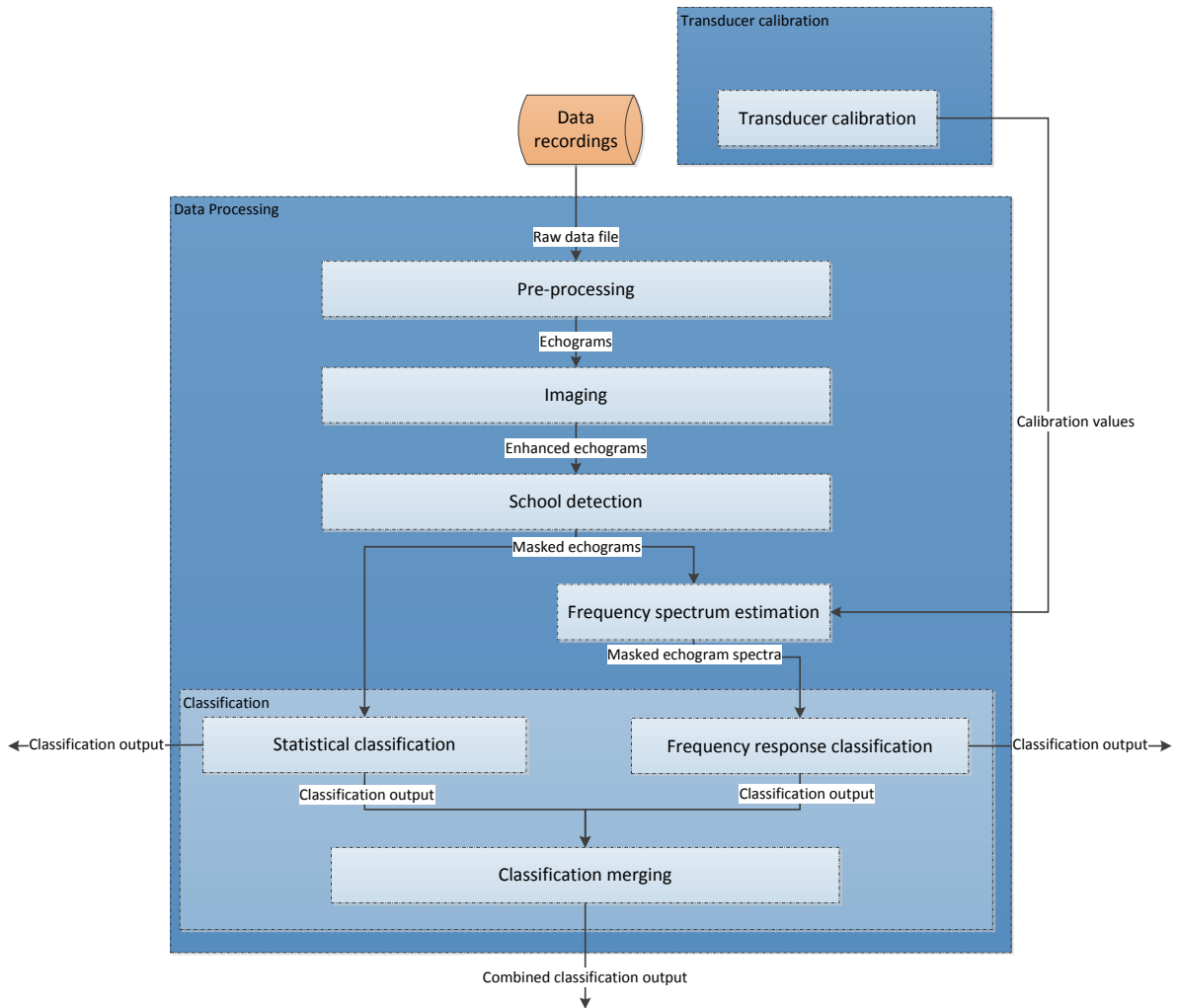


Figure 2.3. Schematic overview of the data processing chain. A raw recorded data file is presented as input to the chain. Individual detected schools and their estimated species type are produced as outputs.

In Figure 2.3, a schematic overview of the data processing is depicted. For each recorded file containing a fixed number of pings, data are pre-processed (section 2.2.1) to reconstruct the original time signal data. Echograms are created and enhanced (section 2.2.2) using image processing techniques. School detection (section 2.2.3) is performed on the enhanced echograms in order to create cluster masks. Thereafter the calibration parameters are computed (section 2.2.4) and applied to the derived frequency spectra of the clusters (section 2.2.5). The masked cluster data are used as an input for further fish school classification (section 2.2.6). All individual modules, given by the light blue boxes, are described in more detail in the following sections. The outputs of the chain are given for both types of classification methods (statistical and frequency response/spectrum classification) as well as for a classifier that merges both outcomes. A brief analysis of the three outcomes will throw light on the best approach in determining the final outcome.

2.2.1 Pre-processing

The data pre-processing module converts the raw echosounder data to echograms. A basic level of pre-processing scripts, which could read the data format produced by the prototype EK80 system used were delivered by the manufacturer of the utilized echosounder, SIMRAD. A schematic overview with the

operations is given in Figure 2.4. The pre-processing is performed for each transducer, delivering three echograms as an output that are fed to the next stage: image enhancement. The individual steps will be described in the following sub-sections.

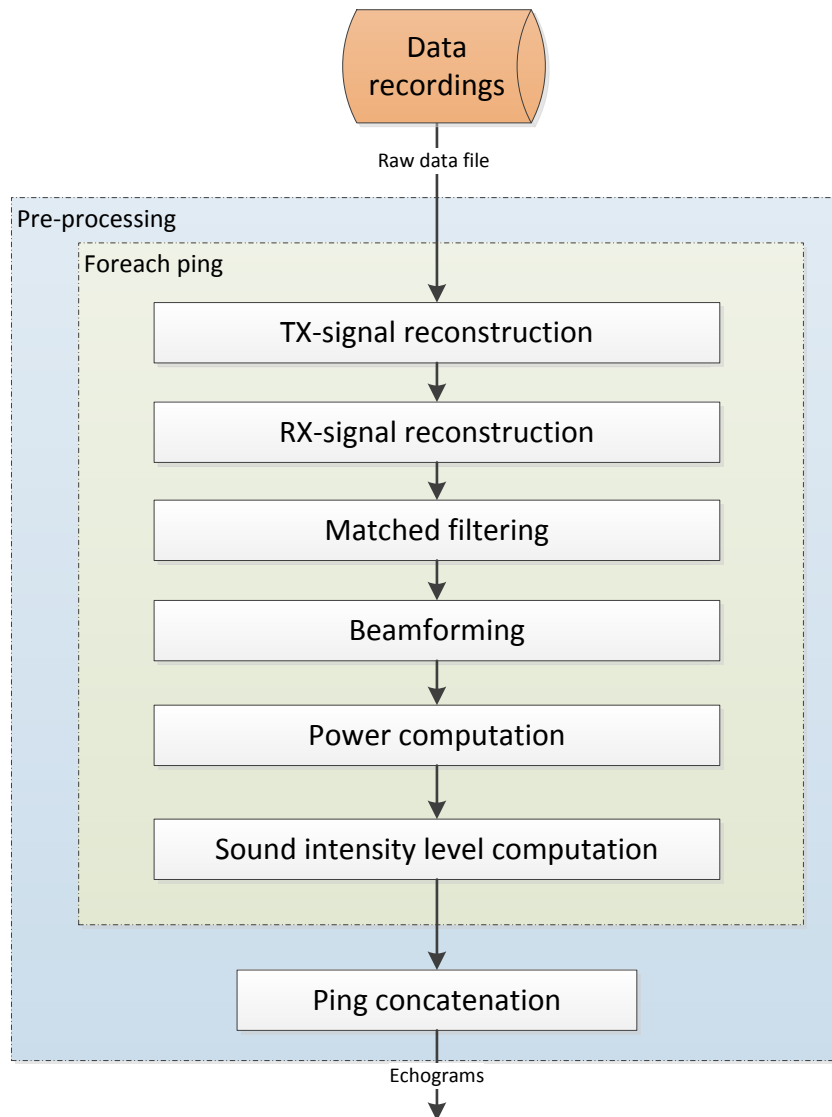


Figure 2.4. Schematic overview of the pre-processing module. Raw file data are pre-processed and converted to sound pressure. All pings in the data are collected to construct an echogram. An echogram is created for each transducer separately.

2.2.1.1 **TX-signal reconstruction**

Based on the properties of the transducer as well as those of the transmission pulse that is used, the signal that was transmitted during data recording, is reconstructed. Reconstruction of the original transmission signal is required to be able to perform matched filtering of the received data (section 2.2.1.3). The transmission pulse is described by its start and stop frequencies, its length in time and the slope of the window that describes the chirp shape. Having the originally transmitted pulse, it is band-pass filtered and down sampled to match the sampling frequency of the received data such that it can be used for matched filtering.

2.2.1.2 **RX-signal reconstruction**

The raw data received by the transceivers are sampled with a very high frequency. In RX-signal reconstruction the data is band-pass filtered and down sampled to obtain the received signal that is used for further processing, without loss of information.

2.2.1.3 Matched filtering

Matched filtering is a technique to detect the presence of a template in an unknown signal. This is achieved by correlating a known signal, the template, with an unknown signal. Here, the transmitted pulse (TX) is the template and the unknown signal is the received data (RX). A matched filter is known as the optimum filter for maximising the Signal-to-Noise Ratio (SNR) in the presence of additive stochastic noise. By performing matched filtering, reflections (by fish, seabed etc.) of the transmitted signal are maintained in the data while noise is filtered out.

2.2.1.4 Beamforming

Each of the transceivers used on the test vessel consists of four receiving elements, positioned in a square. To increase the SNR of the received data, the elements are summed together in this step. This process is called beamforming and is a widely known technique to create directivity and suppress additive stochastic noise as well as the negative contribution of interfering sources coming from other directions than the focus direction (straight downward in this case).

2.2.1.5 Sound intensity level computation

It is important to compute the exact intensity level of the data in order to be able to make comparisons between data of different transducers and/or datasets in the classification stage. Using the physical impedance of the transducer and receiver, the power P (W) of the beam formed data is computed according to the implementation used by SIMRAD:

$$P = 4 * (|d| / (2 * \sqrt{2}))^2 * (RI / (RI + NI))^2 * 1 / NI$$

Where d represents the beam formed data values (V), RI the receiver impedance (Ω) and NI the nominal transducer impedance (Ω). The intensity level I (dB) of the sound is then given by:

$$I = 10 * 10 \log(P)$$

This intensity is corrected with the following compensations.

Time-varying gain

Having the exact intensity levels of the received data, the data is compensated for natural intensity loss as a result of propagation through the water. The amount of intensity loss is directly related to the propagation time of the signal: longer propagation results in more intensity loss. Intensity loss due to propagation is a combination of absorption and spreading loss.

Sea water absorption is calculated as a function of water temperature, salinity, depth, acidity, sound speed and sound frequency. Spreading loss is caused by the geometrical spreading of the sound with respect to the source. A spherical spreading corresponds to a sound wave propagating uniformly in all directions. This case corresponds to a source in open water. A cylindrical spreading corresponds to a sound wave bounded into a waveguide, typically a shallow water scenario. Both are geometrical approximations, SIMRAD is using a spherical spreading compensation for a point target (single fish), and a cylindrical spreading loss for a fish school in order to account for the larger target volume. The spreading compensation is user defined, and at the exception of the calibration procedure (point target), only the cylindrical spreading is used for fish school analysis:

$$PL = 10^{10} \log(r)$$

Where r equals the range distance to the object in meters. For the transducer, also spherical spreading is applied with an additional compensation for the directivity of the combination of four transmitting elements.

Matched-filter gain

The matched-filter gain is the gain obtained by the matched-filter response. By the transmission of a pulse and the matched-filtering of the received data with the transmitted pulse, the gain applied on the transmitted pulse is indirectly measured. By normalising the received signal intensity with the intensity level of the autocorrelation of the transmitted pulse, this additional gain is removed. This is useful in order to be able to compare data sets that have been generated with pulses that have different gains.

Transmission power

The sound intensity level is compensated for the transmission power of the transducing elements. In this case the sound intensity is fully normalised independent of specific transducer settings. Data sets recorded with different transmission power can then still be used for comparison.

2.2.2 Imaging

Once the echograms (one per transducer) are produced, image processing and enhancement is required in order to be able to combine the transducers operating at different frequency bands and with different sampling frequencies. Image enhancement is then applied to remove noise and interferences from the data as a result of interfering sources residing within or around the operating vessel.

In Figure 2.5 a schematic overview of the imaging blocks is depicted. The following sections will outline the individual steps in more detail.

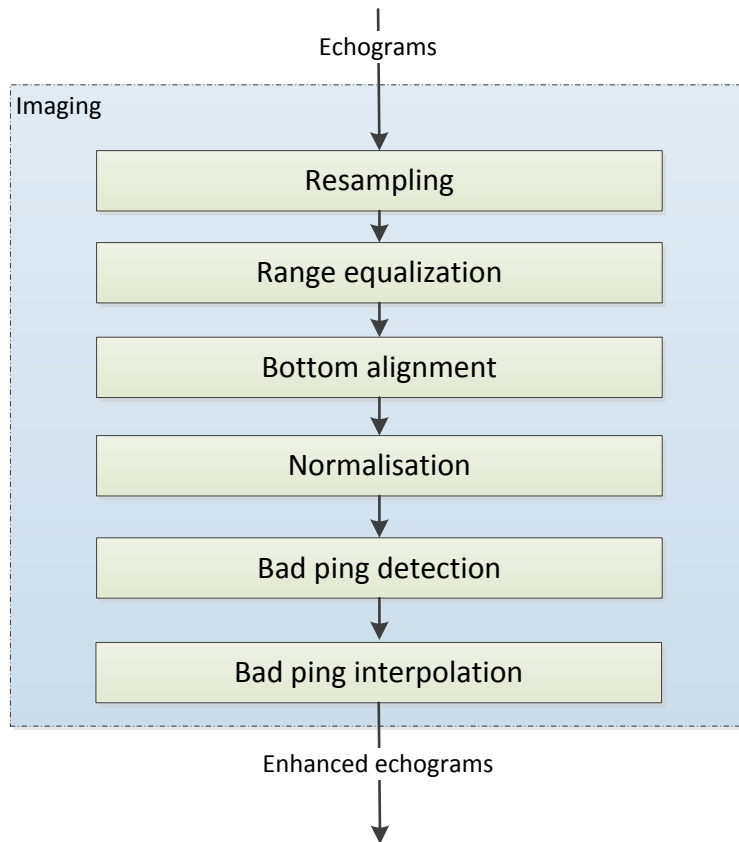


Figure 2.5. Schematic overview of image processing and enhancement blocks applied on the echogram data of each transducer.

2.2.2.1 Resampling

The resampling module upsamples the echogram data of the individual transceivers to the highest sampling frequency of all available transceivers. Upsampling is performed by linear interpolation. By upsampling the data, each sample in the echogram of a transducer corresponds to the same pixel location in the echograms of the other transducers, making it suitable for combining transducers in the following processing steps.

2.2.2.2 Range equalisation

In range equalisation the maximum range of each echogram is cropped to the minimum range of the echograms of the three transducers in order to have the same number of range samples per image. The data being removed in practice is only a small fraction of the image residing below the bottom. This step is necessary in order to easily combine or compare the three transceivers.

2.2.2.3 Bottom alignment

In the bottom alignment step, the transducer images are aligned with the bottom by removing all data below the bottom and adjusting the image for a varying bottom as a result of vertical ship movement due to surface waves. The procedure roughly consists of three steps:

- Global depth estimation

- Ping-based depth estimation
- Ping-based bottom alignment

All three steps are outlined in the following sections.

2.2.2.3.1 Global depth estimation

As a first step, a rough depth estimate is made using the echogram of one of the transducers. The second transducer spanning the frequency range 95-160 kHz was used for that purpose since this band provides a suitable balance between little noise and little bottom penetration.

In practice, to find a global depth estimate, the mean over all pings is taken, resulting in a single-ping vector with average intensity per range. The range value with the maximum intensity is considered the global depth estimate of the image. In case of a very strong sub-bottom reflection, a varying depth (bottom slope) or significant waves, averaging over pings may not provide a clear maximum near the actual bottom since the bottom pixels are not aligned when looking in the ping direction. The averaged *sub-bottom* reflections then may add up to a maximum higher than the actual bottom reflection, resulting in an incorrect depth estimate. To avoid this problem, each ping was low-pass filtered by a moving average filter that divides the ping into moving windows in the range direction and takes the average of each window. The filter length is in the order of a few meters. That way, the bottom reflection in every ping is spread out such that the depth is estimated properly. For the ping-based depth estimation in the next step, the original image is used again. Figure 2.6 shows an example of the global depth derivation of an echogram with Mackerel data.

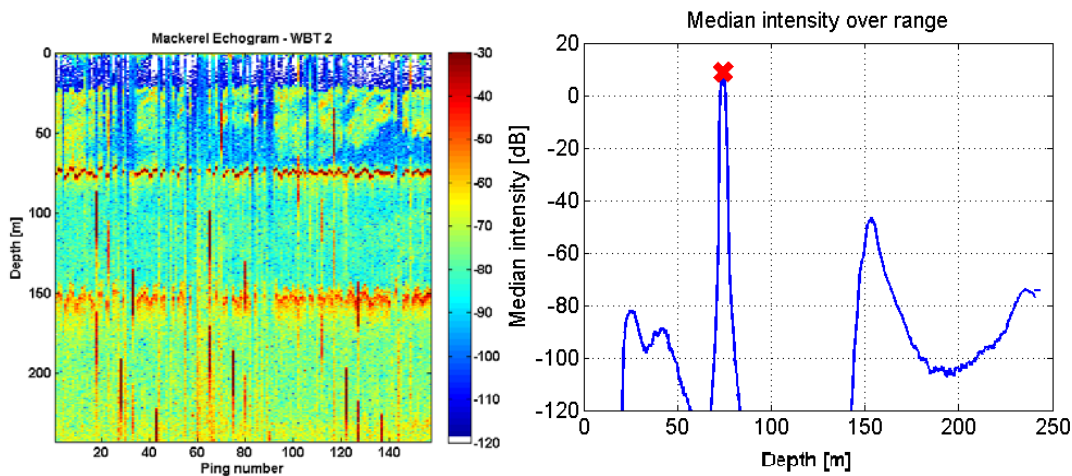


Figure 2.6. Example of global depth derivation. A non-bottom aligned echogram of transducer 2 (left) with a depth of 75 m and a clear duplicated bottom reflection at two times the depth. A plot of the median intensity of the echogram, low-pass filtered in the ping direction, and the found maximum at 75 m (right).

2.2.2.3.2 Ping-based depth estimation

Using the rough depth estimate for each transducer, the actual depth was then estimated for each ping by searching for the ping maximum within a local window around the global depth estimate, as depicted in Figure 2.7 for a herring school. By doing this, the rough depth estimate is adjusted locally for surface waves and a possible bottom slope. The combination of using a global depth estimate and local depth estimates around the global estimates makes it robust against noise.

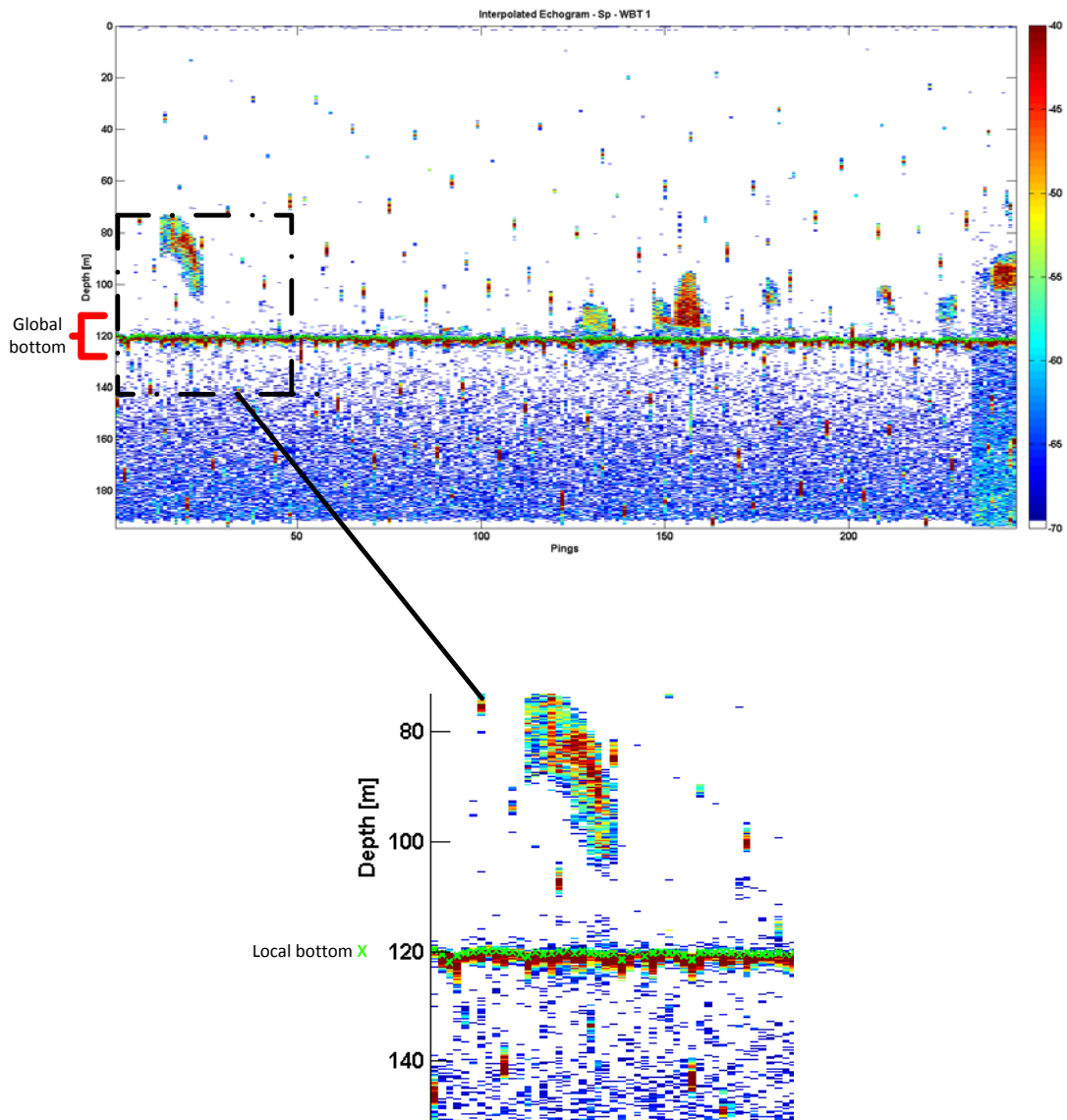


Figure 2.7. Echogram (above) and zoomed echogram (below) of the global depth indicated by the red brackets and the local depth indicated by the green crosses.

2.2.2.3.3 Ping-based bottom alignment

Finally, using the found bottom index per ping, each ping was aligned with its local bottom. This is done by removing the data below the bottom as well as the data with a range smaller than the deepest wave detected in the image. The deepest wave is implicitly given by the closest bottom found in the image. In this way each ping retains the same amount of samples, making it suitable for further processing. Figure 2.8 depicts the bottom-corrected version of Figure 2.7.

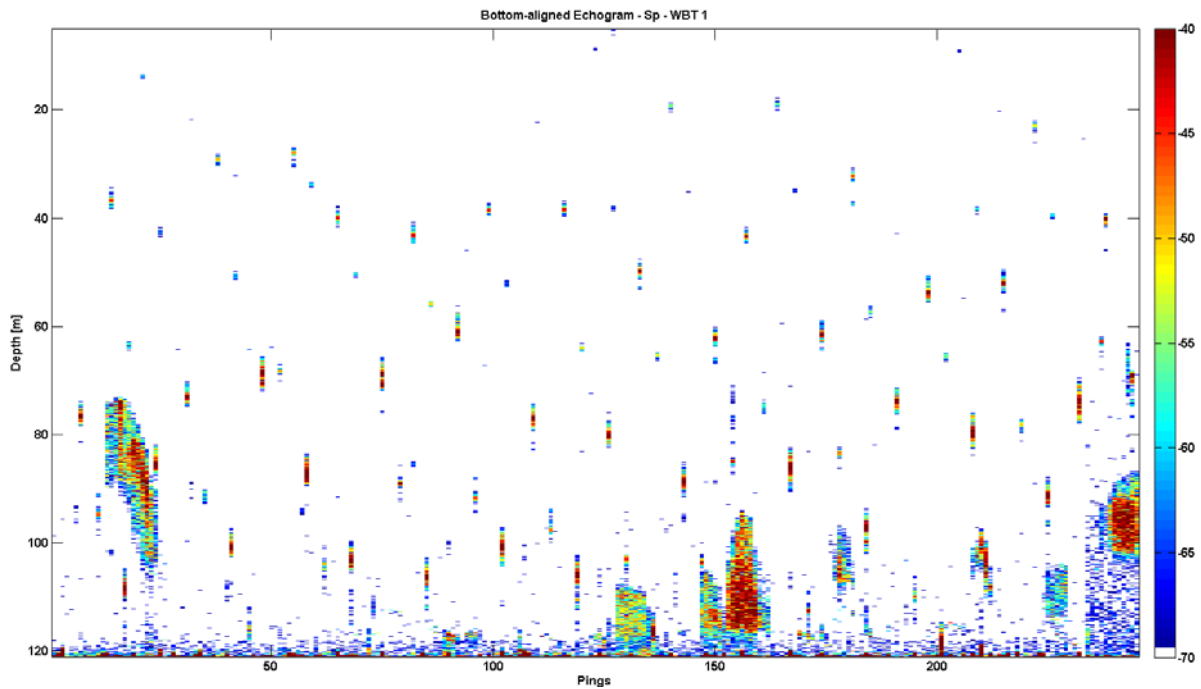


Figure 2.8. Example echogram after ping-based bottom alignment. The bottom of the echogram is now exactly aligned with the estimated local bottom and corrected for vertical ship movement incurred by surface waves.

2.2.2.4 Normalisation

Normalisation of the echograms is done per individual transducer. Normalisation is performed as a supporting step in school detection. The different frequency bands of the transducers resulted in different background intensities. By normalising the images, fixed image data thresholds can be set for initial school mask estimation independent of the frequency band covered by a transducer. Normalisation is performed by subtracting a 'data dependent' value from the intensity values (log values) of the image pixels. For this purpose, the 'data dependent' value was defined as the first quartile of the echogram data of the transducer. That value implicitly represents an intensity value outside a school of fish, assuming a fish school does not cover more than 75% of the echogram. If it does, though, this percentile could be further decreased.

2.2.2.5 Bad ping detection

To enhance the quality of the echograms and to make detection and classification more robust against noise, bad pings were identified, detected and replaced by their interpolated counterparts. Bad pings are parts of the data that reduce the quality of the image. Mostly these are vertical stripes in the image, which are caused by acoustic or electronic interference during the reception of the ping. They can also be 'empty pings', whenever the transducer did not work properly and skipped a ping. For example this situation may occur in bad weather when air bubbles can cover the transducer face and prevent transmission and/or reception of sound energy. These bad pings needed to be removed and interpolated or at least indicated such that they would not be used in classification as bad pings can have a negative effect on the final classification output. If bad pings reside within a school and remain present in the echogram, this may have several consequences:

- Adjacent empty pings may unwantedly split a single school in two sub-schools
- They change the observed (local) signal level of the school

- Their time signal does not represent the actual time signal that would be observed at that location in the school

All points have their effect on school detection and/or classification when it comes to feature computation that is based on, among others, intensity, school shape and size and time signal and frequency response statistics. Not removing or indicating bad pings would negatively influence the classification performance. Still, it neither is beneficial to be too strict and remove too many pings that have a slight deviation from the average good pings, as this decreases available sample size and therefore statistical robustness of a subsequent classification.

Besides the detection and replacement procedure itself, as a preliminary step it is important to identify the exact definition of a 'bad' ping. Figure 2.9 and Figure 2.10 show a normalised, bottom-aligned echogram with several examples of what can be considered bad pings. The blue diamond indicates a bad ping with two neighboring good pings. The black circles indicate bad pings with one or two neighboring bad pings. The red cross indicates a bad ping that contains a red stripe of interference noise. The magenta triangles indicate pings that may still be considered good despite of their noisy 'red stripe' as it is mostly outside the area of interest (fish school).

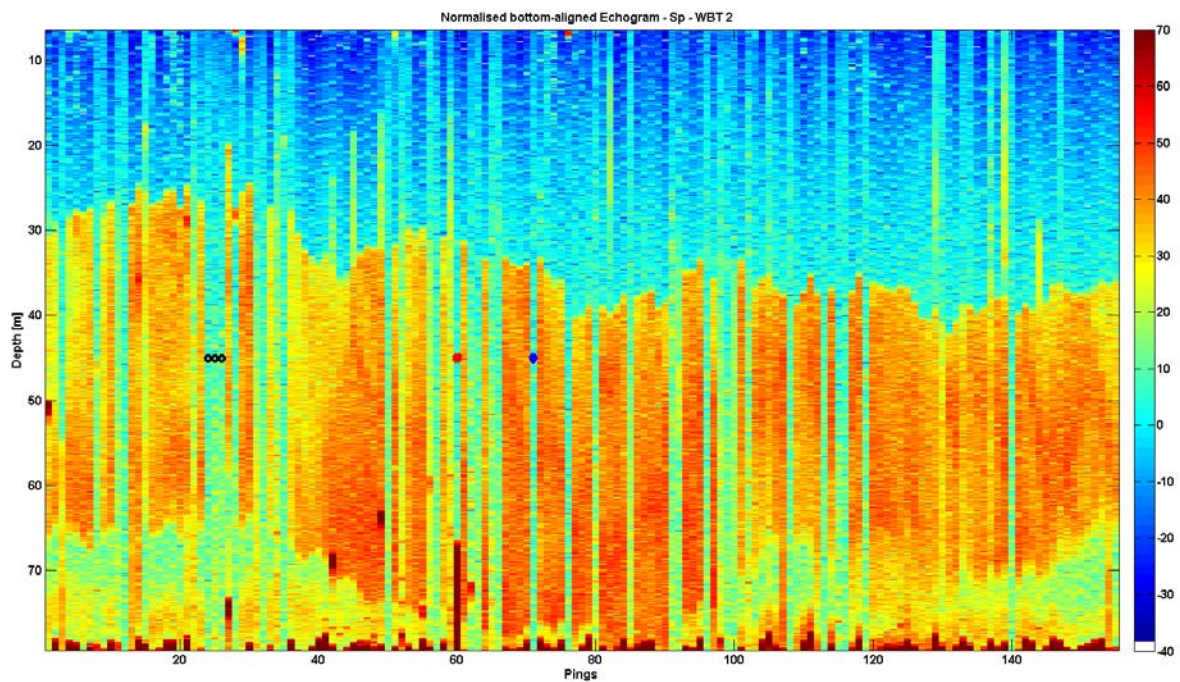


Figure 2.9. Normalized, bottom-aligned echogram with bad pings. The blue diamond indicates a bad ping with two neighbouring good pings. The black circles indicate bad pings with one or two neighbouring bad pings. The red cross indicates a bad ping that has a clear red stripe.

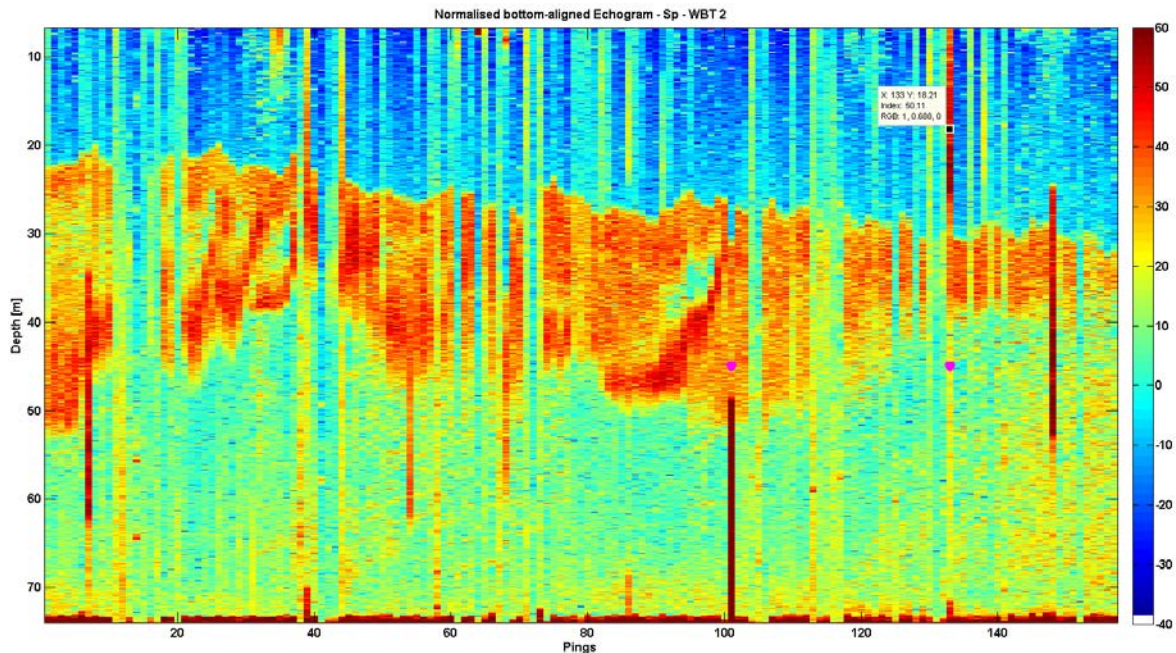


Figure 2.10. Normalised, bottom-aligned echogram with bad pings. The magenta triangles indicate pings that may still be considered good despite their 'red stripe' as the bad part is mostly outside the area of interest (fish school).

From these situations several criteria can be set:

- A bad ping does not necessarily have to have low average intensity (ping with the red stripe is also bad).
- A ping is not per definition good when it resembles its direct neighbors (pings with the black dots).
- A ping is only bad when it is bad in the area of interest.

Conclusively, when trying to come up with a description of a bad ping while looking at the image, a ping can be considered bad when its (locally averaged) intensity in the area of interest (fish schools) deviates too much from a more global pattern both in time and range, constructed from a number of close (in time) *good* pings. Based on this definition, for each transducer the following procedure is executed to determine the bad pings in an echogram:

1. Removal of (strongly reflecting) seabed top layer from the echogram
2. Normalisation to minimum and maximum value in the image
3. Windowed averaging per ping over the range dimension (similar as in bottom detection)
4. Image quality estimation
5. Creating a template by smoothing in ping direction with a smoothing length based on the image quality
6. Determining bad pixels based on deviation of image from template
7. Determining bad pings using bad pixels and their locations

Steps 1 to 3 are self-explanatory; steps 4 to 7 will be further outlined here.

2.2.2.5.1 Step 4: Image quality estimation

As a preparatory step for creating an image template, an image quality estimate is made resulting in a value between 0 and 1 with 1 indicating very good quality. This image quality estimate is directly related to the filter or smoothing length used in template creation. If the image quality is low, there are a lot of

bad pixels and pings and the filter length must be somewhat longer to create a template that resembles the 'big picture' better. Or in other words: one would have to squeeze the eyes a bit more in order to see the contours of the school! A disadvantage of a long filter length is the reduced ability to cope with natural, local school variations. Any natural, rapid variations can be mistakenly qualified as a bad ping. Hence, a high image quality will allow a shorter filter and reduces the amount of mistakenly qualified bad pings.

The image quality is based on the variation of the image in the ping direction: high variation indicates an unnaturally low, local coherency and hence lots of bad pixels and a poor image quality. Figure 2.11 shows a number of echogram images with their associated quality estimates.

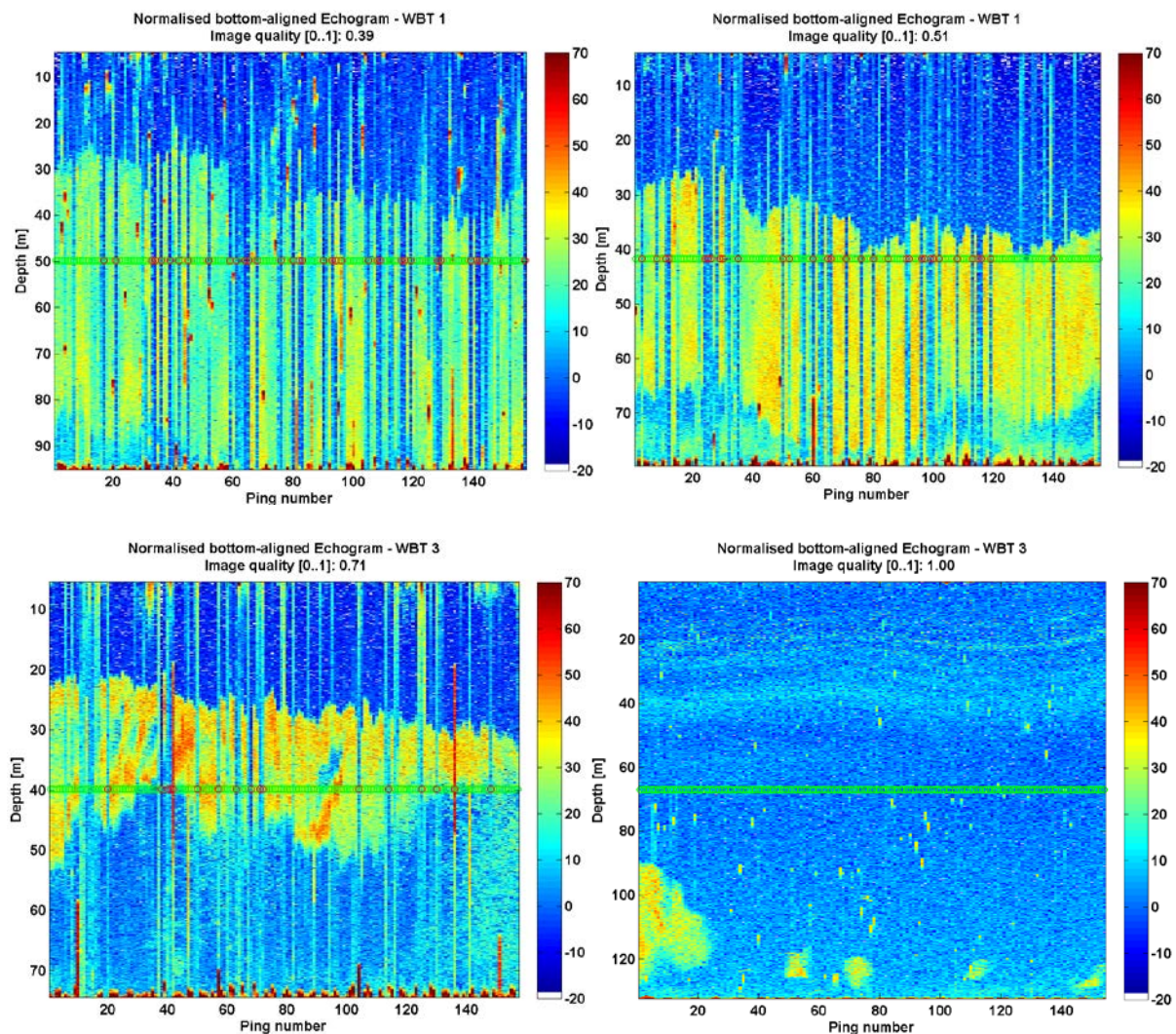


Figure 2.11. Four example echograms with their image quality estimates between 0 and 1 with 1 being good quality. Image quality is based on the amount of variation in the ping direction; high variation indicates poor image quality.

2.2.2.5.2 Step 5: Template derivation

Based on the image quality a template of the image is created; i.e. the image is low-pass filtered in the ping direction. The smoothing length lies between 6 pings for very high quality images and 20 pings for very low quality images. Figure 2.12 shows the templates for the 0.39 and 1.00 quality images in Figure 2.11. Two things become evident from the image quality dependency of the filter length:

- In the left image the bad pings are hardly visible anymore in the template due to the larger filter length. This will ensure that the actual bad pings will also be qualified as bad pings in template matching.
- In the right image, the sharp edges of the sub-schools are maintained due to a short filter length as a result from the high image quality. This will ensure that school edge transitions will not be mistakenly qualified as bad pings.

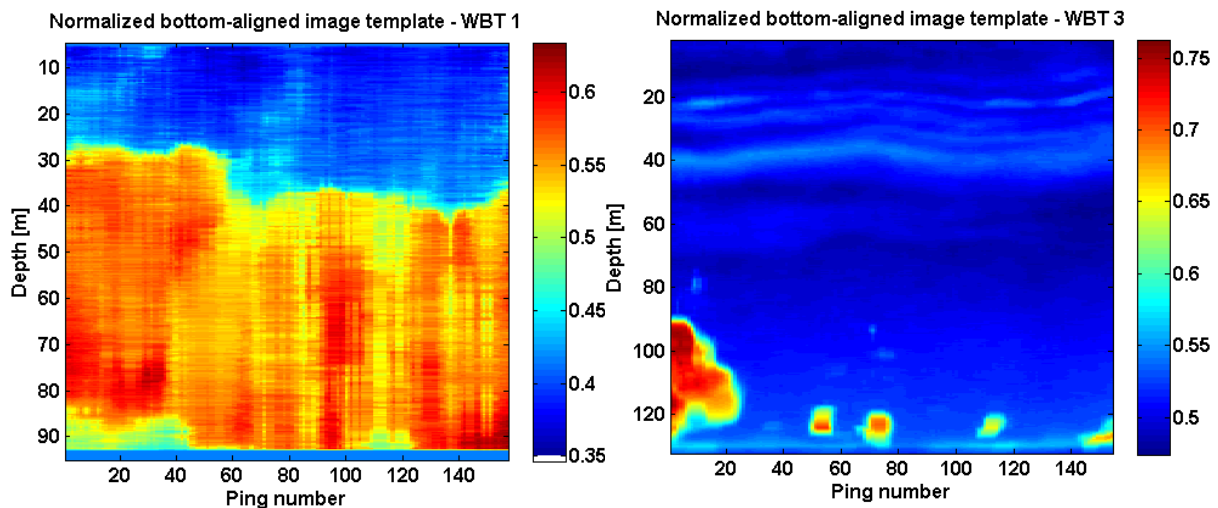


Figure 2.12. Image templates for two of the four example echograms with a relatively poor quality image and hence a longer filter length (left) and a high quality image and hence a shorter filter length (right). The filter length determines the allowed variation in the template.

2.2.2.5.3 Step 6: Bad pixel determination

To determine the bad pixels, the difference between the template and the image was computed. If the difference of a pixel exceeded a certain threshold level, it was assigned a suspicious pixel. Due to local school variations a suspicious pixel does not necessarily have to be a bad pixel, but there is a valid chance. All suspicious pixel indices were stored for usage at a later stage. In bad ping interpolation, the suspicious pixels are not used for interpolation. In this case, one avoids smearing out bad pixels in certain areas of the image as a result of bad ping interpolation. Any high intensity bad pixels otherwise may generate a new invalid 'school'. Figure 2.13 summarises the process of bad pixel determination: template creation, template subtraction and thresholding.

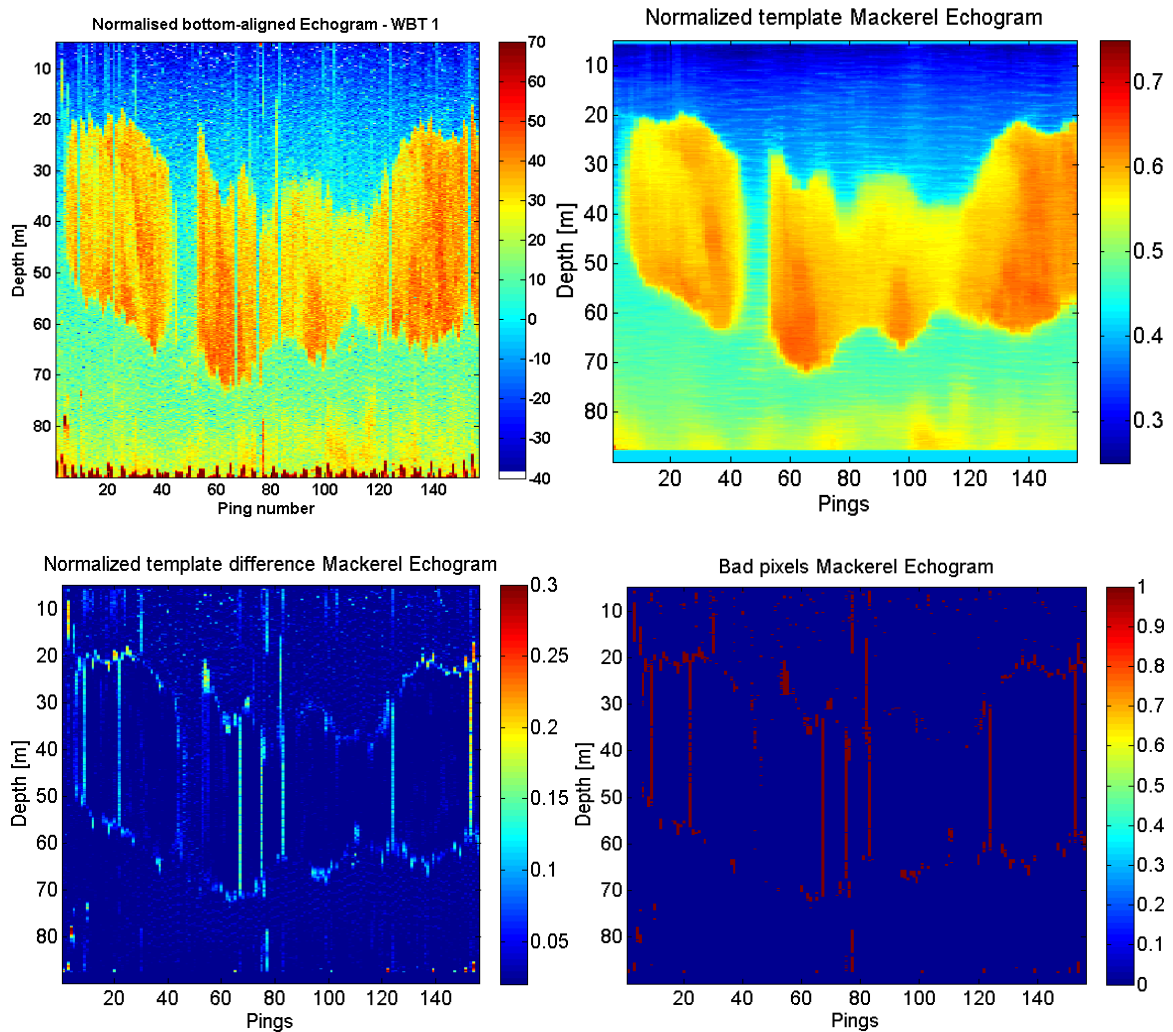


Figure 2.13. Bad pixel determination process. For a transducer echogram (top left) a template is created (top right). By thresholding the difference between the template and the normalized echogram (bottom left), a bad pixel mask is obtained (bottom right).

2.2.2.5.4 Step 7: Bad ping determination

From the template, the areas with high intensity pixels were selected by means of another thresholding step, indicating important data (i.e. fish schools). These were essentially the areas of interest. According to the earlier derived definition, a ping was allowed to be partly bad as long as the bad part was outside the school. Because the template is already a filtered version of the image, the chance of indicating high intensity bad ping parts as ‘important data’ was very small.

Per ping, the number of suspicious pixels was computed in the region where the important data was located. If the number of suspicious pixels was more than half (or another preset part) of the total number of pixels in the important data region of that ping, the ping was classified as bad. Finally, Figure 2.14 shows the result of this procedure for two example echograms of mackerel schools with their pings classified as good (green circles) or bad (red circles).

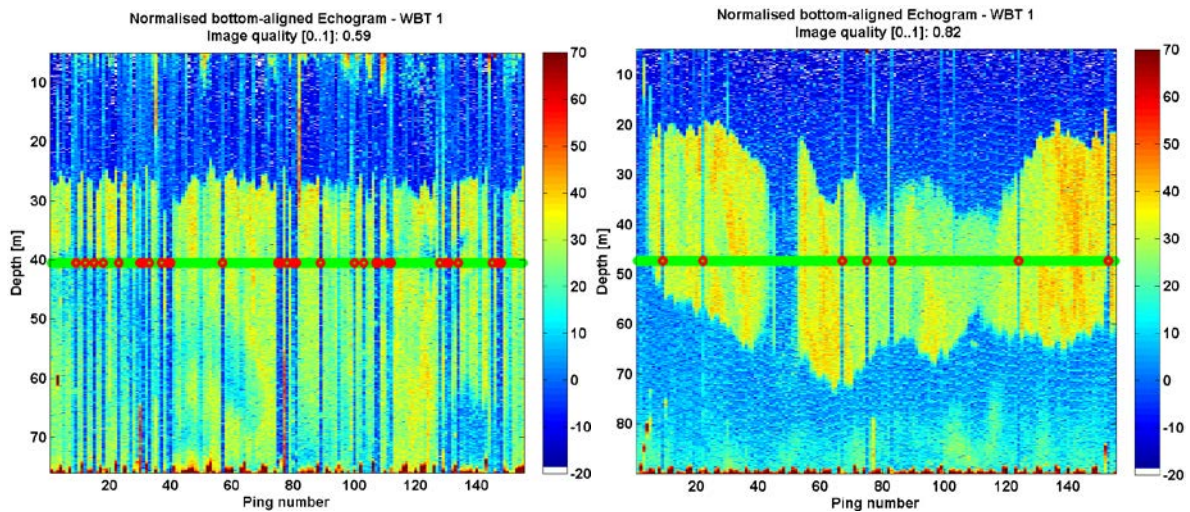


Figure 2.14. Result of bad ping detection for two echograms of mackerel schools with a different image quality. The pings classified as being ‘bad’ are indicated by a red circle, the ‘good’ pings are indicated by a green circle.

2.2.2.6 ***Bad ping interpolation***

The bad pings found in the bad ping detection procedure were linearly interpolated. Interpolation of a bad ping was performed using its two closest, good neighbors. The contribution of each neighbor was weighted based on their relative distance to the ping being interpolated. Any suspicious, bad pixels determined in the previous step were not used for interpolation in order to avoid reproduction of bad pixels throughout the image. As a replacement, the closest good pixels at the same depth were used accordingly.

2.2.3 **School detection**

The school detection module created a mask indicating the image pixels that represented fish; i.e. it detected the schools in an image. For all three transducers, a single school mask was created that accounted for all of them. In Figure 2.15, a schematic overview of the approach is provided. The subsequent description of the procedure is accompanied by figures of the intermediate results for two transducers with data of a herring recording.

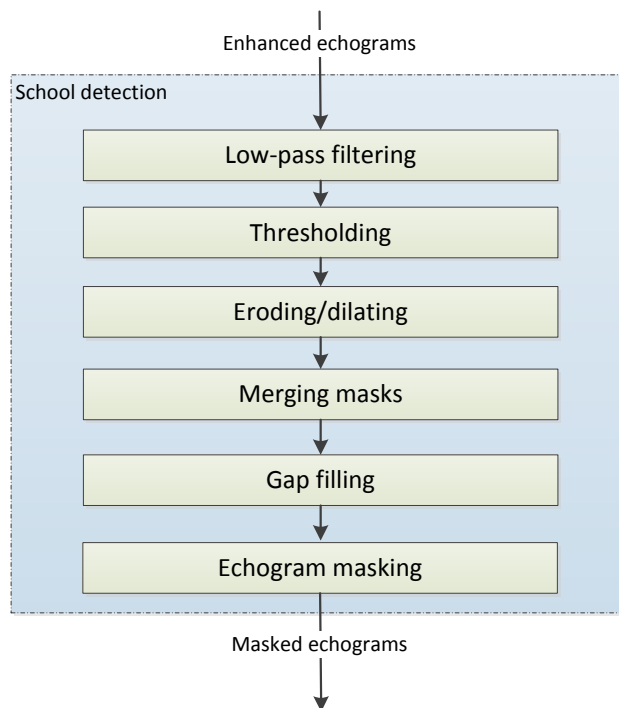


Figure 2.15. Schematic overview of the school detection module. In the individual steps an enhanced echogram is processed to deliver a masked echogram with the detected schools.

First, each pre-processed transducer echogram was processed individually (Figure 2.16). An initial digital school mask was created: the echogram was slightly low-pass filtered (Figure 2.17) to reduce the amount of noisy pixels that may distort school detection. Afterwards pixel values that exceeded a certain threshold level were marked as potential fish (1) or not (0), the result of which being depicted in Figure 2.18. To filter out remaining noise and wrong detections, image eroding and dilating (Serra, 1986) was applied to the mask (Figure 2.19). The resulting detection masks of the individual transducers were combined, resulting in a common detection mask where each pixel was allocated to fish (1) if at least half of the transducers (two in this case) indicate that pixel as fish (Figure 2.20). The reason for using the mask of multiple transducers (frequency bands) is to avoid detection selectivity as a result of frequency dependent differences in target response between different types of species; e.g. a species with hardly any reflectivity in the operating band of transducer 1 could potentially be not or only partly detected if only that transducer would be used in deriving the common detection mask. As a last step, small gaps in the school were filled by dilating and eroding the common detection mask (Figure 2.20). This step was performed in order to make sure that small gaps in a school do not unwantedly split a school in two and to support the ability to detect low density areas in a school in the classification stage. The latter might be a typical property of the school structure of a certain fish species. The mask was finally multiplied with the original, enhanced echogram data (Figure 2.21).

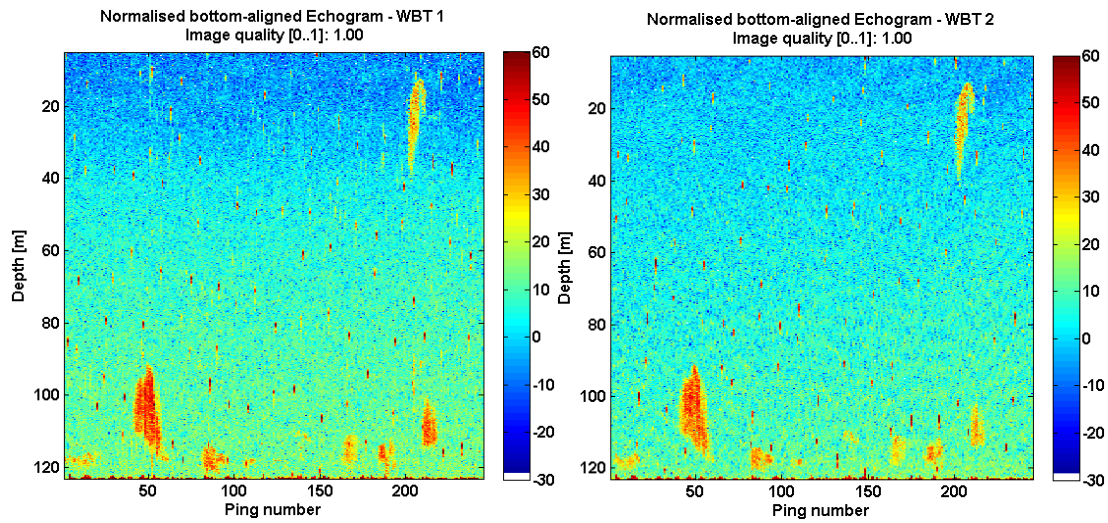


Figure 2.16. Enhanced echograms of the recording of Herring schools. The echograms are two of the three transducer inputs to the school detection module.

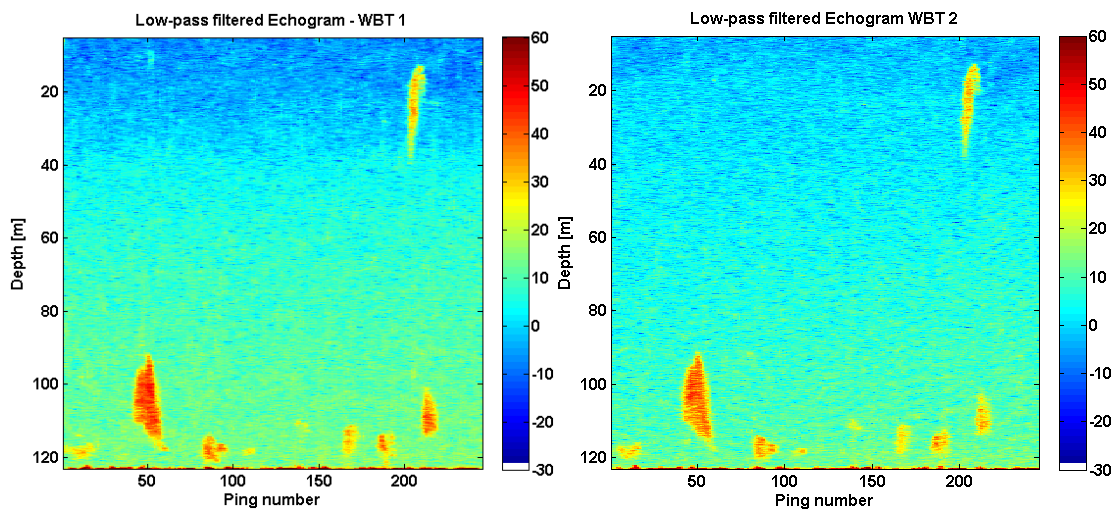


Figure 2.17. Echograms after low-pass filtering. Low-pass filtering reduces the amount of noisy pixels that may distort school detection.

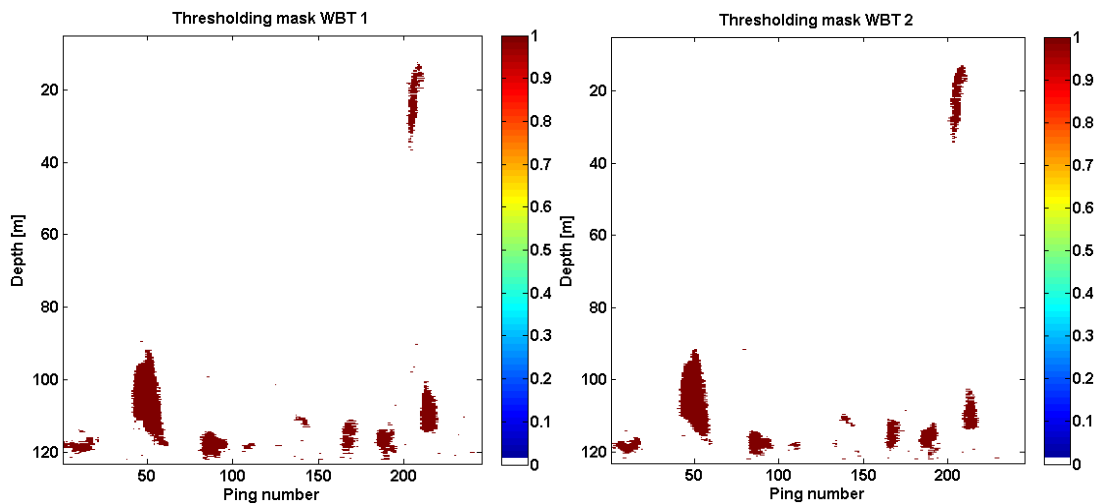


Figure 2.18. Initial school masks after thresholding the low-pass filtered echograms.

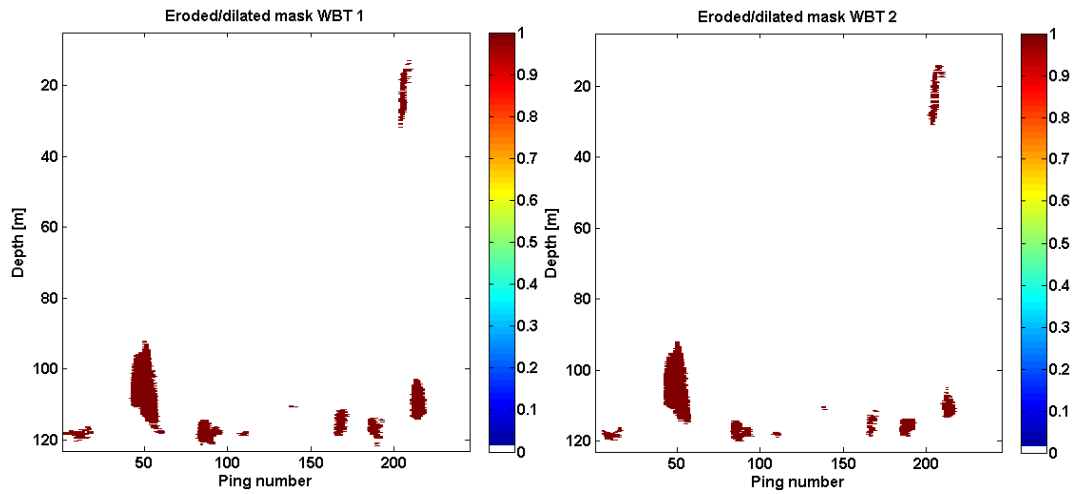


Figure 2.19. School masks after eroding and dilating the initial school masks. Erosion and dilation is used as an additional noise or misdetection removal technique.

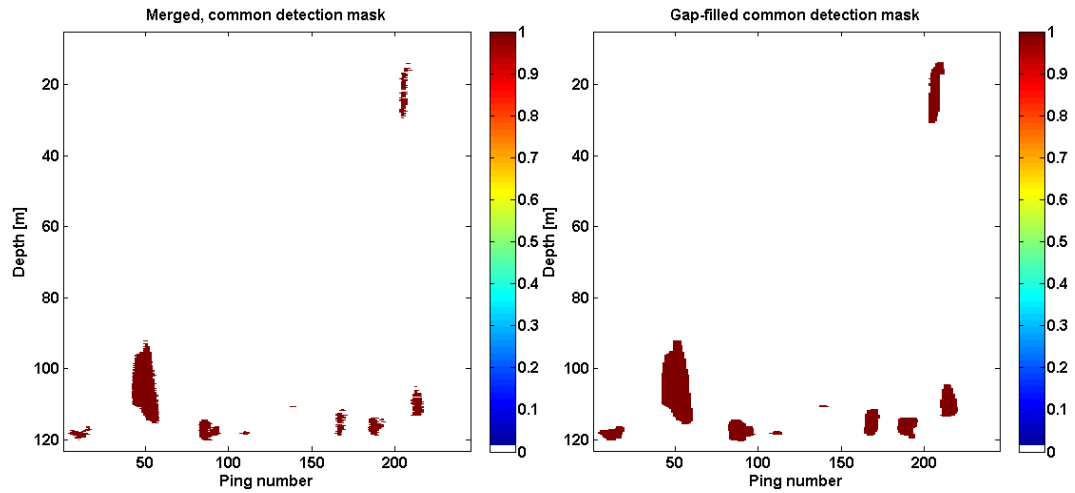


Figure 2.20. School mask after merging the masks of the three transducers (left). Final, common school mask after filling small gaps in the school using dilation and erosion.

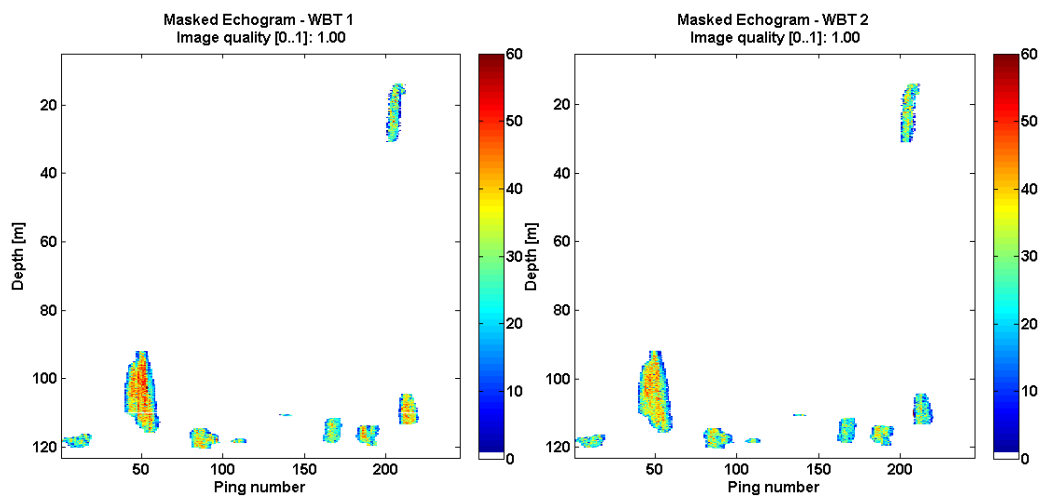


Figure 2.21. Masked echograms of two transducers. The common mask is multiplied with the enhanced echograms of the transducers to result in echograms with school-only data.

2.2.4 Transducer calibration

In order to be able to visualise target strength or biomass directly on the echograms, it is necessary that the transducers are calibrated. In other words, their characteristics are measured and compensated for as a function of frequency. The basic principle is to use a perfectly defined object, with a perfectly defined acoustical response as a reference and to measure it in the water column, at the location of the measurement. Any difference between the theoretical response and the measured response must be compensated for. In the sonar equation, this can be seen as estimating:

$$EL(f) = SL(f) - 2TL(f) + TS(f)$$

with f being the sonar frequency band, EL the echo level as measured on the transceiver, SL the sound level of the transceiver, TL the one way transmission loss and TS the target strength. Note that all these parameters are frequency dependent.

The echo level is measured and it also includes the transmission characteristics of the transceiver as a function of frequency. The target strength of a reference target used during calibration is known. The transmission loss can be estimated as function of frequency (spreading + absorption).

The analytical frequency responses of the different calibration spheres available are known (Figure 2.22), data of these spheres was also available. Specifically, the 38.1mm sphere was selected because of the presence of multiple contrasting features in the form of nulls and peaks over the frequency band of interest.

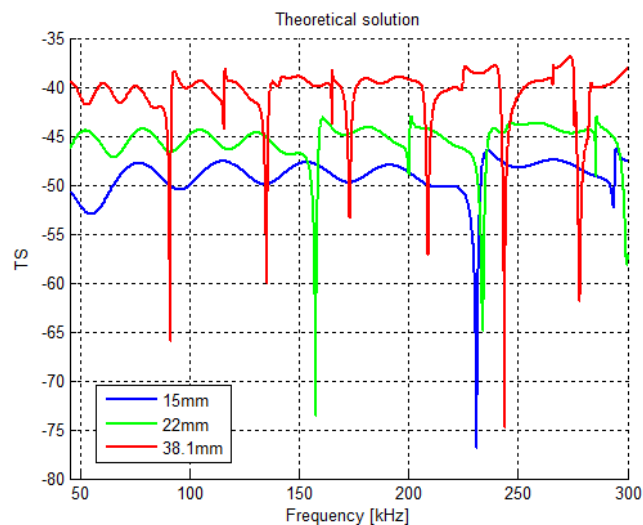


Figure 2.22. Analytical target strength response as a function of frequency in kHz for the 15mm (blue), 22mm (green) and 38.1 mm (red) calibration spheres available.

Implementation

The calibration procedure applied the following four steps:

1. Imaging and depth selection
2. Transmission loss compensation
3. Ping quality selection
4. Computer aided calibration

First the calibration measurement echograms were generated using the processing chain for the three available transceivers. Then, a small depth range (~1m) around the known calibrated target depth range

was selected. The data was oversampled with a factor 32, in order to accurately find the maximum position for each ping (corresponding to the target location).

Then, the transmission loss was compensated for using a spherical spreading and a frequency dependent absorption coefficient.

The pings corresponding to the target being measured exactly in the middle of the transducer were selected to avoid any amplitude fluctuations that could be linked with a bad alignment. This was done by comparing the position of the target (maximum amplitude) in the four quadrants for each transceiver. When the maximum position agrees, the target was assumed to be exactly in the middle of the acoustic beam, where maximum response can be expected. On top of this selection, the amplitudes that were within 10% of the maximum measured amplitude were further selected to avoid any outlier.

The frequency content of the data collected during calibration was plotted on top of the analytical TS solution (Figure 2.23). The offset in amplitude was automatically computed. Per frequency band, the theoretical null that should be visible in the data was identified. The corresponding offset in frequency was then computed. As output, per transceiver, an amplitude and frequency offset were computed and saved. These numbers were then loaded and applied as a compensation for the frequency response computations.

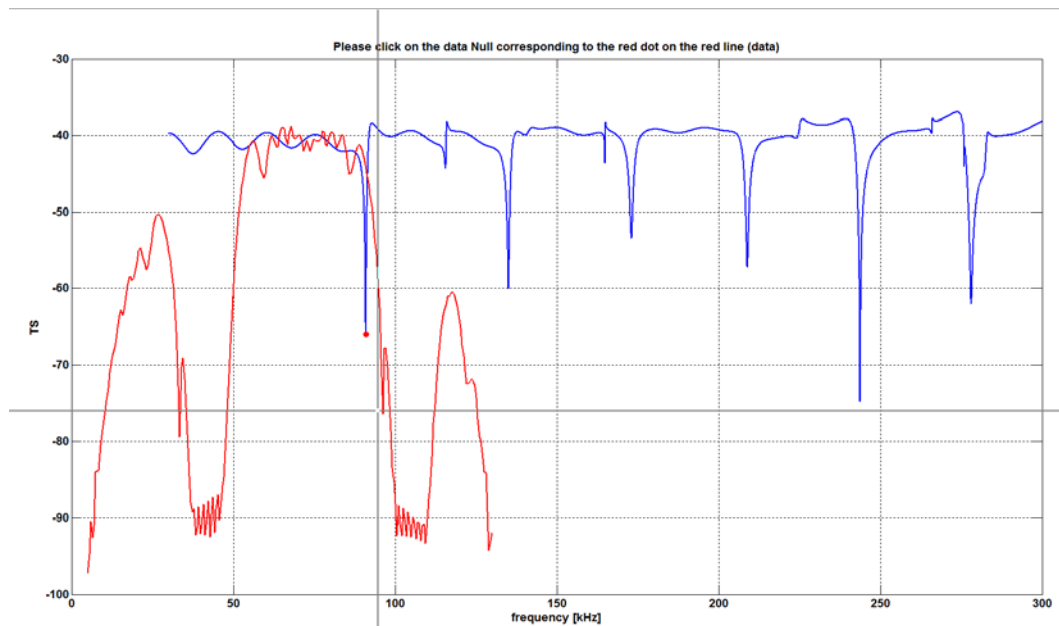


Figure 2.23. Computer aided calibration tool. Example for the first transceiver (45-90 kHz). The analytical TS response from the calibration sphere (blue) is plotted together with the selected calibration data (red). The user is asked to click on the null that corresponds to the position marked with a red disk in the analytical response. A possible offset in frequency is automatically computed.

As an example, the 38.1mm calibration sphere measured by the Alida in January 2014 is plotted versus the analytical response of the very same sphere prior (Figure 2.24) and after (Figure 2.25) the computer aided calibration procedure.

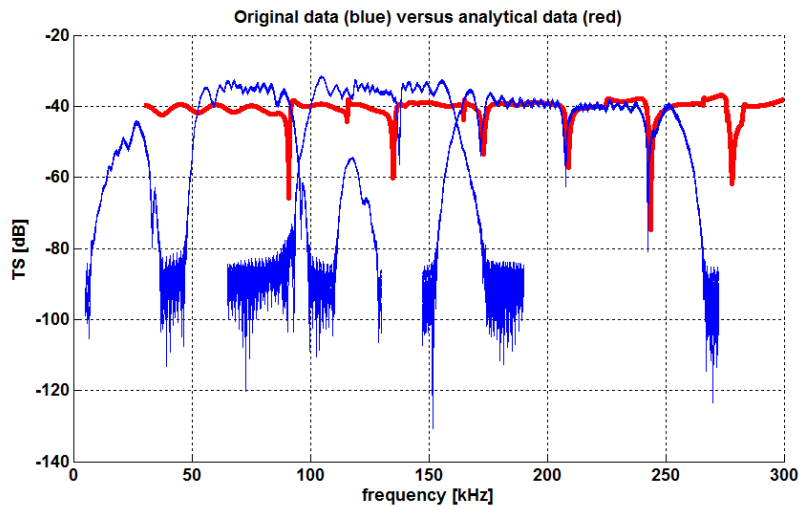


Figure 2.24. Frequency response of the measured 38.1mm calibration sphere in blue versus analytical response in red prior to calibration.

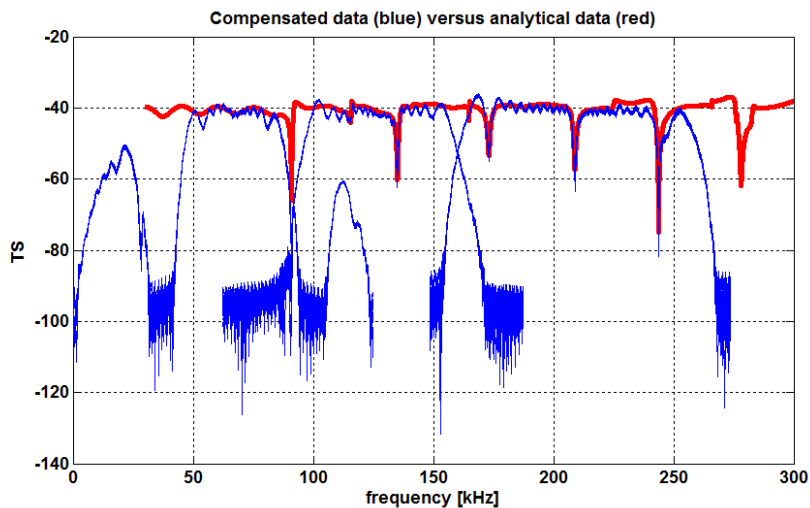


Figure 2.25. Frequency response of the measured 38.1mm calibration sphere in blue versus analytical response in red after calibration.

2.2.5 Frequency spectrum computation

The frequency spectrum computation was an important step of the processing as it generated the spectrum data information necessary as input for the frequency-based classification. This was done by applying the following steps:

First the common frequency array was computed, spanning all available transceivers frequency bands. Then, the pings corresponding to the detection mask and marked as 'good pings', as defined in section 2.2.2 were selected.

Further, per transceiver and for each selected ping:

- The different ranges correspond to different clusters were identified and processed separately.
- The frequency spectrum was extracted using a Fourier transform.
- The calibration frequency offset was applied on the corresponding frequency array and the calibration amplitude correction was applied on the computed spectrum.

The frequency responses were saved in separated structures per ping and per cluster.

2.2.6 Classification

For classification of the school data three approaches were utilised: 1) Statistical classification aimed at identifying species based on statistical features contained in the acoustic data and resulting images; e.g. related to school size, shape, echo intensity distribution, school density, time signals etc; 2) In frequency response classification the focus lied on analysis of the enhanced frequency spectrum available from the broadband data, which should theoretically differ between different types and shapes of fish species; 3) As an additional step, both classification approaches were merged to create a combined classifier. All three approaches will be described in the following sections. All classifications were currently performed on a school (cluster) basis, or finer samples thereof. The verification of acoustically detected fish schools was assessed by use of the vessels' catch logs. The number of species-verified schools available from the fishing trip data and the developed detection module were (see Appendix C):

- 23 herring schools
- 7 horse mackerel schools
- 57 mackerel schools

For 20 out of the 23 recorded herring schools, a pulse with a different window than the one specified in the recommended settings was used during data recording. Windowing is applied to a transmitted pulse to decrease side lobes in the matched filter response. The window used in the data of those 20 schools had a slope that was significantly less steep than the window used for the pulses of all the other recorded schools. This had an effect on the resulting frequency spectrum but also on the time signal data. Some features used in statistical classification were also computed on the data contained just outside of the schools, to serve as a reference and make them more robust against changing environments and interferences. The resulting features in essence were the difference between the feature value outside the school and the feature value inside the school. By doing this, the effect of the use of a different pulse window may have (partly) been accounted for and make these data potentially suitable for classification. However, it must be mentioned that it is still not fully certain whether this measure was realistic or not, but for now these schools were also included in the test sets. For frequency response classification this was not trivial to do. Therefore, the frequency response classification as well as the merged classification was performed with the 3 herring schools that had a correct pulse window.

2.2.6.1 Statistical classification

A number of simple as well as more complex features were derived that are related to statistical properties of the fish schools and that show differences among different types of species. To make classification more robust against environmental and electronic interferences, some of the features were also computed for the background data, i.e. the data in the water column. In this case, classification also became more suitable when using a slightly different pulse, in different environmental conditions or with other transducer properties. Additional robustness against local interferences in the data was achieved by using 'safe' data percentiles and avoided the use of minima and maxima in feature computation. The latter would otherwise increase the vulnerability of the classification for very high or very low intensity parts of a ping.

After having the features computed for all schools of all species, they were used for testing their ability to discriminate between species: their classification performance was assessed. A classifier in general uses features of all classes to derive equations that define the decision boundary between classes. This process is called training. Using this trained classifier, for an unknown test sample (school in this case), the same feature or combination of features are computed and provided as an input to the classifier. The classifier then determines on which side of the decision boundary the sample lays. This is the

classification output. The type of classifier determines how this boundary is derived. Several common classifiers derive their boundary using the following approaches:

- K-nearest neighbours: for each test sample it determines the distance to the K closest training samples of each class. The class with the shortest distance is the classification output.
- NMC: Nearest Mean Classifier. For each test sample it computes the distance to the average of all training samples of a class. This is done for every class; the class with the shortest distance is the classification output.
- SVC: Support Vector Classifier. A support vector classifier is a discriminative classifier defined by a separating hyperplane or maximum margin separator: a linear decision boundary with the largest possible distance from the decision boundary to the training samples it separates.

2.2.6.2 Frequency response classification

Frequency responses over the observed bandwidth were extracted from the example fish schools for all species analysed. Individual frequency response samples were represented by joining 100 subsequent primary pixel samples within each ping and school (cluster). These samples represented a vertical resolution of 0.57m on the echogram. For further frequency response classification analyses, these frequency response samples were averaged over the individual schools to give mean acoustic backscatter over the whole available frequency band for every observed school by species.

Dynamic factor analysis (DFA) was used to investigate the existence of common trends among the relative frequency responses by species. Consequently, the method classified species based on quantified differences in shapes and forms of their frequency responses. The method was initially developed as a multivariate analysis approach to estimate underlying common patterns in sets of time series (Zuur et al., 2003). Here the same principles were applied to model the observed mean frequency response trends by a linear combination of m common trends and a noise component. In matrix notation, the relationship can be written as:

$$\mathbf{Z}_f = \mathbf{A}\mathbf{X}_f + \boldsymbol{\varepsilon}_f$$

where \mathbf{Z}_f is the $n \times 1$ vector containing the frequency response backscatter values at each frequency f , \mathbf{X}_f is the vector with the values of the m common trends at frequency f , and \mathbf{A} is the $n \times m$ matrix of the factor loadings. The factor loadings give an indication of how the n frequency responses, or combinations of them, are related to a particular common trend in the DFA analysis. The magnitude and sign of the factor loadings determine how the respective common trends are related to the original frequency responses by species. The DFA allows for the interactions between the n series of frequency responses to be taken into account and model validations are carried out simultaneously. $\boldsymbol{\varepsilon}_f$ is the $n \times 1$ noise component for every frequency f and is assumed to be normally distributed with mean 0 and covariance matrix \mathbf{R} , hence $\boldsymbol{\varepsilon}_f \sim N(0, \mathbf{R})$. The m common trends are independent of each other. They are represented by Gaussian random walk models estimated using the Expectation Maximization (EM) algorithm with the Kalman filter and smoother algorithm to evaluate the likelihood function (Zuur et al. 2003). The common trends represent the underlying response patterns over the frequency band and are essentially smoothing functions.

A diagonal error covariance matrix \mathbf{Q} lets frequency response values close to each other be modelled with joint noise component contributions. To allow for the linear combination of the trends to move up or down, similar to an intercept in a linear regression model, a constant term \mathbf{C} of dimension $n \times 1$ was also added. The covariance matrix of \mathbf{Z}_f is expressed in the same way as in a factor analysis, except that the factors are now the common trends which are required to be smoothing functions. That covariance

matrix R was chosen to be symmetric non-diagonal, i.e. noise correlated among the components. A non-diagonal matrix allows for adequate model fits even at the low number of common trends applied here. The number of common trends can be chosen in the model but here it was set equal to the number of species to be classified in an attempt to allocate at least one common trend per species. It is possible to use a higher number of common trends and thereby achieve a better fit, however, then more parameters will also have to be interpreted. The procedure of the DFA to derive common trends and link these to the original trend patterns for classification purposes is described in simplified form in Figure 2.26.

In order to evaluate the classification success using this method, frequency response trends of individual schools by species were attempted to be compared to a training dataset. The training data set consisted of a proportion of all frequency responses except those from the school to be classified. That proportion of data samples used to create the training data set was 80% of the available data per species, which were subsequently averaged at every frequency over the available bandwidth. Classification of a particular test school was then performed with the DFA by selecting 4 frequency responses in the model: the mean frequency response of that school and the mean responses of the training datasets of all three species.

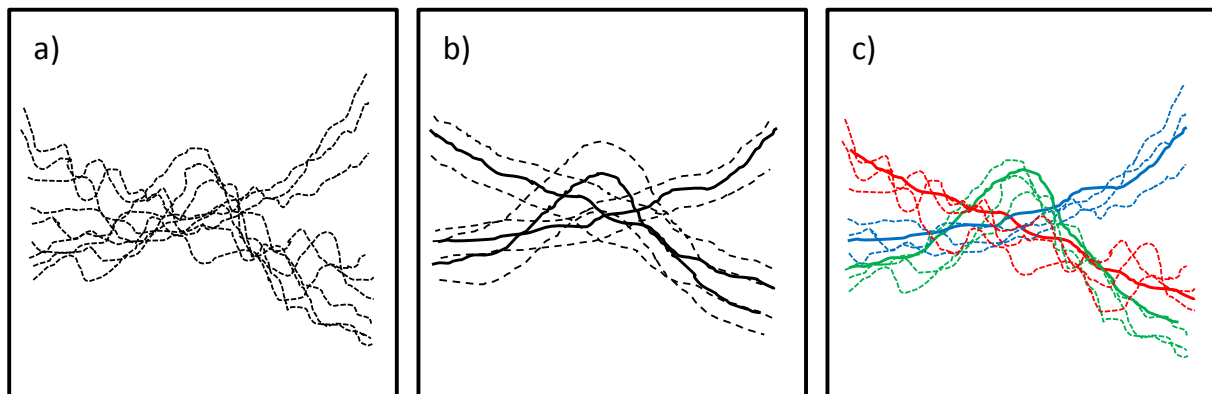


Figure 2.26. Simplified description of the Dynamic Factor Analysis (DFA). Hypothetical trend patterns of different sources along a continuous interval (e.g. different frequency responses) (a). Common trends for the data obtained by the DFA model (b). Based on similarities between the original trends (a) and fitted common trends (b), classes of trend groups with similar properties can be identified (c).

The DFA model was run like that for every observed school by species with 25000 iterations and 20 trials of randomly picked model parameter starting values. The unknown parameters in the DFA model were the elements of \mathbf{A} , \mathbf{R} , \mathbf{Q} and \mathbf{C} . After the 20 runs the starting values that resulted in the lowest AIC were used as starting values in the final run. Canonical correlation analyses were used to identify potential associations of the common trends identified by the DFA with the frequency response data of the training sets per fish species and the tested school. If a canonical correlation was large, then this indicated that the corresponding frequency response of a certain fish species followed the pattern of the particular common trend. If it was low, then it was not related (in a linear context) to the common trend. The difference in canonical correlations between the test school frequency response and the frequency response trends of the training data per species was used as a measure of classification. School samples with a canonical correlation score, combined over all 3 common trends, that was close to the score for a test school (typical) frequency response of a certain species would receive a higher probability to be classified as that species. Eventually, the probability P of the n^{th} school sample having frequency response Z_{school_f} to be classified as a certain species, based on that species' training set typical frequency response (Z_{typical_f}), was estimated to be:

$$P = 1 - \sqrt{\frac{\sum_{i=m}^3 (\text{cancorr}(X_{f_m}, Z_{\text{typical}_f}) - \text{cancorr}(X_{f_m}, Z_{\text{school}_{f_m}}))^2}{k}}$$

k was a constant set per school sample so that the combined probability for the different species classes for that sample equalled to one.

2.2.6.3 ***Classification merging***

A potential performance gain could be achieved when merging the classification outcomes of the two classification methods. There are several ways to do this. Firstly, it would be possible to merge the features of both approaches and use that collection to perform classification with. Another method would be to use the class output confidences of both classifiers as new features that are then fed into another classifier, which implies having two classification stages. A class confidence is a percentage indicating how likely it is that the test sample belongs to a certain output class. For each test sample, the output confidences for each test class together add up to 100%. A final, more straight-forward way, is to take the average or maximum of the class confidences between the two methods and to assign the species with the maximum confidence as the final outcome. This last approach was applied here.

2.3 **Backscatter modelling**

Theoretical backscattering models were developed in an attempt to estimate the backscattered broadband target strength (TS, in dB) of five important pelagic species commonly targeted (or encountered and to be avoided) by the RVZ: herring, sprat, boarfish, horse mackerel and mackerel. The models were used to identify specific regions along the complete frequency spectrum, 16 – 260 kHz, where differences in the scattering response are likely to occur between these species. Identification can help to identify bandwidths that have high potential for distinguishing between these species. Furthermore, the models are used to identify features in the scattering spectrums for different length classes of the five species to enable us to improve size-class recognition.

Backscatter models are generally based on representing different body components of the fish in terms of their shape, orientation and acoustic properties. The predominant scattering feature is the air-filled or partly air-filled swimbladder, which can contribute up to 95% of the acoustic backscatter (Foote, 1980). For species which lack a swimbladder other body parts contribute to the overall backscatter, including backbone, skull and other small bones (Nesse et al. 2009). In the past morphological data was attained using fixed depth slicing microtomes, injection modelling or through the dissection of frozen specimens (Foote, 1985; Ona, 1990). However, more recent studies follow less invasive digital techniques. The true shapes of fish, swimbladders, and other scattering organs can be derived from radiographs (Sawada et al. 1999), computed tomography (CT) and magnetic resonance imaging (MRI; Peña and Foote, 2008, Fässler et al. 2013).

2.3.1 **Morphological measurements of body components**

During the current project, morphological measurements were obtained from pre-existing data (made during past studies) or literature values. All fish had been imaged on their dorsal and lateral aspects. Based on swimbladder condition identified from inspection of the digital images only specimens with intact swimbladders were considered for use in this project. External morphology of the fish body (total length (TL, in cm), standard length (SL, in cm), height (H, in cm) and width (W, in cm)) were obtained for five fish species using various imaging techniques. For species which possess swimbladders (i.e. herring, sprat, boarfish and horse mackerel) additional measures of swimbladder length (SB_L , in cm), height (SB_H , in cm), width (SB_W , in cm), tilt with respect to fish axis (SB_θ , in °) and position on the x-y plane (SB_X and SB_Y , in cm, respectively) were taken (Figure 2.27). For species which lacked a swimbladder (i.e. mackerel) measurements of the backbone were made instead; backbone length (BB_L ,

cm), height (BB_H , cm), width (BB_W , in cm) and position on the x-y plane (BB_x and BB_y , in cm, respectively) (Figure 2.28).

Herring and sprat data were taken from Fässler et al. (2009). Mackerel measurements of fish body and backbone were derived from radiographic images taken with a specialised 'soft' x-ray machine (Scoulding et al., unpublished data). Measurements of boarfish were obtained from radiographs and MRI scans taken by Fässler et al. (2013). Measurements for horse mackerel were not available and therefore MRI measurements made by Pena and Foote (2008) on a related species Chilean Jack mackerel *Trachurus murphyi*, were scaled down to the expected size range of horse mackerel. Ratios between dimension pairs were assumed to be the same for both species.

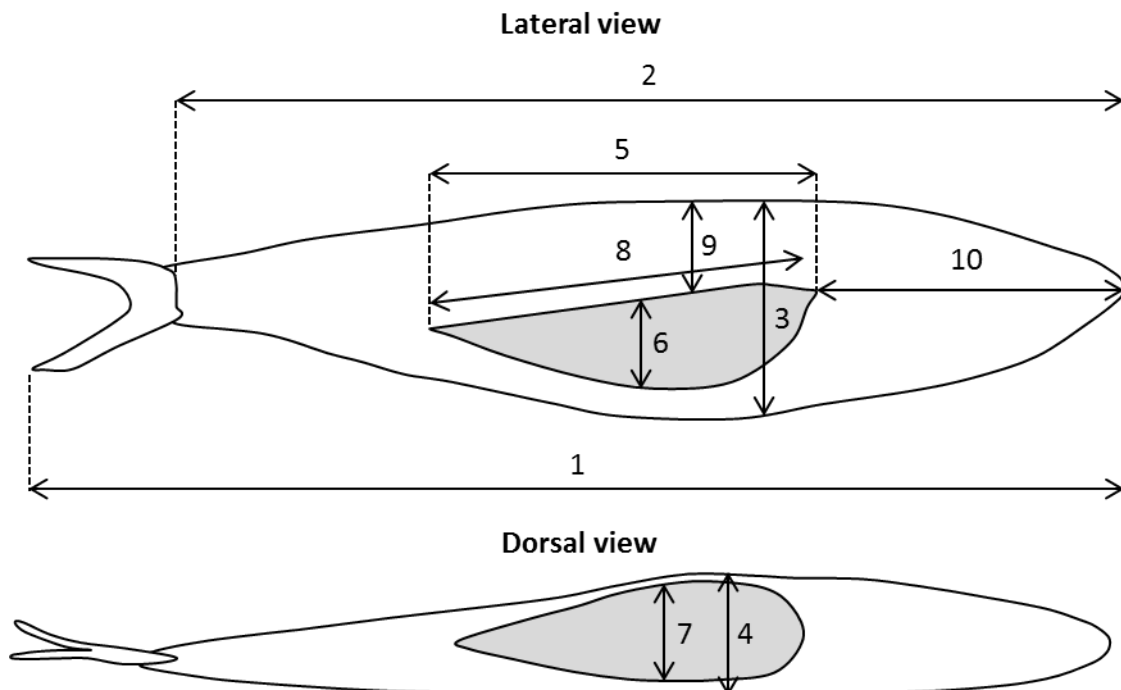


Figure 2.27. Schematic of a swimbladder fish showing measurements required to create simplified geometric shapes. (1) Total fish length (cm); (2) standard fish length (cm); (3) fish height (cm); (4) fish width (cm); (5) swimbladder length (cm); (6) swimbladder height (cm); (7) swimbladder width (cm); (8) swimbladder tilt ($^{\circ}$); (9) distance from dorsal fin to swimbladder (cm); and (10) distance from snout to swimbladder (cm).

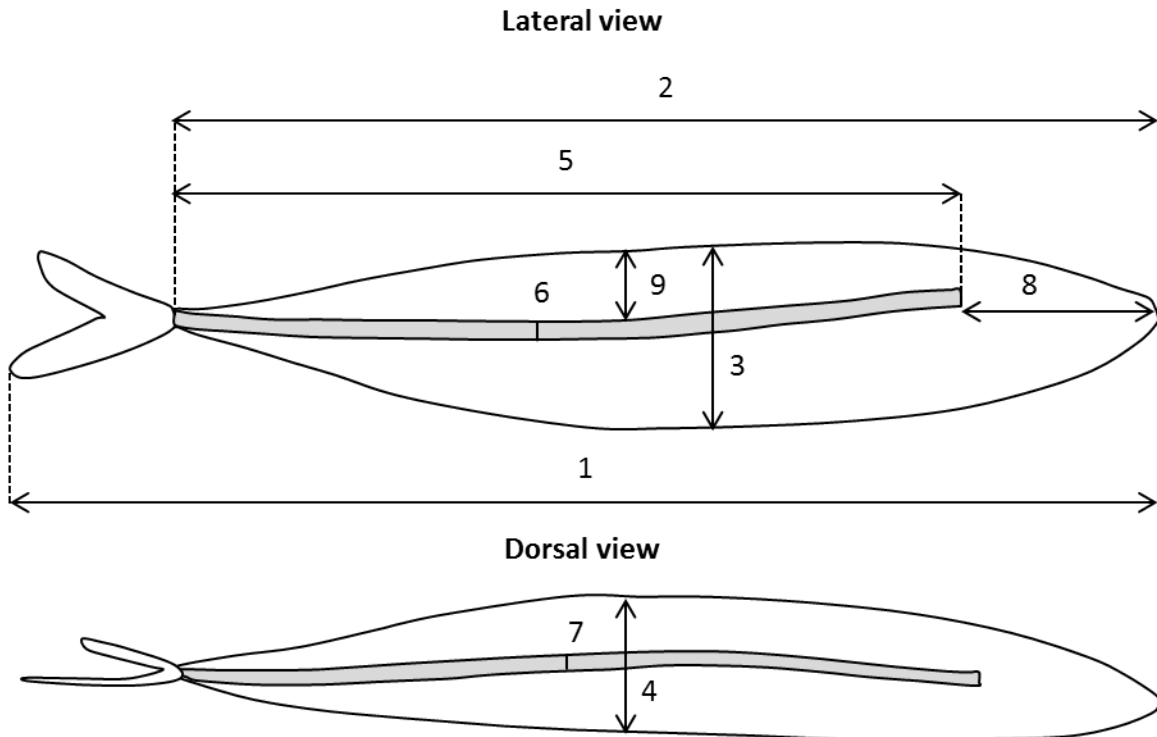


Figure 2.28. Schematic of a bladderless fish showing measurements required to create simplified geometric shapes. (1) Total fish length (cm); (2) standard fish length (cm); (3) fish height (cm); (4) fish width (cm); (5) backbone length (cm); (6) backbone height (cm); (7) backbone width (cm); (8) distance from dorsal fin to backbone (cm); and (9) distance from snout to backbone (cm).

2.3.2 Model definition

A Finite Element Method (FEM), as implemented in the Acoustics Module of the COMSOL Multiphysics software (Anonymous, 2015a; Anonymous, 2015b) was used to estimate the broadband scatter for the five pelagic species mentioned above. Two dimensional (2D) implementations of the model were performed across the frequency spectrum 16 – 260 kHz for different size-classes of each species. Three dimensional (3D) implementations of the model were ran from 16 – 100 kHz for fixed fish lengths of each species. Computational loads above this range were not possible given the computing power and time available during the project. The number of elements required to construct the 3D mesh was an extreme limiting factor.

A scattering model of fish was developed that incorporated simplified numerical solutions of idealised fish morphology, and models the complex interactions of an incident acoustic wave (p_{inc}) of amplitude p_0 (1 Pa) travelling in the direction e_k (Figure 2.29). The governing equations in COMSOL were applied as a scattered field formulation such that only the scattered field from the fish (p_f) was solved for. The total acoustic field p_t is given by the summation of p_f and p_{inc} such that: $p_t = p_{inc} + p_f$, where, $p_{inc} = p_0 e^{i(e_k \cdot x)}$.

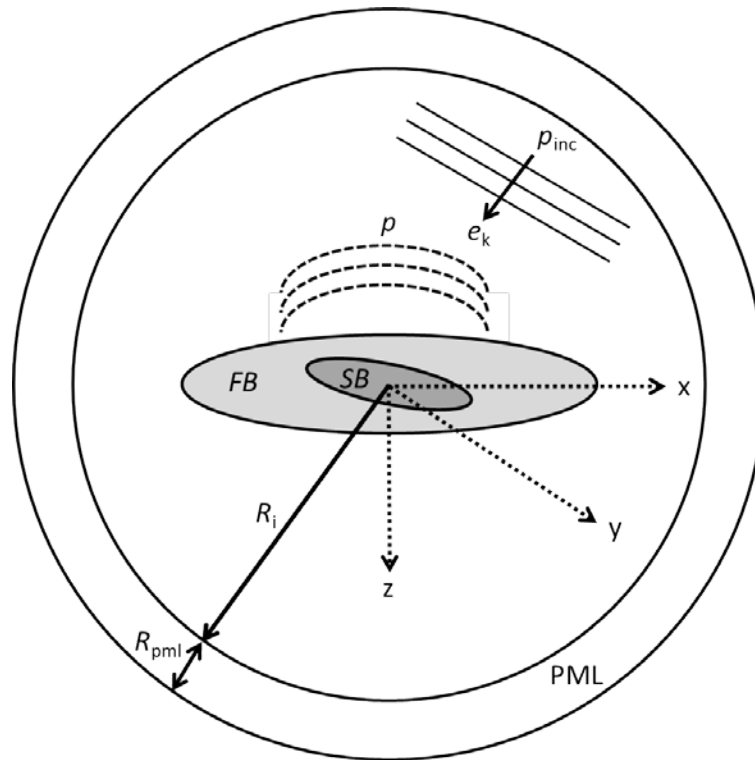


Figure 2.29. Simple schematic of the modelled system for a swimbladder bearing fish. The schematic shows the incident wave p_{inc} , the scattered field p , fish body FB, swimbladder SB and water geometric scales and the PML. Adapted from COMSOL 2015a Acoustic Scattering off an Ellipsoid.

The model domain was constructed in several parts. For 2D models the central region was constructed of rigid ellipses or rectangles which represented the swimbladder (SB) or backbone (BB) respectively, contained within a rigid ellipse which gave an approximation of the fish body (FB) (Figure 2.29). For the 3D implementation of the model a mix of ellipsoids and cylinders were used instead. In both models the geometry could be scaled for any fish length based on the aspect ratios between different dimensional pairings. The modelled fish was located within a simulation domain consisting of a water domain (circle (2D) or sphere (3D)) and a perfectly matched layer (PML, Berenger, 1996; Zampolli et al. 2007) (which emulates a non-reflecting and absorbing boundary domain which extends to infinity and is independent of the shape and frequency of the incident wave front) (Figure 2.29). The outer boundary of the PML region contained a radiation boundary condition to reduce the amplitude of any reflections back into the model domain. The simulation domain had a total radius of $r_i + r_{pml}$, where r_i is the radius of the water domain and r_{pml} is the thickness of the PML. The model was constructed so that the size of the water domain and PML, as well as the mesh size, changed automatically as a function of the frequency (in kHz) being studied. The PML maintained a thickness (r_{pml}) of 3 and 6 elements for 2D and 3D models, respectively, whilst the water domain was constructed to maintain a minimum distance of 3 elements from any edge of the fish body. The water domain in the model had approximately the same physical properties (temperature = 15 °C, salinity = 35 psu and sound speed 1506 ms⁻¹) as those commonly encountered during real situations. All model regions were solved for as one fully coupled system.

It is recommended to use a minimum of 6 elements per wavelength which sets a limit to the maximum element size for the mesh. This is in line with Macaulay (2009) who found that results converged at 5.88 elements per wave length. In order for the PML to dampen the outgoing waves optimally, a swept mesh containing 6 elements was used. The free triangle node created a tetrahedral mesh on the two inner circles and the boundary layer node created the single boundary layer at the far-field boundary. This provided sufficient resolution of the incident waves.

The scattered pressure field was estimated using the Helmholtz-Kirchoff (H-K) integral on the outer boundary of the scattered pressure field region. COMSOL uses a numerical evaluation of the Helmholtz-Kirchoff (H-K) integral to compute the scattered [sound] field from the object surface (made up of selected boundaries) (Anonymous, 2015b). The selected boundaries form a closed surface around all sources and scatterers. The far-field calculation is performed on the boundary between the normal domain (fish geometry and water domain) and the PML. In this model we used the H-K version which solves the full integral and can thus determine the exact far-field pressure (including phase) at any point and distance outside the computational domain. In order to get a precise evaluation of the far-field variable the evaluation of the H-K integral must be accurate. This required having a good numerical estimate of the normal derivative of the pressure on the far-field calculation surface (adjacent to the PML layer). This was achieved by adding a single boundary layer mesh element on the inside of the acoustic domain. The thickness of this layer was one tenth of the element size in the domain.

The acoustic pressure is the pressure field (p) in pascals (Pa), whereas the sound pressure level (L_p) is given as a logarithmic decibel (dB) value, to the reference sound pressure (P_{ref}). The P_{ref} for water is used when computing the L_p in the model, which is $1 \mu\text{Pa}$ ($1 \cdot 10^{-6}$ Pa). The L_p is evaluated back in the direction of the incident wave at 1 m from the target (i.e. fish). The background pressure field (p_b) represents how the pressure field would be without the scattering object, implying that it is ubiquitous and uniform. Thus, it is defined in all domains and uses the same speed of sound for reference. The far-field L_p is computed from the scattered sound pressure which means the reflected L_p is calculated directly. The pressure was converted to TS as:

$$L_p = 20\text{Log}_{10} \left(\frac{P_{rms}}{P_{ref}} \right) = 10\text{Log}_{10} \left(\frac{\frac{1}{2}pp^*}{p_{ref}^2} \right),$$

where sound pressure level is based on the root mean square pressure P_{rms} as:

$$P_{rms} = \sqrt{\frac{1}{2}pp^*}$$

where p_{ref} of water $1 \mu\text{Pa}$ and * denotes the complex conjugate.

Using a parametric sweep we computed the TS for the complete frequency spectrums 16 - 260 kHz and 16 - 100 kHz for 2D and 3D implementations of the model, respectively. The mesh was scaled automatically to the wavelength of the frequency. The data was then exported as a table containing the TS value at 1 m from target along the direction of the incident wave for all frequencies.

For each species, a simulation was carried out at a range of appropriate lengths. Each model run produced the far-field backscattered pressure. For validation purposes an image of the scattered field immediately surrounding the fish was inspected (for an example see Figure 2.30). For all simulations, the sound speed and density of the different body parts used in the model were set according to the values in Table 2.1.

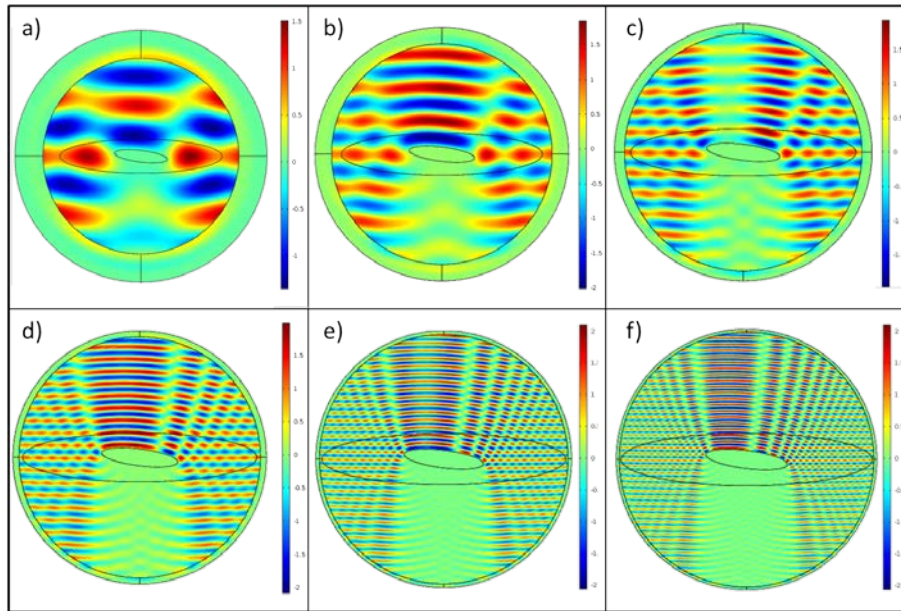


Figure 2.30. Sequence total scattered field immediately surrounding a 24 cm herring at: a) 18 kHz; b) 38 kHz; c) 70 kHz; d) 120 kHz; e) 200 kHz; and f) 260 kHz. Note how the PML thickness changes with frequency. The colour scales is the total scattering pressure field (Pa), which is different for each frequency.

Table 2.1. Material properties used in model simulations.

Physical parameter	Value	Unit	Source
<i>Fish body</i>			
Density	1070	kg/m ³	Fässler et al. (2007)
Sound speed	1570	ms ⁻¹	Fässler et al. (2007)
<i>Swimbladder (air)</i>			
Density	13.62	kg/m ³	Fässler et al. (2007)
Sound speed	340	ms ⁻¹	Fässler et al. (2007)
<i>Backbone</i>			
Density	1129	kg/m ³	Gorska et al. (2005)
Sound speed	1957	ms ⁻¹	Gorska et al. (2005)
<i>Seawater</i>			
Density	1027	kg/m ³	Measured
Sound speed	1506	ms ⁻¹	Measured
Temperature	15	°C	Measured
Salinity	35	psu	Measured

3 Results

3.1 Backscatter modelling

3.1.1 Model validation and limitation

The accuracy of the three-dimensional FEM model was tested by simulating the backscattered TS from a sphere of radius 19.05 mm submersed in water (density 1027 kg/m³ and sound speed 1506 ms⁻¹ as used in the model). A homogenous solid Tungsten carbide sphere (density 14900 kg/m³ and sound speed 6853 ms⁻¹ [longitudinal waves]) was simulated at frequencies of 1 to 125 kHz in 1 kHz steps and compared to a theoretical solution for a standard Tungsten carbide sphere as given in Simmonds and MacLennan (2005). The variations of TS with frequency are presented in Figure 3.1. Results indicate that the model can correctly simulate the scattering response from spheres, however the amplitude is

consistently underestimated. This discrepancy may be explained by the fact that the model implementations do not account for directionally dependent material properties (e.g. as those found in bone or the swimbladder), or for acoustic attenuation with range (Macaulay, 2009). For the range of interest here (1 m) attenuation is less significant, however, at higher frequencies (> 125 kHz) the effect of not modelling directionally dependent material properties may be very important. The null observed in the theoretical backscattered TS at ~90 kHz is partly due to the use of two sound speeds; longitudinal (6853 ms^{-1}) and transverse (4174 ms^{-1}) waves in the calculation. These transverse waves could not be modelled in COMSOL. Based on these results we can be confident that the governing physics used in the model are correct. The same underlying physics are used in the 2D and 3D implementations of the models.

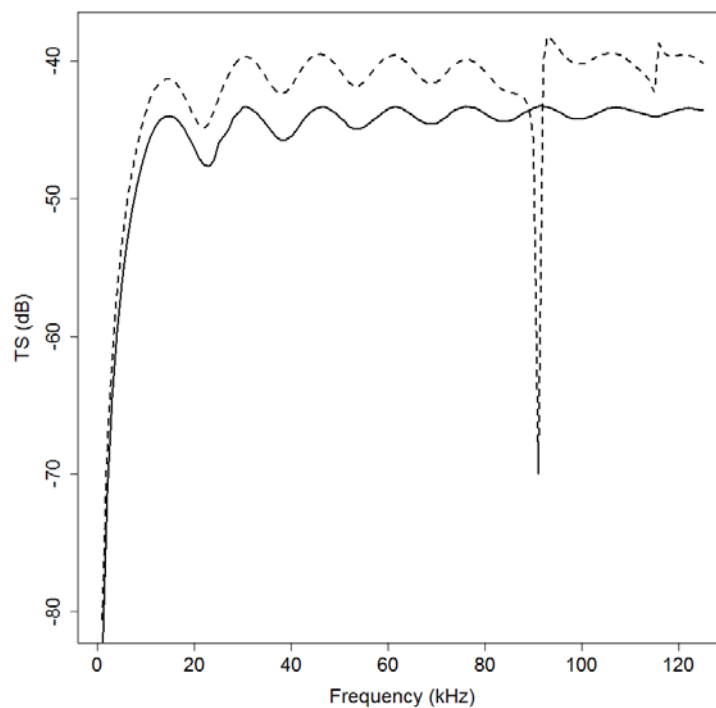


Figure 3.1. Comparisons between three dimensional model and theoretical backscatter TS. The solid line is the model TS and the dotted line is the theoretical TS.

The limited frequency range (16 – 100 kHz) in the 3D models is due partly to the memory required to construct mesh at higher frequencies. It is difficult to maintain the minimum six elements per wavelength that is needed. To give an example of these requirements at high frequencies, the total memory requirements were estimated using a polynomial 3-order regression which gave the equation: $y = 2E-05x^3 - 0.0024x^2 + 0.1498x - 0.4362$, which gives the curve shown in Figure 3.2. This results in an estimated total memory requirement of 100 GB at 200 kHz. Many modern computers have more than 200 GB useable hard memory, however, the memory other than RAM (swap file) is much slower and represents an additional limitation. Given the computing power and time available the 3D models were only used to show the differences between fish species at frequencies between 16 and 100 kHz. An example of 2D mesh sequencing is shown in Figure 3.3, when extrapolated to a 3D geometry the problem becomes evident.

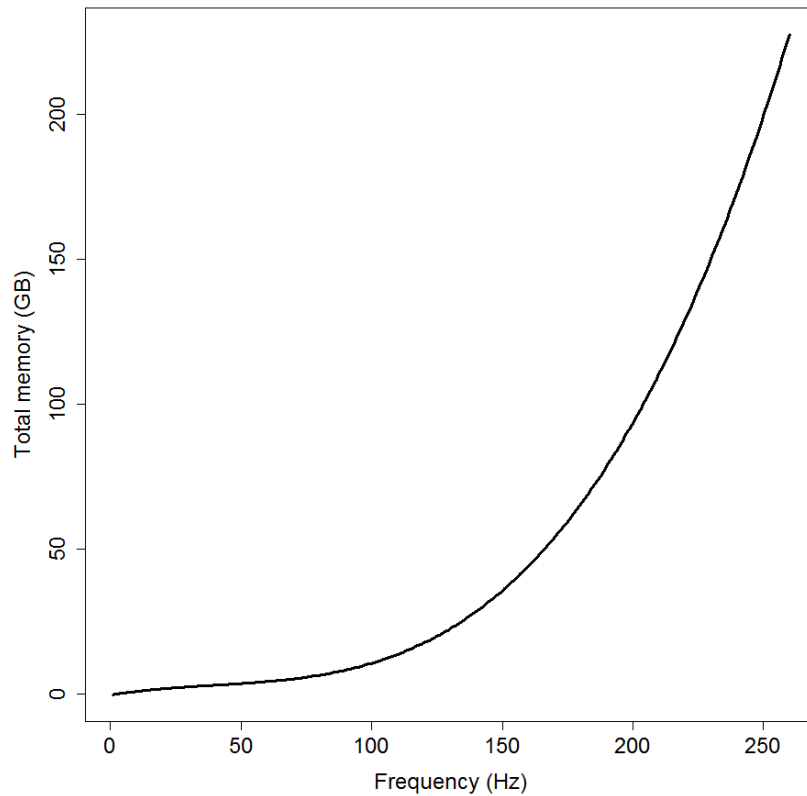


Figure 3.2. A polynomial 3-order regression showing total memory requirements for the frequency range 1 – 260 kHz.

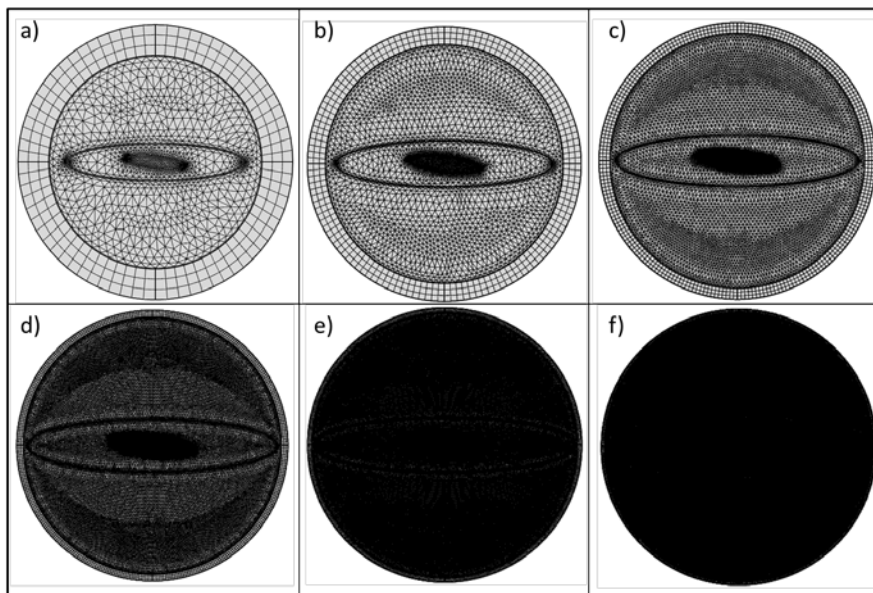


Figure 3.3. Mesh sequence of a 2D model for a 24 cm herring at: a) 18 kHz; b) 38 kHz; c) 70 kHz; d) 120 kHz; e) 200 kHz; and f) 260 kHz. Note how the PML thickness changes with frequency.

3.1.2 Two-dimensional and three-dimensional model comparison

As 3D implementations of the model at high frequencies (> 100 kHz) were not possible due to time and memory restrictions, they were compared to 2D implementations between 16 –100 kHz to investigate

similarities in the frequency response (Figure 3.4). Small sized individuals for each species (with a length less than the expected mean length) were compared. This was because fewer problems were encountered when modelling smaller individuals during 3D implementations of the model. The comparison identified similarities, at least in relative terms, between 2D and 3D models for all species, with the exception of Atlantic mackerel. Sprat show close agreement, particularly between 16 and 38 kHz and 70 and 100 kHz (Figure 3.4). Similarly herring revealed good agreements displaying similar trends in the responses, however, issues with memory meant that herring could not be modelled successfully above 40 kHz. Similar memory issues were encountered for horse mackerel, which could not be modelled above 44 kHz. However, initial results between this narrow frequency show good agreement. Boarfish showed very similar trends between 16 and 65 kHz, however at frequencies above 65 kHz the 3D model showed a decrease in backscattered TS, whilst in the 2D model the response remained relatively flat. Two dimensional model implementations for Atlantic mackerel are not considered representative of actual mackerel backscatter as *in situ* TS is shown to decrease from 18 to 38 kHz and then increase again at higher frequencies (> 100 kHz) (Scouling et al. in prep). Therefore, direct trend comparisons between 2D and 3D models for Atlantic mackerel are not possible.

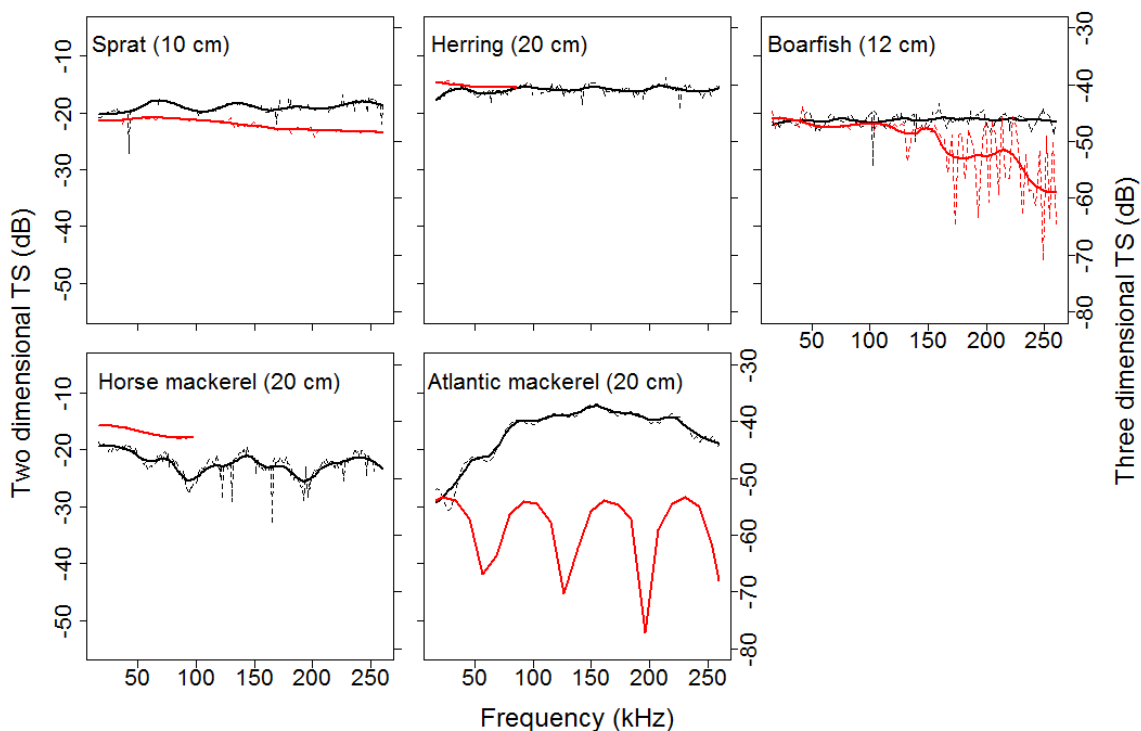


Figure 3.4. Comparisons between 2D (black line) and 3D (red line) model outputs from 16 to 100 kHz at steps of 1 kHz for all species. LOESS curves (solid lines) are fitted to the model data (dashed lines). The first y axis represent 2D TS values and the second y axis represents the 3D TS values. Note the different scales between the first and second y axis. Note that herring and horse mackerel were only modelled up to around 45 kHz due to memory issues.

The results indicate that 2D models can be useful for identifying regions along the complete frequency spectrum of interest (16–260 kHz) where the five species may differ in their response, with the exception of Atlantic mackerel. Although the differences are not precisely estimated using the 2D approach, particularly with respect to amplitude, they do provide an indication to where differences may occur between species. Furthermore, differences were apparent between different size-classes of each species.

3.1.3 Model outputs

When 2D model outputs were compared for each species obvious differences were observed (Figure 3.5). The results show that sprat and herring are clearly distinguishable from one another at the size modelled, SL = 10 and 20 cm, respectively (Figure 3.5a). It is expected that these differences will be a lot less obvious for more similarly sized individuals of both species, which can be inferred from the results shown in Figures 3.6a and 3.6b. Boarfish (SL=12 cm) and horse mackerel (SL=20 cm) are easily separated from herring and sprat as they show weaker standardised backscattering TS values. However, they are not easily distinguished from one another as their frequency responses shows periodic overlap (Figure 3.5a). Boarfish has a relatively flat response whilst horse mackerel has an undulating response. Narrow bands along the frequency spectra may be used to separate these species. For example, the model estimates are quite different at frequencies around 90 and 180 kHz. However, it is worth noting that these particular regions of differences will shift according to the size of both boarfish and horse mackerel as shown in Figures 3.6c and 3.6d, respectively. As mentioned above mackerel is poorly represented and therefore results are considered inconclusive. Despite some of the limitations of 2D models they show clear differences between the fish lengths of each species modelled, thus reinforcing their usefulness in species classification.

The 3D implementations of the model also show differences, however, they are more slight compared to 2D at the frequency range explored. For the same length fish (as modelled in 2D) there is much less of a difference between sprat and boarfish between 16-60 kHz, whilst there are large differences from 60-100 kHz (Figure 3.5b). At low frequencies between 16 and 45 kHz horse mackerel have stronger backscatter compared to sprat and boarfish (similar to 2D implementations) and show more similar scattering characteristics of herring. At higher frequencies the opposite is true with horse mackerel having weaker scatter. It may be possible to exploit these differences for classification, paying particular attention to the switch between horse mackerel being the stronger scatterer at low frequencies (< 45 kHz) and the weaker scatterer at higher frequencies (> 45 kHz). Mackerel have a much lower response than the other species because of its lack of an air-filled swimbladder. The undulating response is because the backscatter at the frequency range investigated is dominated by scatter from the fish flesh. The backbone is expected to contribute to the backscatter between 100 and 150 kHz and therefore the contribution is not apparent in this frequency spectrum. However, it is clear that mackerel are easily separable from other species at this frequency range. Despite the identification of differences, which can be useful in the development of species classification tools, the limited frequency spectrum investigated here may fail to identify the key areas of differences at higher frequencies between the species.

Lessons learned from both the 2D and 3D models can be combined to provide a more detailed understanding of the expected regions of difference between species which can be exploited to provide improved classification and discrimination. It therefore becomes necessary to develop models capable of estimating the backscattered TS at the entire frequency range on interest for all species. Currently the model does not yet account for variations in tilt angle, which will have large effects on the estimated TS and may show higher levels of species overlap or improved levels of separation. Tilt angle should be considered in future model simulations.

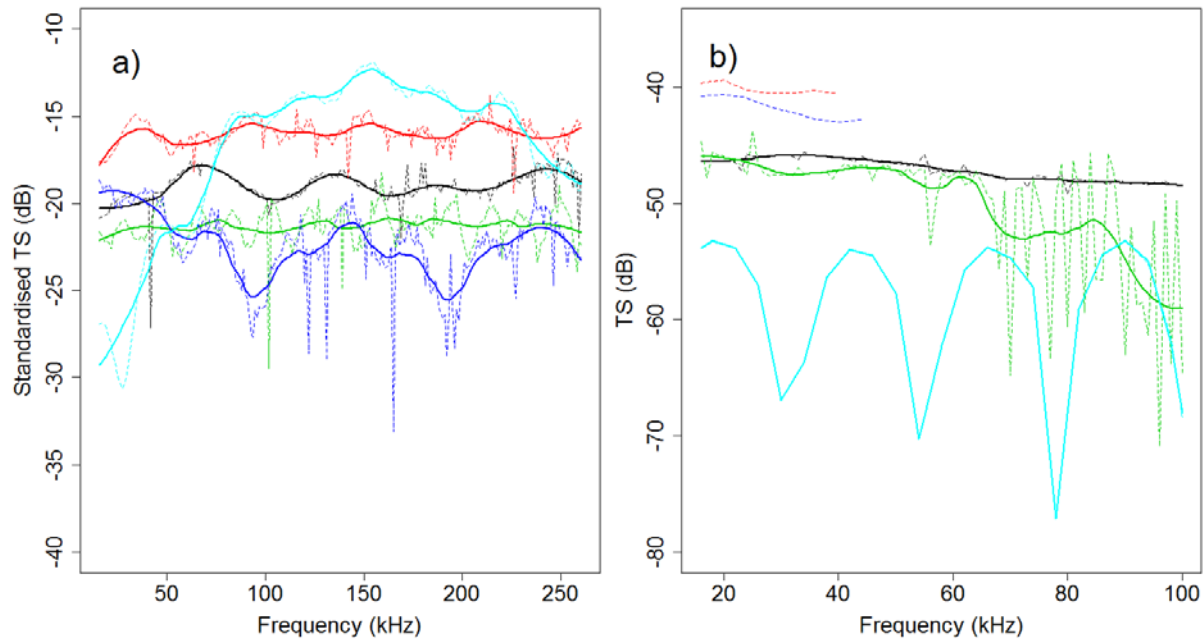


Figure 3.5. Broadband frequency response from 16 – 260 kHz for fixed fish lengths of: sprat (black, SL = 10 cm); herring (red, SL = 20 cm); boarfish (green, SL = 12 cm); horse mackerel (dark blue, SL = 20 cm) and Atlantic mackerel (cyan, SL = 20 cm), modelled using: a) 2D and b) 3D implementations of the FEM in COMSOL Multiphysics software. LOESS curves (solid lines) were fitted to the theoretical estimates (dashed lines). Note the differences scales on the x and y axis. Note that 3D implementations of herring and horse mackerel were only possible up to around 45 kHz due to memory issues.

3.1.4 Size-class modelling

For each species, a number of simulations were carried out using the 2D model at a range of selected size-classes Figure 3.6. This was done in order to identify regions along the frequency spectrum which could be used to separate size-classes. Similar differences are expected to exist in 3D model estimates of backscatter TS, however, due to limitations in time and computing power it was not possible to do direct size comparisons.

3.1.4.1 *Herring*

Standardised TS for herring showed an undulating response over the entire frequency spectrum (Figure 3.6a). As expected larger individuals had a stronger scattering response compared to smaller individuals. Different sized fish had an overlapping response at particular frequencies, especially when looking at some of the variability in the estimated backscattered TS from the model output which shows large and dramatic increases and decreases in response (as represented by dashed line in Figure 3.6). Shifts in the peaks and troughs (as represented by the LOESS curves in Figure 3.6a) of the frequency response may provide the most useful information for distinguishing between different size-classes. For example the first and second peaks occurred at lower frequencies for large individuals (SL = 28 and 30 cm) compared to smaller individuals (SL = 20 and 22 cm) where these peaks occurred at higher frequencies. Monitoring these peaks closely may provide information on the length class of individuals in the wild. Furthermore, paying particular attention to the occurrence of these peaks between species can also aid in species discrimination (Figure 3.5).

3.1.4.2 *Sprat*

Standardised TS for sprat showed higher amplitude differences between the peaks and troughs in the response (Figure 3.6b). The response for small sprat (i.e. 8 cm) showed long undulations with greater differences in amplitude compared to larger individuals where the undulations were more frequent with

shallower differences in their amplitude. The differences between sprat of similar lengths was less obvious compared to herring, as the response overlapped heavily. However, small (i.e. 8 cm) and large (i.e. 16 cm) fish were easily distinguished. Similarly to herring the locations of the peaks and trough can be used to determine the size-class of the individuals according to the location of these features along the frequency spectrum.

3.1.4.3 Boarfish

Although the standardised TS for boarfish as shown by the LOESS curves in Figure 3.6c (solid lines) show no overlap there exist large amounts of overlap between the actual model output (dashed lines in Figure 3.6c). This level of difference between variability may be closer to the levels expected for wild fish (e.g. due to changes in tilt angle distributions). Therefore, distinguishing between different sizes of boarfish may not be as easy as in the cases of herring and sprat where variability is less. Detailed trend analysis of the size-dependent response will be required to identify key regions along the spectrum where individuals can be separated according to their size.

3.1.4.4 Horse mackerel

Horse mackerel show the highest levels of overlap between different size-classes across the entire spectrum, particularly at frequencies between 16 – 100 kHz (Figure 3.6d). Therefore, it is unlikely that this frequency range will be useful for separating different sized horse mackerel. Even at higher frequencies there is substantial overlap between the response for all size-classes, with the exception of the smallest fish (10 cm) which is lower than the rest. Similarly to boarfish trend analysis is required to help with separation of size-classes. Further studies may also be required to investigate the effect tilt has on modelled TS and whether this can in part explain the observed similarities between the backscattered TS of difference sized fish. It is worth noting that as fish body and swimbladder shape were based on Chilean Jack mackerel the modelled geometry may not be entirely representative. Species specific scans covering a suitable size distribution are required.

3.1.4.5 Atlantic mackerel

As mentioned above Atlantic mackerel backscatter is poorly represented using a 2D implementation of the current FEM model (Figure 3.6e). This is assumed to be because the 2D interpretation of the backbone cannot model the curvature of the backbone vertebrae accurately. Instead a straight rectangle is used. Alternatively, as the backbone is given very basic physical properties (density and sound speed) it is likely that these are inadequate for describing the key material properties used to imitate the bone. Further investigation will be required to identify the causes of the observed response. It is therefore difficult to infer anything useful from these results. However, past studies have shown that changes in mackerel length result shifts in the peaks and troughs, as well as their amplitude and frequency of occurrence from 1 to 70 kHz (Scoulding et al. in prep), similar to other species described in this project. Thus there is potential for 3D models to identify differences along the frequency spectrum for different sized fish. Future studies should focus solely on the development of 3D implementations of the model for mackerel.

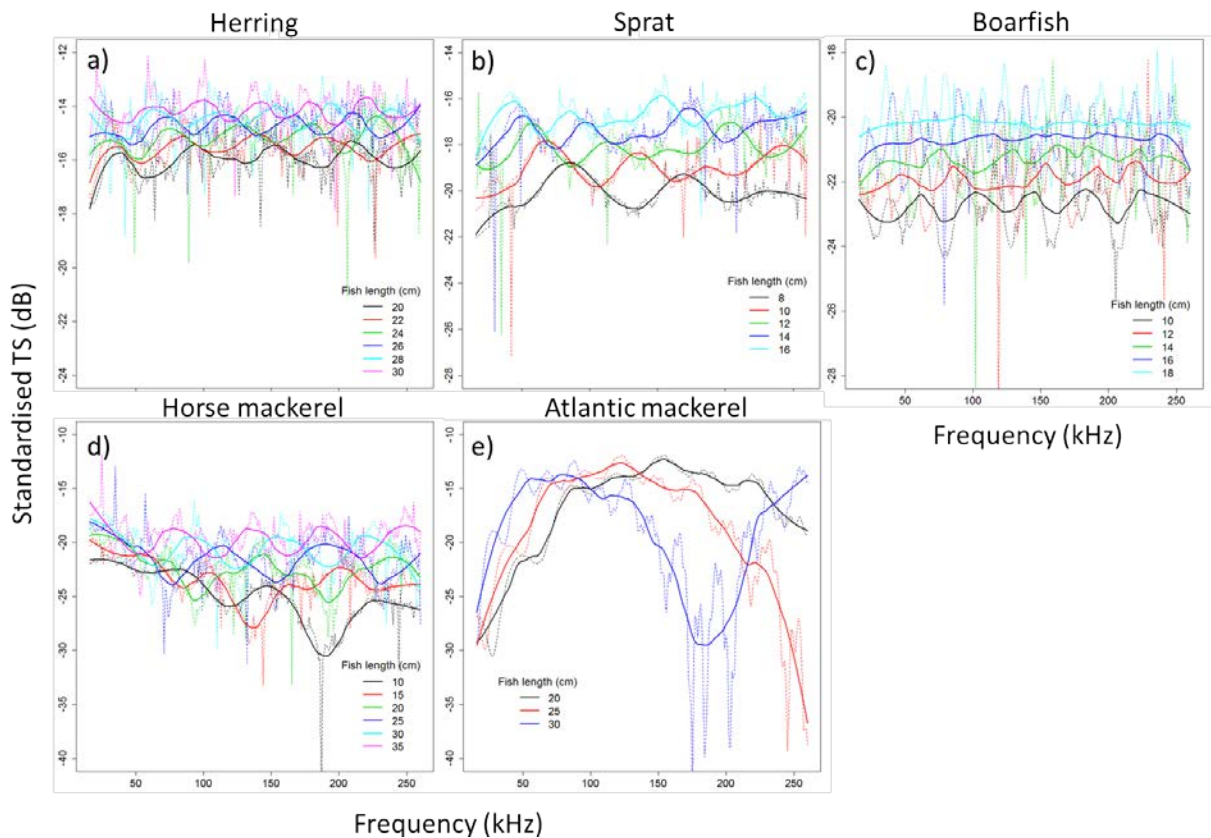


Figure 3.6. Broadband frequency spectrum from 16 – 260 kHz for different standard length of: a) Herring (SL = 20 to 30 cm, steps of 2 cm); b) Sprat (SL = 8 to 16 cm, steps of 2 cm); c) Boarfish (SL = 10 to 18 cm, steps of 2 cm); d) Horse mackerel (SL = 10 to 35 cm, steps of 5 cm); e) Atlantic mackerel (SL = 20 to 30 cm, steps of 5 cm); modelled using a 2D implementation of an FEM in COMSOL Multiphysics software. The different colours indicate different fish lengths. LOESS curves (solid lines) were fitted to the theoretical estimates (dashed lines). Note the different scales on the y-axis.

Fish models of TS depends largely on the accuracy of density and sound speed contrasts. Differences in these values between two mediums determines the intensity of the backscatter. Generic values for herring were assumed for all swimbladdered species in this project (Fässler et al. 2008; Brawn, 1966), whilst mackerel were assumed to have those given by Gorska et al. (2005). However, it is not really appropriate to merely assume that values for one species are correct for another. Future studies involving modelling techniques should investigate species-specific material properties for the time of year the fish are encountered so that the models can be as representative as possible of the study population. The effect of this is not readily apparent as it is the change in acoustic impedance that determines the scattering strength. Furthermore, the physics of the model may require further validation. Increased computational power is required to provide truly accurate estimates of TS using the FEM in COMSOL. Increased computational power is needed if three-dimensional FEMs are going to be used in the wideband evaluation of these pelagic fish species.

3.2 Species classification

3.2.1 Statistical classification

The assessment of the classification performance of the computed statistical features delivered percentage outputs of correct classification per school. The basis for this was the trained classifier using any of three common classifier approaches to derive boundaries between classes. Figure 3.7 shows a-

called feature plot for two statistical features used for classification, together with the computed decision boundary for the three different example types of classifiers.

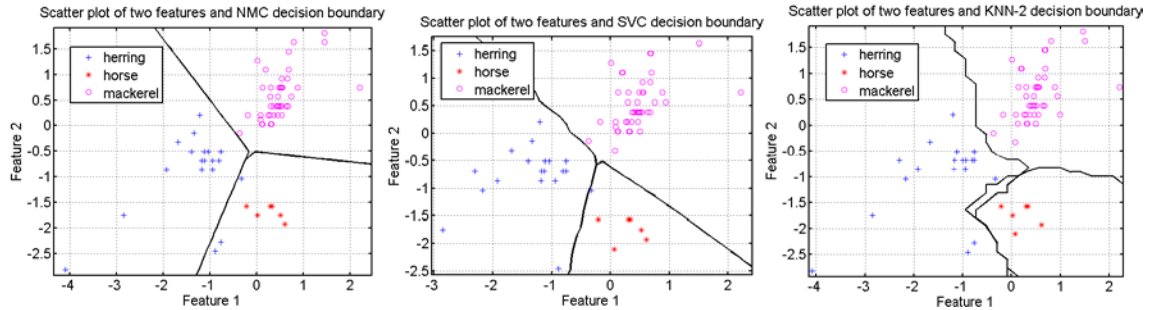


Figure 3.7. Three plots of two statistical features computed for the three species together with the decision boundary of a Nearest Mean Classifier (top left), a Support Vector Classifier (top right) and a 2-Nearest Neighbour Classifier (bottom).

Additionally, in Figure 3.8 some other computed statistical features are plotted that discriminate between species and could be used in classification.

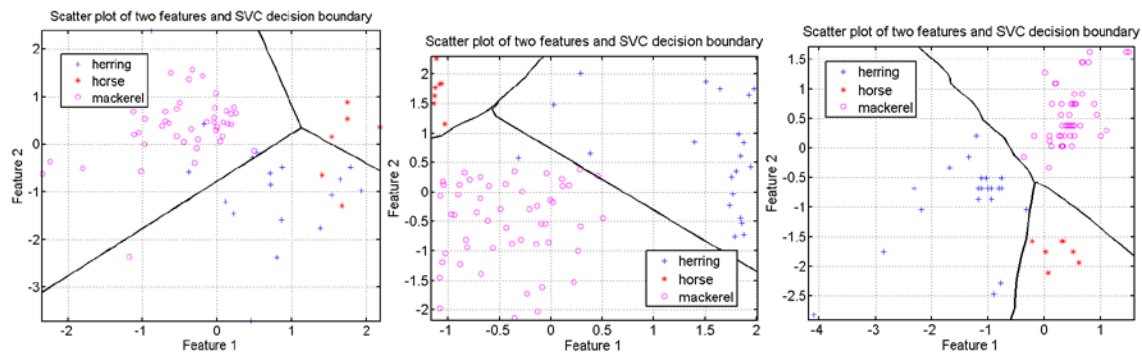


Figure 3.8. Plots of three times two statistical features computed for the three species together with the decision boundary of a Support Vector Classifier. The (total of) six statistical features can be useful in classification.

To assess the classification performance, different classifiers were then tested with a selection of the computed features as input. The procedure was as follows: All schools of each species are split up in a training set and a test set. 200 iterations were performed and in each iteration the test and training set are randomly selected, leading to two independent sets per iteration. For the 200 iterations the minimum score, 25-, 50- and 75-percentiles and the maximum score is given where 0% corresponds to all misclassifications and 100% to all correct classifications. Also, the median score per species type is given. The a priori class information going into the classifier is automatically extracted from the available number of samples per species. Per test, all three species were put into the classifier simultaneously. The used classifiers were: KNN-x (k-nearest neighbor classifier using x neighbors), Fisher (Fisher classifier), and SVC (Support Vector Classifier). Table 3.1 shows the classification performance for the mentioned classifiers, having a training set of 80% of the available data and a test set of the remaining 20% of the data.

Table 3.1. Classification performance statistics of three types of classifiers, performing 200 iterations on 20% test, 80% training data sets.

Classifier	Min. score	25-prct	50-prct	75-prct	Max. score	Median score Herring	Median score Horse	Median score Mackerel
KNN - 2	94.1 %	97.1 %	98.53 %	100 %	100%	97.2 %	100 %	100 %
KNN - 3	85.3 %	95.6 %	97.1 %	98.5 %	100 %	88.9 %	100 %	100 %
Fisher	76.4 %	95.6 %	97.1 %	98.5 %	100 %	94.4 %	100 %	100 %
SVC	94.1 %	98.5 %	100 %	100 %	100 %	100 %	100 %	100 %

Table 3.2 shows the classification performance for the mentioned classifiers, but having a training set of 70% of the available data and a test set of the remaining 30% of the data.

Table 3.2. Classification performance statistics of three types of classifiers, performing 200 iterations with random data sets of 30% test and 70% training data.

Classifier	Min. score	25-prct	50-prct	75-prct	Max. score	Median score Herring	Median score Horse	Median score Mackerel
KNN - 2	92.0 %	96.0 %	100 %	100 %	100%	100 %	100 %	100 %
KNN - 3	88.0 %	96.0 %	100 %	100 %	100 %	100 %	100 %	100 %
Fisher	88.0 %	96.0 %	100 %	100 %	100 %	100 %	100 %	100 %
SVC	96.0 %	100 %	100 %	100 %	100 %	100 %	100 %	100 %

The performance increased slightly when using a larger training set. This is expected since the classifier is better able to determine the best fit of the decision boundary with respect to the data. The use of a relatively large training set, however, is not straight-forward for getting a proper impression of the performance during operational application of the classifier. Therefore, a rather small training set is more suitable due to the fact that only a fraction of potential data recordings are available at this stage, mimicking real life application performance best. Still, when training a classifier to operate in real life, all available data would be used for training to achieve maximum performance.

3.2.2 Frequency response classification

From the clusters of all schools available per species, 2452 frequency response samples were available for herring, 2619 for horse mackerel, and 98337 for mackerel. To generate more balanced datasets, the mackerel samples were randomly subsampled and reduced to 10% of the original dataset. Each sample was subsequently standardised to the largest backscatter observation over the whole frequency band and converted to backscatter coefficients in the linear scale. Training datasets were created consisting of the mean of these standardised frequency response per species. Only samples were considered that contained observations at all recorded frequencies over the bandwidth. Data by channel band were truncated at the edges of the bands where signal levels usually decrease and observations become more variable. The actual bands per channel used were eventually: 58-79 kHz, 107-149 kHz, and 178-240 kHz. Observed mean standardised frequency responses per species and the three channel frequency bands used are shown in Figures 3.9-11.

Differences in shape and relative magnitude were evident between species and bands. Horse mackerel gave on average a more curved and elevated response pattern in the first and second band. The response for mackerel was rather flat throughout these bands, while herring showed a steeper decrease. A higher overall relative frequency response could be observed for mackerel at the highest frequency band observed with a distinct downward trend beyond about 215 kHz. For the other two species, relative frequency responses were comparatively lower and slightly decreasing throughout that band.

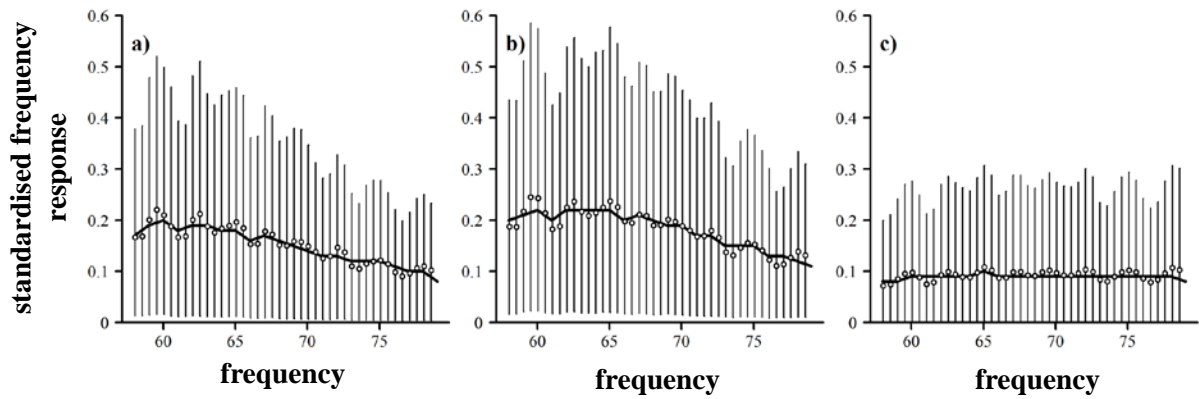


Figure 3.9. Standardised relative frequency response values over the first WBT channel (nominal frequency 70 kHz) for herring (a), horse mackerel (b), and mackerel (c). Averaged mean (\pm sd) values of training data sets (circles and vertical lines) with fitted trends from the DFA model (thick black line) are given.

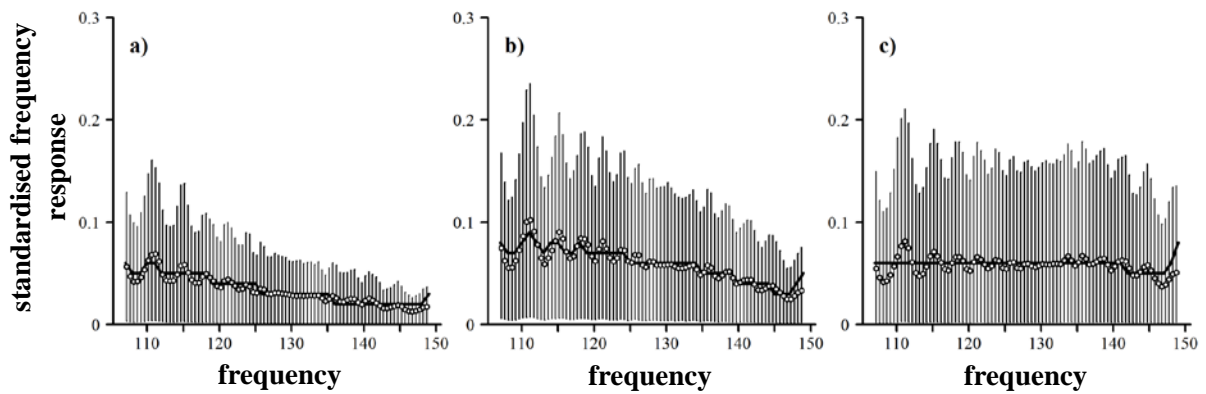


Figure 3.10. Standardised relative frequency response values over the first WBT channel (nominal frequency 120 kHz) for herring (a), horse mackerel (b), and mackerel (c). Averaged mean (\pm sd) values of training data sets (circles and vertical lines) with fitted trends from the DFA model (thick black line) are given.

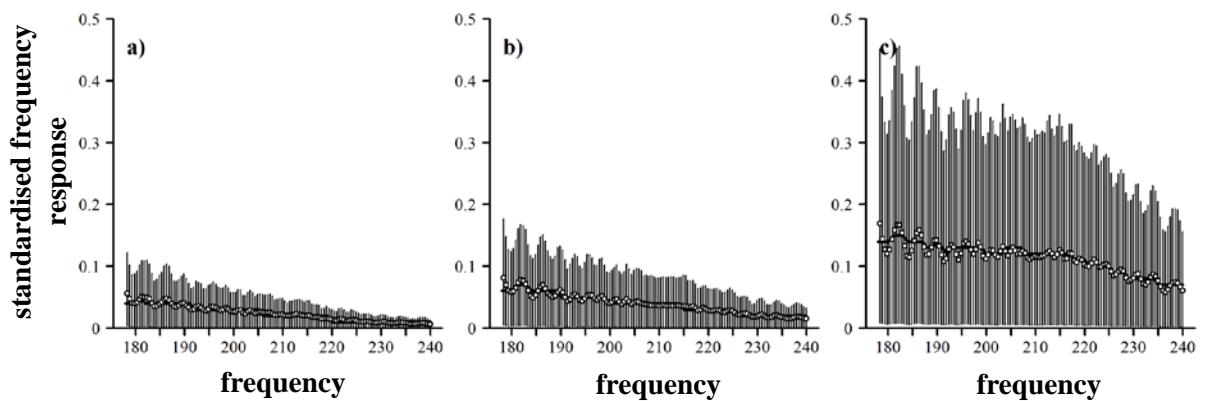


Figure 3.11. Standardised relative frequency response values over the first WBT channel (nominal frequency 200 kHz) for herring (a), horse mackerel (b), and mackerel (c). Averaged mean (\pm sd) values of training data sets (circles and vertical lines) with fitted trends from the DFA model (thick black line) are given.

Using Dynamic Factor Analysis (DFA) and three potential common trends between the species training frequency response data revealed the pattern shown in Figure 3.12. The first common trend showed a gradual decrease over the entire frequency band and was positively associated with training data of both herring and horse mackerel (Figure 3.13). The second common trend showed peak features over the first two bands and a more gradual decrease over the last band. It had the highest positive association with the horse mackerel training dataset, emphasising the curvature in the response observed in the first band, and a slightly higher overall response in the second band. The herring training data showed intermediate positive association to the second common trend, whereas the mackerel training dataset was strongly negatively correlated to it (Figures 3.12 and 3.13). The third common trend represented an increase in response from low to higher frequencies with a plateau and slight decrease over the last band. Consequently, it was strongly positively correlated with the mackerel training dataset and negatively with both herring and horse mackerel (Figures 3.12 and 3.13).

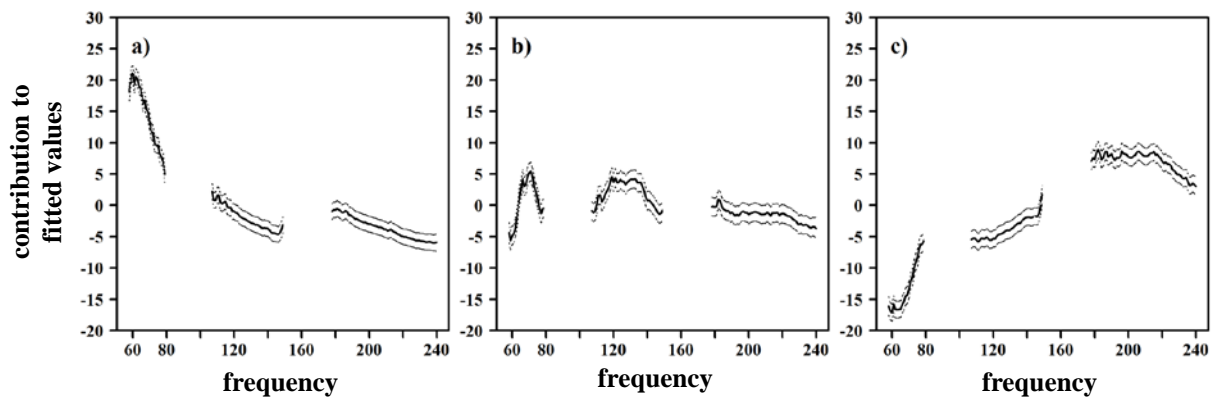


Figure 3.12. First (a), second (b), and third (c) common trends in broadband frequency responses of training data sets from herring, horse mackerel, and mackerel, identified by the dynamic factor analysis (DFA) with 95% confidence intervals.

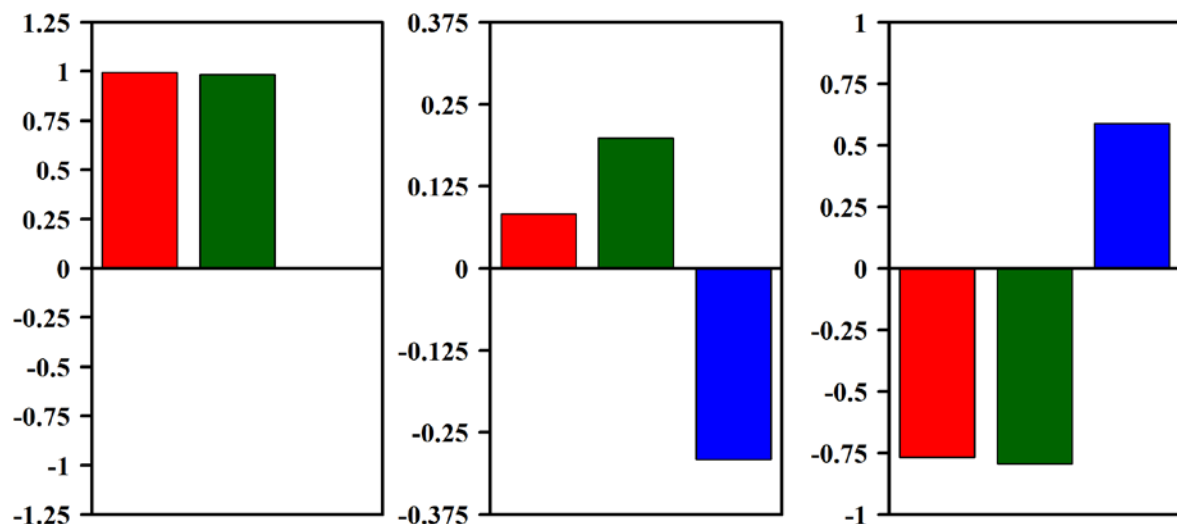


Figure 3.13. Canonical correlations between training data sets of mean relative frequency response trends of different species (herring: red; horse mackerel: green; mackerel: blue) and common trends identified by the Dynamic Factor Analysis (DFA).

Data samples of whole schools were subsequently averaged and these 'test' datasets then compared to training datasets of the different species. In order to assess the potential for correct classification based on the observed frequency response trends and their relation to the common trends identified by the

DFA, the 3 training dataset and the test dataset of each school were run through the DFA model to generate canonical correlation scores between the different datasets and common trends. Figure 3.14 illustrates an example case where a school was selected on an echogram and its average frequency response, based on all the samples contained in that school, compared to those of the training datasets. Eventually, that example classified the school as being mackerel with a certainty of 79%. The result is based on the similarities of the canonical correlation between the test school frequency response pattern with the 3 common trends of the DFA, and those of the mackerel training data with the 3 common trends. The training datasets of the herring and horse mackerel frequency responses on the other hand showed canonical correlations to the common trends that were more different than those of the test school dataset (see bottom left panel in Figure 3.14).

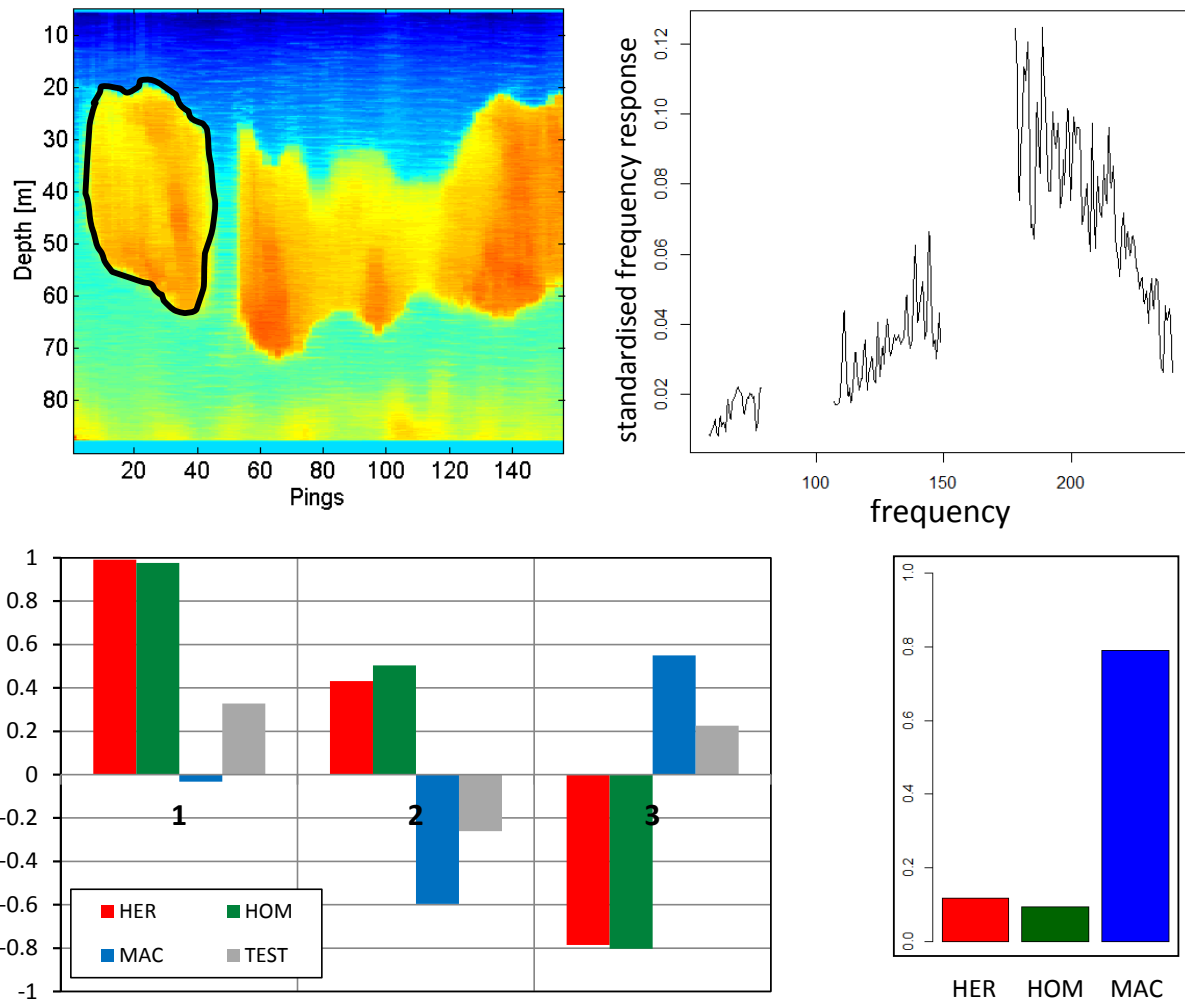


Figure 3.14. Example of a test mackerel school (black border) on an echogram (top left panel) with averaged frequency response of all samples in the school (top right panel). Canonical correlations of the training datasets of the three species (HER: herring; HOM: horse mackerel; MAC: mackerel) and that of the test school (TEST) with the three common trends from the Dynamic Factor Analysis (DFA) (bottom left panel). The resulting classification score is then based on the similarities of the canonical correlations of the test school with those of the training datasets (bottom right panel).

Overall scores when giving each school the chance to be classified as either of the three species were around 70% correct probability for herring and horse mackerel, and over 80% correct probability for mackerel schools (Figure 3.15). All schools but one horse mackerel school were correctly classified by receiving the highest classification probability for the true species class (Table 3.4).

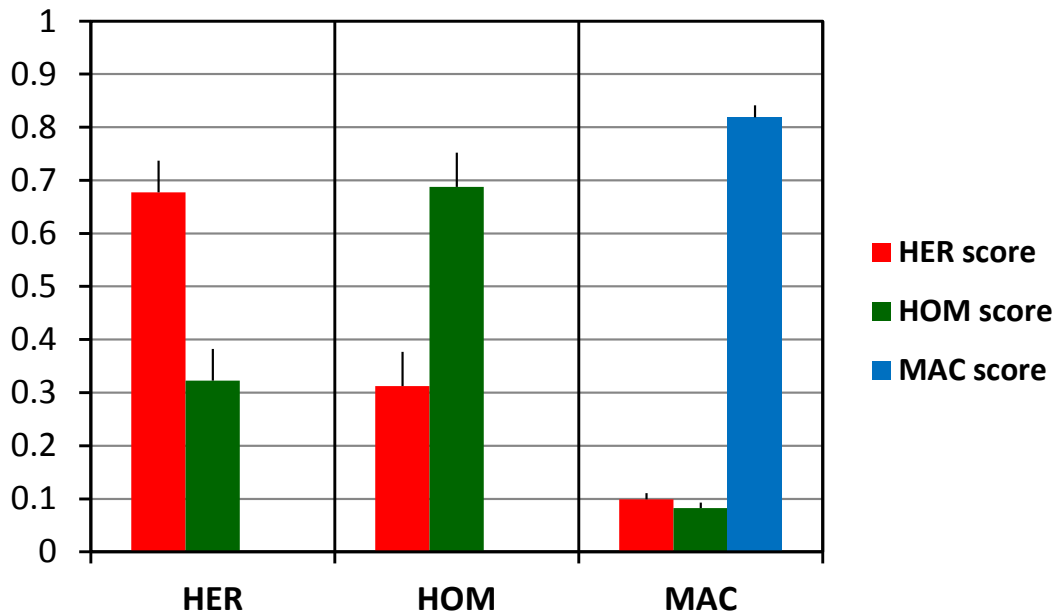


Figure 3.15. Overall classification performance using Dynamic Factor Analysis (DFA) to identify and associate common trend patterns based on differences in frequency responses between species. The three sections represent scores for respective species groups given to schools of herring (HER), horse mackerel (HOM), and mackerel (MAC). Error bars represent standard errors.

3.2.3 Combined classifier

As a different pulse window was applied during data recordings for 20 out of the 23 available herring schools, only 3 herring schools could be evaluated in the combined classifier when the frequency response and statistical approach were merged to contribute to a joint classification score. The individual class output confidences of both approaches are given in Table 3.3 and Table 3.4. These results present the differences in using an SVC or KNN-3 classifier for the statistical classification. Due to the nature of the SVC classifier, determining a class confidence is strongly dependent on the sample size and may produce over-confident results if naturally occurring variability is not fully represented in the training dataset. Therefore, care must be taken in combining classification outputs using the SVC approach.

Though the scores of the individual classification methods are sometimes in the order of 95 to 100%, merging scores of the two classification approaches seems to deliver a potential advantage. As previously mentioned, due to the nature of the SVC classifier, classification confidences for this type of classifier are not very meaningful at this stage, due to the still small dataset. Therefore, for the combined classifier it is more suitable to use a classifier that delivers more stable and realistic confidence outcomes, such as the KNN-x classifier.

Table 3.3. Individual school classification confidences of the statistical classification (Conf. 1) using an SVC classifier and frequency response classification (Conf. 2) and the species outcome, based on confidence combination using a max function (Outcome max. operator) or a mean function (Outcome mean operator). In this table *H* stands for Herring, *HM* Horse Mackerel and *M* Mackerel. A green box indicates a correct classification, a red box indicates an incorrect classification.

School	Conf. 1 H	Conf. 1 HM	Conf. 1 M	Conf. 2 H	Conf. 2 HM	Conf. 2 M	Outcome max. operator	Outcome mean operator
H1	100 %	0.0 %	0.0 %	60.1 %	39.9 %	0.0 %	H	H
H2	58.0 %	42.0 %	0.0 %	79.5 %	20.5 %	0.0 %	H	H
H3	50.8 %	49.2 %	0.0 %	63.7 %	36.3 %	0.0 %	H	H
HM1	0.0 %	100.0 %	0.0 %	60.9 %	39.1 %	0.0 %	HM	HM
HM2	0.0 %	100.0 %	0.0 %	25.2 %	74.8 %	0.0 %	HM	HM
HM3	0.0 %	100.0 %	0.0 %	37.3 %	62.7 %	0.0 %	HM	HM
HM4	0.0 %	100.0 %	0.0 %	20.9 %	79.1 %	0.0 %	HM	HM
HM5	0.0 %	100.0 %	0.0 %	19.8 %	80.2 %	0.0 %	HM	HM
HM6	0.0 %	100.0 %	0.0 %	23.3 %	76.7 %	0.0 %	HM	HM
M1	0.0 %	0.0 %	100 %	5.9 %	3.7 %	90.4 %	M	M
M2	0.0 %	0.0 %	100 %	6.5 %	3.6 %	89.9 %	M	M
M3	0.0 %	0.9 %	99.1 %	7.7 %	4.9 %	87.4 %	M	M
M4	0.0 %	0.0 %	100 %	10.9 %	8.0 %	81.0 %	M	M
M5	0.0 %	0.0 %	100 %	8.8 %	7.5 %	83.8 %	M	M
M6	0.0 %	0.0 %	100 %	0.7 %	1.1 %	98.2 %	M	M
M7	0.0 %	0.0 %	100 %	14.4 %	11.3 %	74.3 %	M	M
M8	0.0 %	0.0 %	100 %	2.1 %	0.8 %	97.0 %	M	M
M9	0.0 %	0.0 %	100 %	5.3 %	2.3 %	92.4 %	M	M
M10	0.0 %	0.0 %	100 %	14.1 %	11.5 %	74.4 %	M	M
M11	0.0 %	0.0 %	100 %	31.4 %	28.6 %	40.0 %	M	M
M12	0.0 %	0.0 %	100 %	20.9 %	20.1 %	59.0 %	M	M
M13	0.0 %	0.0 %	100 %	13.3 %	10.8 %	75.9 %	M	M
M14	0.0 %	0.0 %	100 %	5.0 %	5.0 %	90.0 %	M	M
M15	0.0 %	0.0 %	100 %	6.5 %	5.3 %	88.2 %	M	M
M16	0.0 %	0.0 %	100 %	13.1 %	12.9 %	74.0 %	M	M
M17	0.0 %	0.0 %	100 %	8.0 %	6.9 %	85.1 %	M	M
M18	0.0 %	0.0 %	100 %	9.8 %	8.2 %	82.0 %	M	M
M19	0.0 %	0.0 %	100 %	11.9 %	10.8 %	77.3 %	M	M
M20	0.0 %	0.0 %	100 %	9.0 %	7.3 %	83.7 %	M	M
M22	0.0 %	0.0 %	100 %	11.3 %	10.2 %	78.5 %	M	M
M23	0.0 %	0.0 %	100 %	10.5 %	10.4 %	79.1 %	M	M
M24	0.0 %	0.0 %	100 %	12.1 %	11.3 %	76.7 %	M	M
M25	0.0 %	0.0 %	100 %	9.7 %	8.1 %	82.2 %	M	M
M26	0.0 %	0.0 %	100 %	2.3 %	0.5 %	97.2 %	M	M
M27	1.1 %	0.0 %	98.9 %	3.2 %	2.3 %	94.5 %	M	M
M28	0.0 %	0.0 %	100 %	2.7 %	0.8 %	96.5 %	M	M
M29	0.0 %	0.0 %	100 %	7.3 %	6.8 %	86.0 %	M	M
M30	0.0 %	0.0 %	100 %	11.7 %	9.2 %	79.1 %	M	M
M31	0.0 %	0.0 %	100 %	19.3 %	17.1 %	63.6 %	M	M
M32	0.0 %	0.0 %	100 %	33.0 %	28.6 %	38.4 %	M	M
M33	0.0 %	0.0 %	100 %	7.7 %	5.6 %	86.7 %	M	M
M34	0.0 %	0.0 %	100 %	4.4 %	1.8 %	93.8 %	M	M
M35	0.0 %	0.0 %	100 %	8.7 %	7.3 %	84.0 %	M	M
M36	0.0 %	0.0 %	100 %	3.5 %	2.8 %	93.7 %	M	M
M37	0.0 %	0.0 %	100 %	7.7 %	6.9 %	85.4 %	M	M
M38	0.0 %	0.0 %	100 %	13.1 %	12.1 %	74.8 %	M	M
Overall							100 %	100 %

Table 3.4. Individual classification confidences of the statistical classification (Conf. 1) using a KNN-3 classifier and frequency response classification (Conf. 2) and the species outcome, based on confidence combination using a max function (Outcome max. operator) or a mean function (Outcome mean operator). In this table *H* stands for Herring, *HM* Horse Mackerel and *M* Mackerel. A green box indicates a correct classification, a red box indicates an incorrect classification.

School	Conf. 1 H	Conf. 1 HM	Conf. 1 M	Conf. 2 H	Conf. 2 HM	Conf. 2 M	Outcome max. operator	Outcome mean operator
H1	33.3 %	50.0 %	16.7 %	60.1 %	39.9 %	0.0 %	H	H
H2	50.0 %	33.3 %	16.7 %	79.5 %	20.5 %	0.0 %	H	H
H3	50.0 %	33.3 %	16.7 %	63.7 %	36.3 %	0.0 %	H	H
HM1	16.7 %	66.7 %	16.7 %	60.9 %	39.1 %	0.0 %	HM	HM
HM2	16.7 %	66.7 %	16.7 %	25.2 %	74.8 %	0.0 %	HM	HM
HM3	16.7 %	66.7 %	16.7 %	37.3 %	62.7 %	0.0 %	HM	HM
HM4	16.7 %	66.7 %	16.7 %	20.9 %	79.1 %	0.0 %	HM	HM
HM5	16.7 %	66.7 %	16.7 %	19.8 %	80.2 %	0.0 %	HM	HM
HM6	16.7 %	66.7 %	16.7 %	23.3 %	76.7 %	0.0 %	HM	HM
M1	16.7 %	16.7 %	66.7 %	5.9 %	3.7 %	90.4 %	M	M
M2	16.7 %	16.7 %	66.7 %	6.5 %	3.6 %	89.9 %	M	M
M3	16.7 %	16.7 %	66.7 %	7.7 %	4.9 %	87.4 %	M	M
M4	16.7 %	16.7 %	66.7 %	10.9 %	8.0 %	81.0 %	M	M
M5	16.7 %	16.7 %	66.7 %	8.8 %	7.5 %	83.8 %	M	M
M6	16.7 %	16.7 %	66.7 %	0.7 %	1.1 %	98.2 %	M	M
M7	16.7 %	16.7 %	66.7 %	14.4 %	11.3 %	74.3 %	M	M
M8	16.7 %	16.7 %	66.7 %	2.1 %	0.8 %	97.0 %	M	M
M9	16.7 %	16.7 %	66.7 %	5.3 %	2.3 %	92.4 %	M	M
M10	16.7 %	16.7 %	66.7 %	14.1 %	11.5 %	74.4 %	M	M
M11	16.7 %	16.7 %	66.7 %	31.4 %	28.6 %	40.0 %	M	M
M12	16.7 %	16.7 %	66.7 %	20.9 %	20.1 %	59.0 %	M	M
M13	16.7 %	16.7 %	66.7 %	13.3 %	10.8 %	75.9 %	M	M
M14	16.7 %	16.7 %	66.7 %	5.0 %	5.0 %	90.0 %	M	M
M15	16.7 %	16.7 %	66.7 %	6.5 %	5.3 %	88.2 %	M	M
M16	16.7 %	16.7 %	66.7 %	13.1 %	12.9 %	74.0 %	M	M
M17	16.7 %	16.7 %	66.7 %	8.0 %	6.9 %	85.1 %	M	M
M18	16.7 %	16.7 %	66.7 %	9.8 %	8.2 %	82.0 %	M	M
M19	16.7 %	16.7 %	66.7 %	11.9 %	10.8 %	77.3 %	M	M
M20	16.7 %	16.7 %	66.7 %	9.0 %	7.3 %	83.7 %	M	M
M22	16.7 %	16.7 %	66.7 %	11.3 %	10.2 %	78.5 %	M	M
M23	16.7 %	16.7 %	66.7 %	10.5 %	10.4 %	79.1 %	M	M
M24	16.7 %	16.7 %	66.7 %	12.1 %	11.3 %	76.7 %	M	M
M25	16.7 %	16.7 %	66.7 %	9.7 %	8.1 %	82.2 %	M	M
M26	16.7 %	16.7 %	66.7 %	2.3 %	0.5 %	97.2 %	M	M
M27	16.7 %	16.7 %	66.7 %	3.2 %	2.3 %	94.5 %	M	M
M28	16.7 %	16.7 %	66.7 %	2.7 %	0.8 %	96.5 %	M	M
M29	16.7 %	16.7 %	66.7 %	7.3 %	6.8 %	86.0 %	M	M
M30	16.7 %	16.7 %	66.7 %	11.7 %	9.2 %	79.1 %	M	M
M31	16.7 %	16.7 %	66.7 %	19.3 %	17.1 %	63.6 %	M	M
M32	16.7 %	16.7 %	66.7 %	33.0 %	28.6 %	38.4 %	M	M
M33	16.7 %	16.7 %	66.7 %	7.7 %	5.6 %	86.7 %	M	M
M34	16.7 %	16.7 %	66.7 %	4.4 %	1.8 %	93.8 %	M	M
M35	16.7 %	16.7 %	66.7 %	8.7 %	7.3 %	84.0 %	M	M
M36	16.7 %	16.7 %	66.7 %	3.5 %	2.8 %	93.7 %	M	M
M37	16.7 %	16.7 %	66.7 %	7.7 %	6.9 %	85.4 %	M	M
M38	16.7 %	16.7 %	66.7 %	13.1 %	12.1 %	74.8 %	M	M
Overall							100 %	100 %

3.3 Dissemination activities

Results and progress of the project were disseminated and communicated at various intermediate stages to project partners and different external audiences. Audiences ranged from project participant fishing industry stakeholder, to scientists, and ministry members. A brief overview is given here with additional information in the Appendix of this report.

- Project preparation meeting, with aim for SIMRAD to give an update on the technical developments and latest status of the new scientific broadband echosounder EK80 prototype, Rijswijk (June 2014). Audience: project partners and hardware manufacturer/engineers.
- Project progress meeting, preliminary results presentation and data discussion, Den Haag (October 2014). Audience: science and industry project partners.
- Project progress meeting, progress and data processing discussion, Den Haag (January 2015). Audience: science project partners.
- Acoustic projects progress meeting, Den Haag (March 2015). Presentation entitled: "Broadband ECHO project – progress and way ahead" (Appendix B). Audience: science and industry project partners.
- SCH6 crew update, Beverwijk (March 2015). Presentation entitled: "ECHO broadband classification with the EK 80" (Appendix B). Audience: skippers and trawler crew.
- ICES Symposium on Marine Ecosystem Acoustics (SomeAcoustics), Nantes, France (May 2015). Presentation entitled: "Identification of commercially important species by wideband acoustic data collected on pelagic fishing vessels" (Appendix B). Audience: fisheries acoustic scientists.
- Preliminary progress results (September 2015). Presentation by correspondence: "Broadband ECHO project Results – September 2015". Audience: industry project partners (Appendix B).
- Dutch Bioacoustics Day, IMARES, IJmuiden, Netherlands (November 2015). Presentation entitled: "Broadband Identification of Fish Species". Audience: bioacoustic scientists, industry representatives, government ministry representatives.

4 Conclusions

A processing chain allowing the offline reading, pre-processing and imaging of the EK80 echosounder data has been successfully implemented. The processing chain also includes detection and classification of fish schools and a separate module for calibration. It has successfully been used for the generation of input data to develop and test several classification algorithms.

The first results of statistical and frequency response classification are overall good and promising for the available data. Average statistical classification scores for allocation of schools to the correct highest-scoring species class, based on iterative resampling procedures, was between 95-100%. Similar results were found for the frequency response classification done on a school basis where 98% were correctly classified.

For the available herring dataset, it remains questionable whether it offered a good representation since the biggest part of the data were recorded with a different pulse window. Also, only relatively little horse mackerel data were available (7 schools). Operationally speaking, the presented results demonstrate the enhanced potential of the broadband technique for improving species classification, however, more data will be necessary to confirm and make the classification more representative with respect to the naturally observed variation in data. The results presented here therefore show the expected capabilities but are so far only based on a relatively limited data. Input data for robust classifiers should be representative with respect to the diversity (environments, fish sizes, swimming depths etc.) observed at sea. Hence, more data will be necessary to confirm these results.

The combination of the two independent classification methods suggests a valuable option as it can make use of the advantages unique to both individual approaches. Based on the available datasets, it resulted in a correct school species classification performance of 100%.

Two- and three-dimensional backscattering models have been successfully implemented. The results highlight the potential of 3D models to deliver representative estimates of broadband backscatter, however, limitations in computational power reduced the realisable frequency range. The 2D implementations for swimbladdered fish provided useful in identifying key regions along the frequency spectrum where species could be distinguished according to difference in backscattering features. Based on modelling results, differences were observed between different size-classes of fish.

5 Recommendations

- The most important aspect of developing a robust classification algorithm is to have access to as much (representative) data as possible. These data should be documented and combined with metadata information (e.g. environment, hardware setup, biology) in order to be able to link the ground truth to the data. It is therefore recommended to continue with the gathering of acoustic broadband data together with as much complementary metadata as possible for the fisheries used so far, but also on additional species.
- The current (and proposed additional) data, can also be used to evaluate the classification performances in terms of average fish size and mixed schools (if available).
- Different ways to merge the classification algorithms should be evaluated in order to maximise its benefits.
- Addition and use of further frequency channels during data collection will deliver even more elaborate data that may reveal useful information for improving species (and size) classification. Figure 5.1 shows an example of broadband data recently collected at 6 transducer channels on R/V 'Tridens'. Especially note the additional differences in backscatter observed between the three species at some of the channels and especially the highest frequency channel (spanning 270-450 kHz), which was not available in this project.
- Auxiliary data, such as swimming depth, geographical position etc., have been left out in order to evaluate the performance of the classification algorithm alone. The additional performance benefit from these parameters should be evaluated separately.
- Predictions of enhanced scatter models can be used to identify differences in the backscattering spectrum. Ultimately this can be applied to real-time algorithms of species and size classification. Combination of modelling and statistical classification can allow the inference of size-based information in addition to species classification. An application may then be to infer sizes of individually detected fish targets from broadband data, e.g. when detected at the edges of schools.
- Modelling has demonstrated its potential for predicting size- and species-based differences. These methods can be expanded to include a wider range of size-classes and species as well as for modelling the highest frequency channels of the EK80 (270-450 kHz) if the limitations associated with computational loads can be overcome. Additionally, the model can be used to estimate and utilise the expected variability around the measurements to improve classification.
- Calibration will remain a tedious but important quality assurance method. However, the implemented calibration tool available in the latest EK80 software release will simplify the procedure and allow collection of calibrated raw data. Nonetheless, it may be worthwhile to explore the application of an un-calibrated and therefore relative frequency response classification approach, which is possible provided enough training data is collected and stability of the hardware assured otherwise.

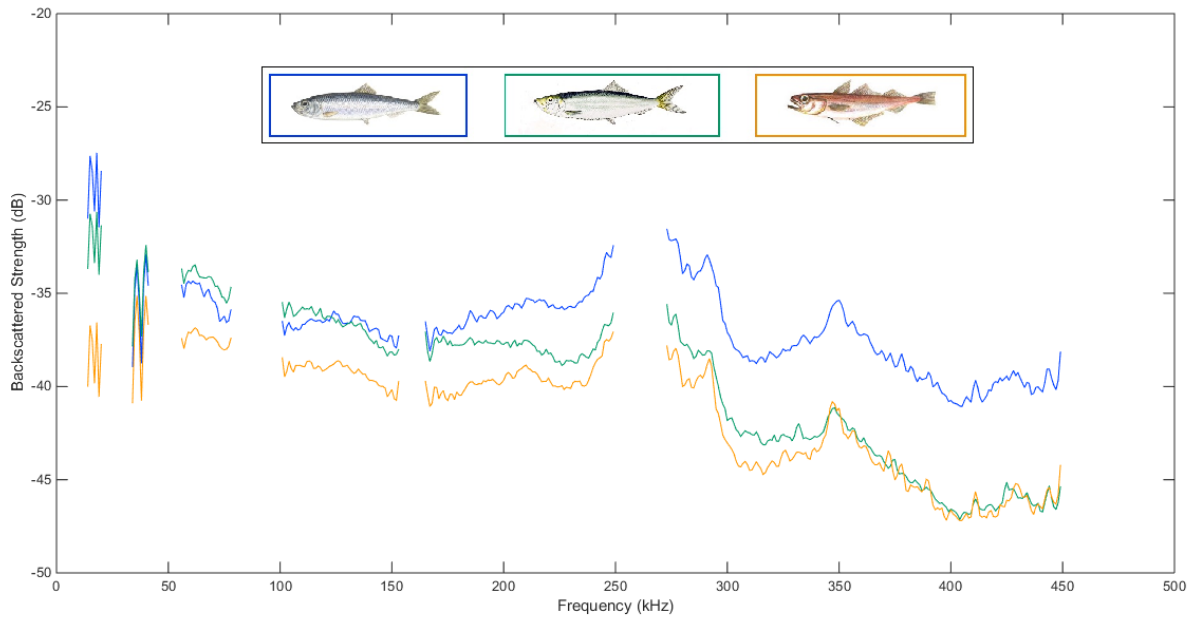


Figure 5.1. Frequency response spectra of herring (blue), sprat (green), and Norway pout (orange) recorded by a EK80 broadband echosounder on R/V 'Tridens' using 6 transducer channels.

6 Quality Assurance

IMARES utilises an ISO 9001:2008 certified quality management system (certificate number: 124296-2012-AQ-NLD-RvA). This certificate is valid until 15 December 2015. The organisation has been certified since 27 February 2001. The certification was issued by DNV Certification B.V. Furthermore, the chemical laboratory of the Fish Division has NEN-EN-ISO/IEC 17025:2005 accreditation for test laboratories with number L097. This accreditation is valid until 1th of April 2017 and was first issued on 27 March 1997. Accreditation was granted by the Council for Accreditation.

References

- Anonymous. 2015a. COMSOL Multiphysics User's Guide. COMSOL AB.
- Anonymous. 2015b. COMSOL Multiphysics. Acoustics Module Users' Guide. COMSOL AB.
- Berenger, J.P. 1996. Three-dimensional Perfectly Matched Layer for the Absorption of Electromagnetic Waves. *Journal of Computational Physics*, 127: 363-379.
- Brawn, V. M. 1969. Buoyancy of Atlantic and Pacific herring. *Journal of the Fisheries Research Board of Canada*, 26: 2077–2091.
- Sawada, K., Ye, Z., Kieser, R., and Furusawa, M. 1999. Target-strength measurements and modelling of walleye pollock and pacific hake. *Fisheries Science*, 65: 193-205.
- Ona, E. 1990. Physiological factors causing natural variations in acoustic target strength of fish. *Journal of Marine Biology Association UK*, 70: 107-127.
- Nesse, T. L., Hobæk, H., & Korneliussen, R. J. 2009. Measurements of acoustic-scattering spectra from the whole and parts of Atlantic mackerel. *ICES Journal of Marine Science: Journal du Conseil*, 66(6): 1169-1175.
- Gorska, N., Ona, E., and Korneliussen, R. 2005. Acoustic backscattering by Atlantic mackerel as being representative of fish that lack a swimbladder. Backscattering by individual fish. *ICES Journal of Marine Science*, 62: 984-995.
- Fässler, S. M. M., Gorska, N., Ona, E., and Fernandes, P. G. 2008. Differences in swimbladder volume between Baltic and Norwegian spring spawning herring: consequences for mean target strength. *Fisheries Research*, 92: 314–321.
- Fässler, S. M. M., Fernandes, P. G., Semple, S. I. K., and Brierley, A. S. 2009. Depth dependent swimbladder compression in herring *Clupea harengus* observed using magnetic resonance imaging. *Journal of Fish Biology*, 74: 296-303.
- Fässler, S. M. M., O'Donnell, C., and Jech, J. M. 2013. Boarfish (*Capros aper*) target strength modelled from magnetic resonance imaging (MRI) scans of its swimbladder. *ICES Journal of Marine Science*, 70: 1451–1459.
- Foote, K. G. 1980. Importance of the swimbladder in acoustic scattering by fish: A comparison of Gadoid and mackerel target strengths. *Journal of Acoustical Society of America*, 67: 2084-2089.
- Foote, K. G. 1985. Rather-high-frequency sound scattering by swimbladdered fish. *Journal of the Acoustical Society of America*, 78(2): 688-700.
- Macaulay, G. J. 2009. Target strength of mackerel icefish (*Champsocephalus gunnari*) from a scattering model. SG-ASAM-09/06.p.
- Peña, H., and Foote, K.G 2008. Modelling the target strength of *Trachurus symmetricus murphyi* based on high resolution swimbladder morphometry using MRI scanner. *ICES Journal of Marine Science*, 65(9): 1751-1761.
- Serra, J. 1986. Introduction to Mathematical Morphology. *Computer Vision, Graphics and Image Processing*, Vol. 35, Pages 283-385.
- Scoulding, B., Fässler, S. M. M., MacLennan, D.N., and Fernandes, P.G. (In prep). In situ target strength measurements of Atlantic mackerel at multiple frequencies.
- Simmonds, J. E. and MacLennan, D. N. 2005 *Fisheries Acoustics: Theory and Practice*, 2nd ed. Oxford: Blackwell Science Ltd.
- Zampolli, M., Tessi, A., Jensen, F., Malm, N., and Blottman III, J. 2007. A computationally efficient finite element model with perfectly matched layers applied to scattering from axially symmetric objects. *Journal of the Acoustical Society of America*, 122(3): 1472-1485.
- Zuur, A.F., Fryer, R.J., Jolliffe, I.T., Dekker, R., and Beukema, J.J. (2003) Estimating common trends in multivariate time series using dynamic factor analysis. *Environmetrics* 14: 665-685.

Justification

Report number: C171/15
Project number: 4301503201

The scientific quality of this report has been peer reviewed by the a colleague scientist and the head of the department of IMARES.

Approved: Thomas Brunel
Researcher

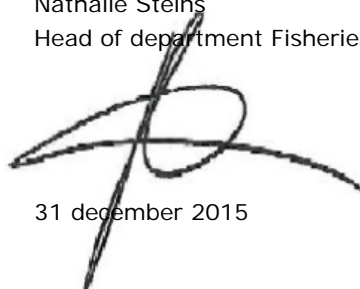
Signature:



Date: 31 december 2015

Approved: Nathalie Steins
Head of department Fisheries

Signature:



Date: 31 december 2015

Kalibratie en data log protocol voor Simrad EK80 breedband echolood

Versie: 2.0
Datum: 06/08/2015



Europees Visserijfonds: Investerings in duurzame visserij

Dit rapport is tot stand gekomen met financiering van het Europees Visserijfonds: Investerings in duurzame visserij.

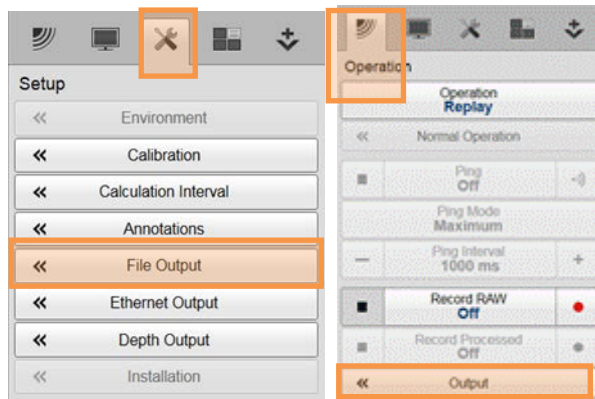
Inhoudsopgave

1	instellingen & data opslag	65
1.1	EK80	65
2	TIJDENS DE REIS: controleer de data opslag & echosounder werking	70
3	KALIBRATIE	71
3.1	voorbereiding	71
3.2	Procedure	72

1. Instellingen & data opslag

1.1 EK80

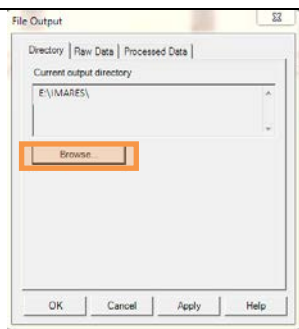
1. configureer de data opslag en kies de echosounder instellingen in de EK80:



software versie 1.6.0 (beeld links)

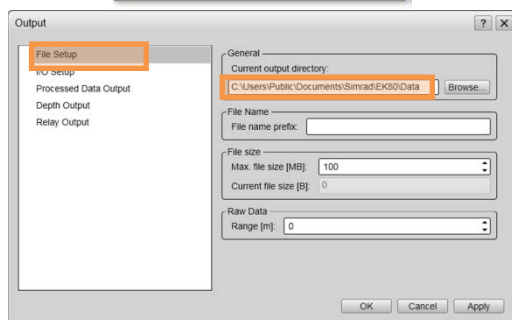
software versie 1.7.0/1.8.0 (beeld rechts)

Operation → Output



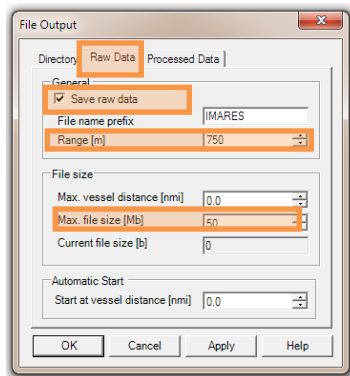
software versie 1.6.0 (beeld boven)

software versie 1.7.0/1.8.0 (beeld beneden)



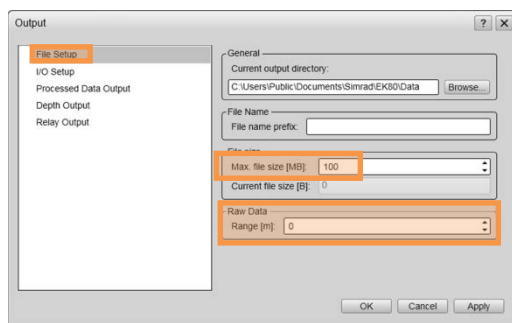
Kies de 'destination folder' voor de EK80 data

Output → General → current output directory -> bijvoorbeeld: D:\IMARES EK80 DATA.



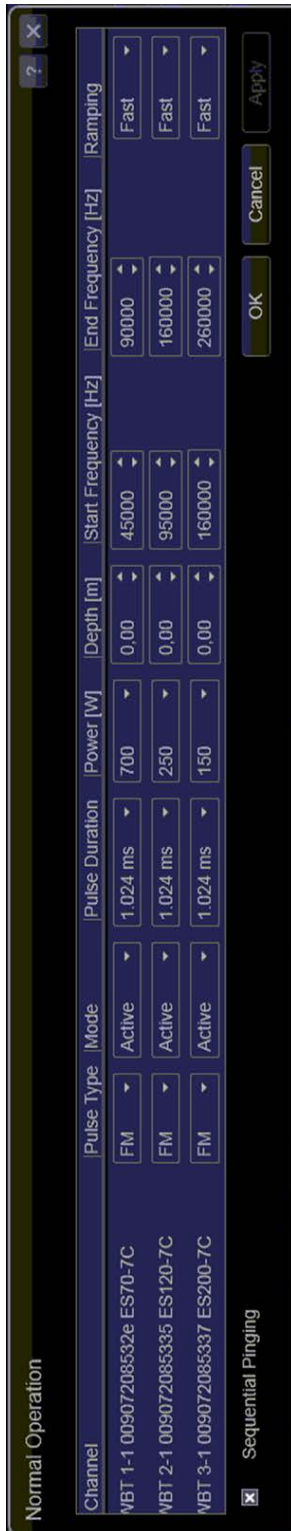
software versie 1.6.0 (beeld
boven)

software versie 1.7.0/1.8.0
(beeld beneden)



Selecteer de file size en range

- stel de Range [m] op: 750
- stel de Max. file size [Mb] op:
1000000



Eenmalig de PulsType, PulsDuration, Power, en Start/End Frequency instellen:
(niet veranderen tijdens de reis!!!)

Operation → Normal Operation

Pulse Type → **FM**

Mode → **Active**

Pulse Length → **1.024** (niet op 'Auto'!!!!!!)

Power [W] Settings

(met de volgende waarden per WBT):

ES70-7C → 700W

ES120-7C → 250W

ES200-7C → 150W)

Depth [m] → **0.00**

Start Frequency [Hz]

(met de volgende waarden per WBT):

ES70-7C → **45000**

ES120-7C → **95000**

ES200-7C → 160000

End Frequency [Hz]

(met de volgende waarden per WBT):

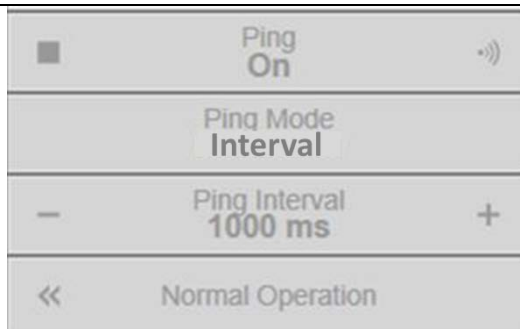
ES70-7C → 90000

ES120-7C → 160000

ES200-7C → 260000

Ramping → Fast

Sequential Pinging → ☒

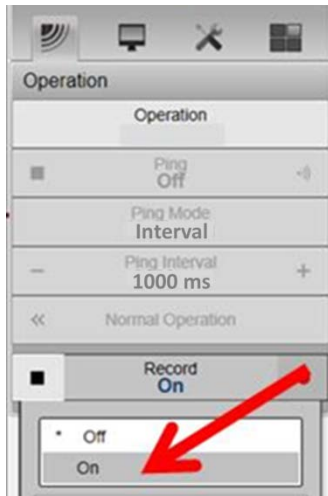


Stel de ping interval in op 1 per seconde:

OPERATION → PING MODE:
"INTERVAL".

OPERATION → PING INTERVAL:
select 1000 ms.

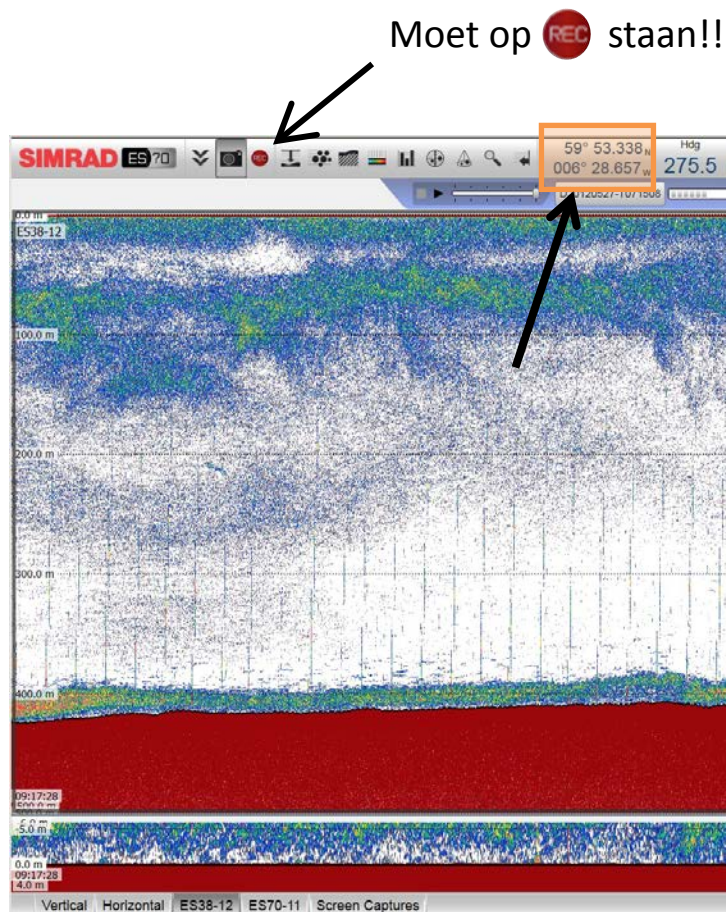
Maar dit is niet kritisch en soms is het wel verstandig een langere /hogere ping interval te hebben (diepte afhankelijk).



Activeer de ruwe data opslag van de echosounder

Operation → Record RAW: "On"

2 TIJDENS DE REIS: controleer de data opslag & echosounder werking



- Mocht de EK80 opnieuw gestart worden, dan **niet de factory settings kiezen**, maar de "Most Recent State". Anders zijn de settings niet juist en wordt de ruwe data niet (of alleen maar naar de C-schijf) opgeslagen.
- Tijdens data recording controleren of de **GPS informatie** op de EK80 binnenkomt, en de **record button rood** is, en de data files (extensions .raw) naar juiste locatie op de harde schijf geschreven wordt: bij voorbeeld op "D:\IMARES EK80 DATA"
- Let op tekening van storing door interferentie van een andere transducer in het echogram (zie scherm hieronder). Als dit zichtbaar is dan de andere transducer uitschakelen. Valse bodem echo's (=storing) kunnen ontstaan als de ping interval te hoog is ingesteld.

3 KALIBRATIE

3.1 voorbereiding

- De kalibratie kan gedaan worden wanneer dit het beste uitkomt tijdens de reis, het is niet noodzakelijk dit vooraf te doen.
- Kalme weersomstandigheden en diep water (>20-30m onder het schip!!) zijn nodig. Vermijd gebieden met grote verschillen in getij hoogte of dicht bij rivier mondingen.
- De hoofd motor moet als mogelijk uitgeschakeld worden tijdens de kalibratie.
- Zorg dat er weinig tot geen individuele vissen aanwezig zijn in de waterkolom onder de echosounder. Bij daglicht is de kans op vis minimaal, kalibratie s'nachts is moeilijk doordat er meer vis aanwezig kan zijn aan de oppervlakte.

3.2 Procedure

a) Kalibrate kit opstelling

Voordat het anker neergelaten wordt!!: Zet de hengels op zodat de sphere het beste in de beam gepositioneerd kan worden:

b) De kalibratie sphere in positie brengen onder het schip



Dompel de schone en droge kalibratie sphere's in een emmer of bakje water met afwasmiddel (b.v, 'drecht'). Dit om te voorkomen dat de sphere microbubbles van lucht vasthoudt en een foute echo waarde geeft.

- Verbind de eerste tungsten sphere (22mm diameter) met een lus van monofilament vislijn van een meter aan het punt waar de drie(of vier) monofilament vislijnen aan elkaar gekoppeld zijn. Die afstand is nodig om het knooppunt voldoende afstand van de 22mm sphere te houden, de 120kc en 200kc kunnen de knopen in het monofilament "zien".
- Verbind de tweede sphere (38,1mm diameter), 3 tot 5 meter onder de eerste sphere, deze werkt als stabilisator gewicht.



De sferes moeten nu voorzichtig overboord gezet worden, hierbij moet contact van de sferes met het schip vermeden worden.

- Vier zoveel lijn uit dat alle hengels dezelfde lijnlengthe hebben, een de bovenste sphere 10 tot 20 meter onder de transducer in de beam komt te hangen.

c) De kalibratie op de brug uitvoeren (EK80)

Set alleen maar de Channel die wordt gekalibreerd op actief, set de anderen Channels op passief!

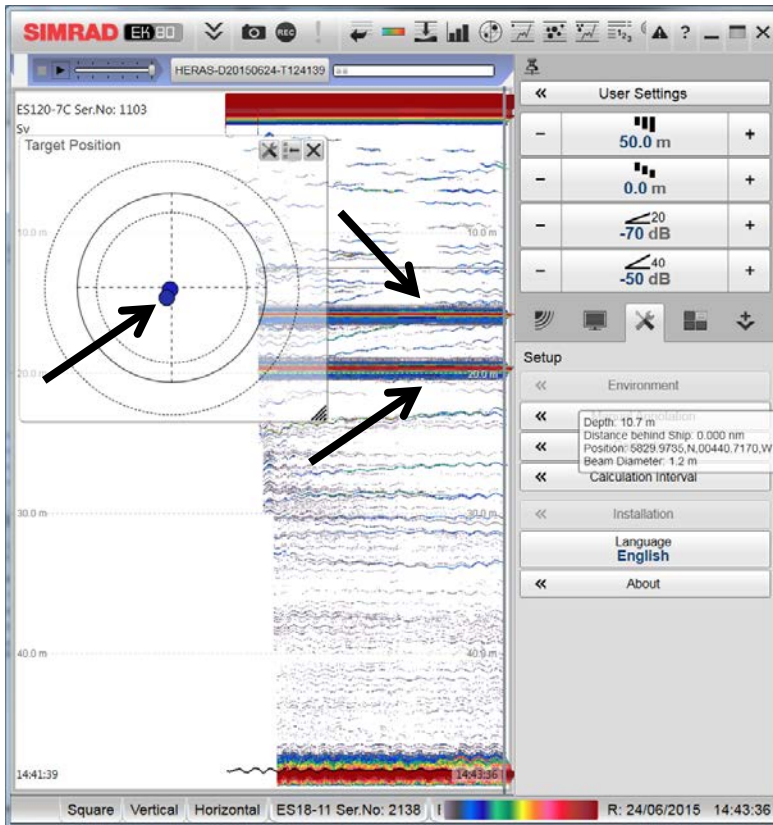
Operation → Normal Operation

Channel die wordt gekalibreerd

Mode → **ACTIVE**

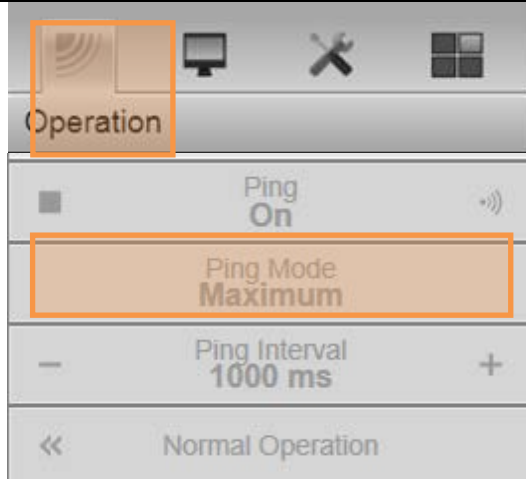
Channels die niet worden gekalibreerd

Mode → **PASSIVE**



Zoek in het echogram van de frequentie die je wil kalibreren de echo's van de twee sphere's op (deze zijn te zien als twee donkere lijnen). Vier de lijnen van de winches, met de remote control, uit tot ze zichtbaar zijn op het EK80 scherm. De bovenste sphere moet tussen de 10 tot 20 meter onder de transducer hangen!!

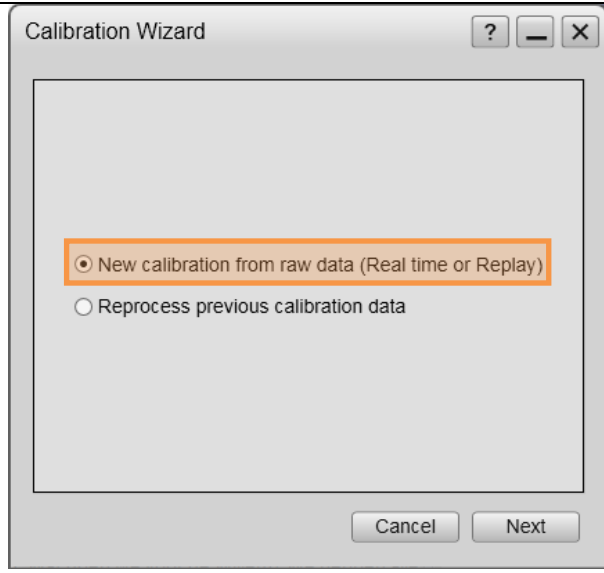
Sla de .raw data zoals gewoon op de harde schijf tijdens de kalibratie.



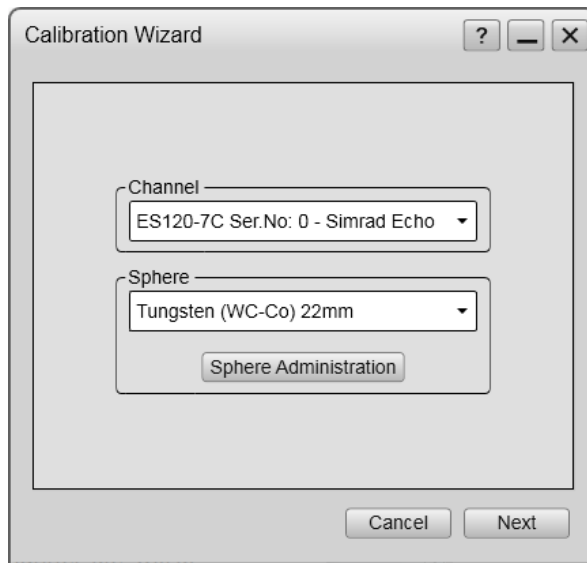
Zet de Ping interval op Maximum tijdens de calibratie: OPERATION → PING MODE: "MAXIMUM".



SETUP → CALIBRATION

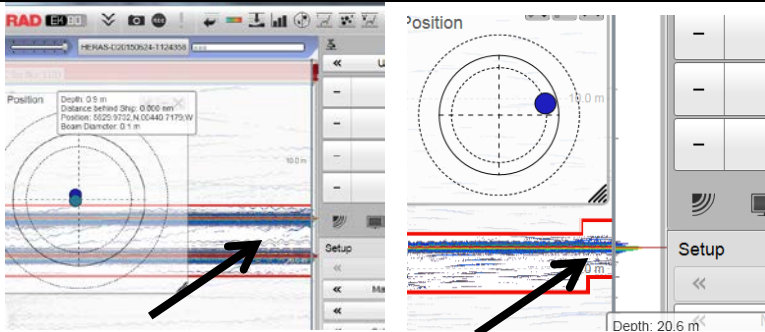


kies: New calibration from raw data

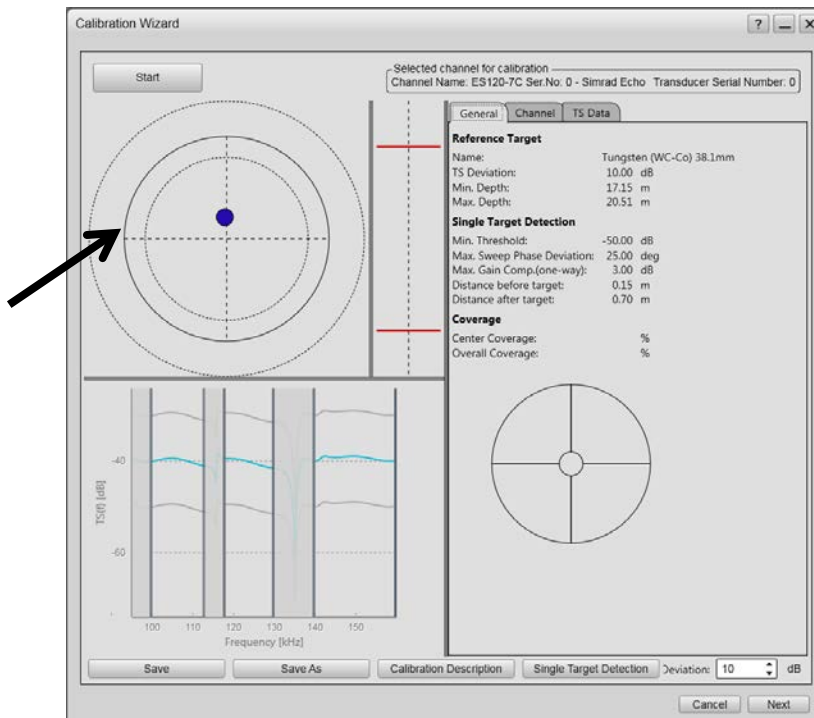


kies de Channel die wordt gekalibreerd. Sphere type, kies de bovenste sphere:
Tungsten (WC-Co) 22mm

Next → de 'Calibration Wizard' scherm wordt geopend

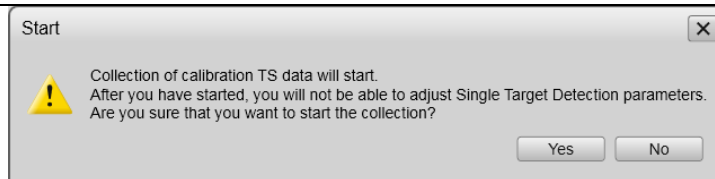


stel de diepte limieten van de 2 rode lijnen op het echogram zo in dat ze boven/onder de bovenste sphere te liggen komen.

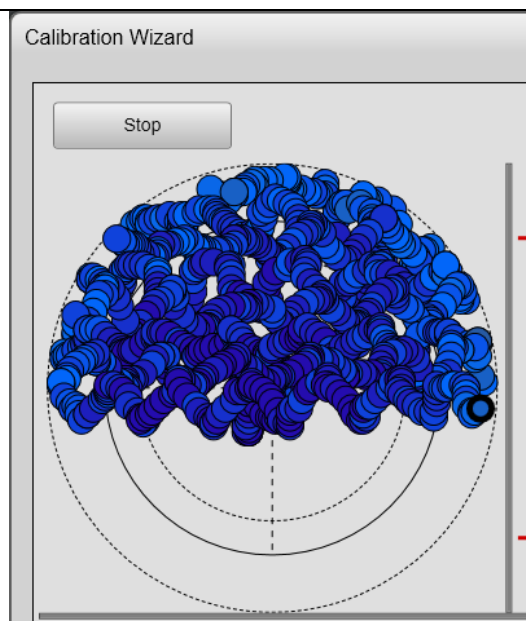


de sphere moet nu in het Target Position window (boven links) in de 'Calibration Wizard' te zien zijn.

start de kalibratie door op 'Start' te drukken.

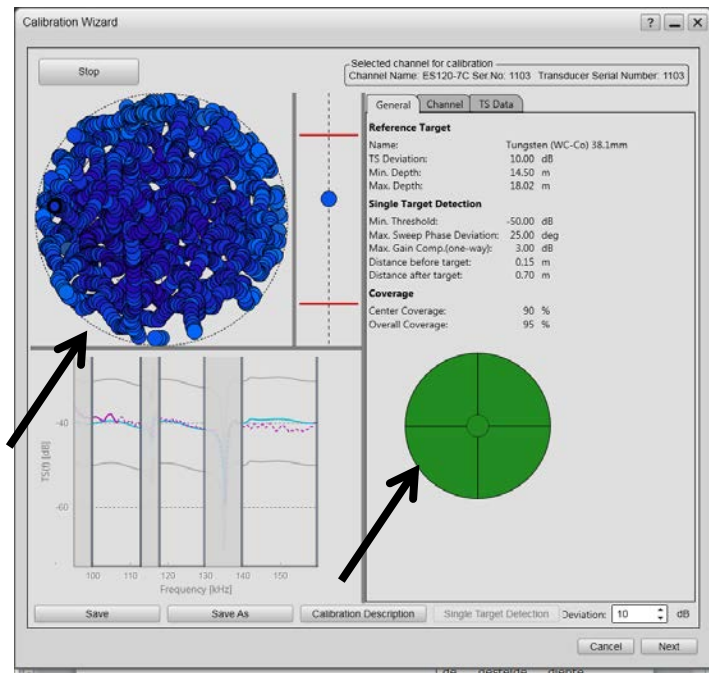


in het volgende window, druk op 'Yes'

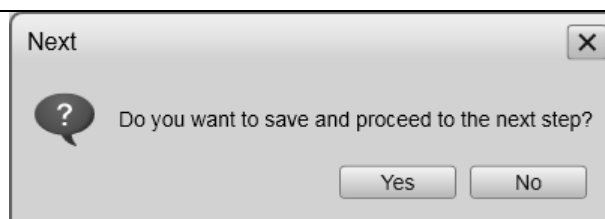


de sphere moet nu rustig door de akoestische beam gemanoeuvreerd worden en de gedetecteerde data punten worden zichtbaar in het 'Calibration

Wizard' scherm.
Zorg dat er genoeg data punten worden gedetecteerd gelijk verdeeld over de akoestische bundel. Als de sphere door de bundel gemanoeuvreerd wordt let dan op de diepte van de sphere in het EK80 scherm, zodanig dat de sphere binnen de gestelde diepte limieten van de 2 rode lijnen blijft.



Als er genoeg data punten gedetecteerd zijn, en alle segment in de beam rechts beneden in de 'Calibration Wizard' groen oplichten, kan de kalibratie voor deze WBT Channel gestopt worden: Click op de 'Stop' button en dan op 'Next'

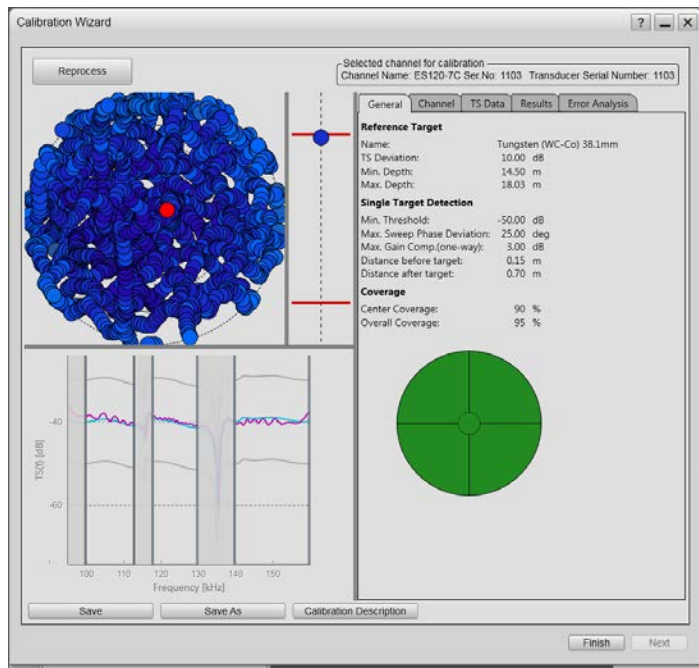


Click op 'Yes'

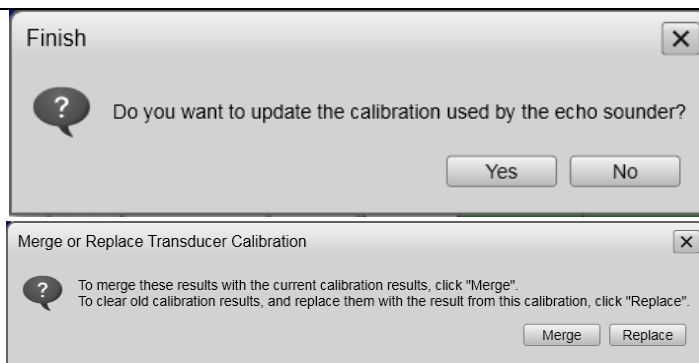
Kies een 'File name' die het datum, scheepsnaam en akoestische frequentie Channel omvat:

b.v. 'ALIDA_14062013_38kHz.xml'

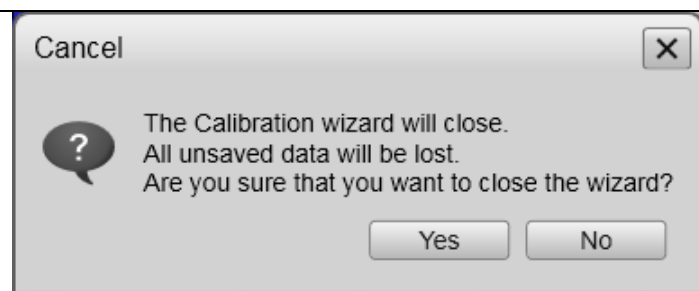
Sla de file op in de data folder op de externe harde schijf (b.v. "E:\IMARES\data").



als de processing klaar is, druk op 'Finish'



update de WBT Channel met de kalibratie: druk op 'Yes' en daarna op 'Replace'



Na de kalibratie kan het SIMRAD kalibratie tool worden beëindigd: druk op 'Yes'

De kalibratie procedure moet voor elke van de WBT Channels herhaalt worden.



Na de kalibratie:

- Haal de sphere's binnen zonder de huid van het schip te raken.
- Ontmantel de kalibratie equipment.
- Spoel de sphere's af in warm zoet water, en droog ze goed af met een doek, en bewaar ze droog in de doos met schuimrubber uitsparingen.


Appendix B: dissemination & presentations

Acoustic projects progress meeting (March 2015)

Broadband ECHO project

Progress and way ahead

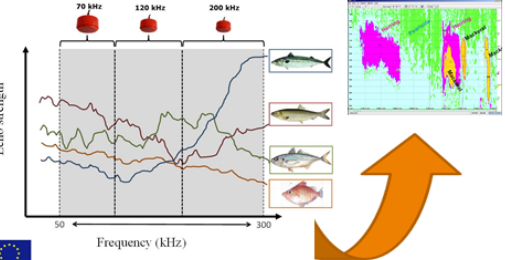
Sascha Fässler, Ben Scouling, Benoit Quesson, Peter Beerens, Jeroen van de Sande, Toon Beeks, Ad van Heijningen



Contents

- Project context and plan
- Progress overview
- Planning of activities
- Data collection progress
- Software progress

Project context



Project planning and progress

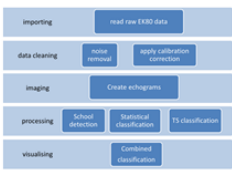
	2014			2015			
activity	Q2	Q3	Q4	Q1	Q2	Q3	Q4
Installation							
Testing & Calibration							
Data collection							

Project planning and progress

	2014			2015			
activity	Q2	Q3	Q4	Q1	Q2	Q3	Q4
Data analysis							
Software development							
Reporting							

Planned activities

- Generalize and test detection algorithm on broad dataset Q2
- Test classifiers: first results in Q2 (may -> SomeAcoustics)
- Mid term report end of June
- Final report Q4 (ready for review end of October)
- Incorporate additional collected datasets for robustness (Q4 if time allows)



Data collection – progress

Fig 17. ALIDA-D20141205-T104601.raw/T105105.raw/T105608.raw

Software chain progress

- Generate echograms in the three WBT bands from raw EK80 data
- Isolate pixels that correspond to (a school of) fish
- Label schools per species

Imaging

Software chain overview Imaging

Actions

- Simrad matlab script analysis (reverse engineering) and validation using EK80 data
- Imaging architecture re-organized and processing optimized.

Results

- Easy and quick generation of echograms from EK80 raw data format.
- Easy access to sub-functionalities

Imaging

Software chain overview Imaging

Detection

Software chain overview Detection

- Detection algorithm developed and tested:
 - Robust against bad quality pings
 - Robust against noise
 - Tested on EK80 data

Imaging

Detection

Classification

Scatter modelling

TNO Innovation for life
IMARES Wageningen UR

ECHO broadband classification with the EK 80

Processing overview
 Sascha Fässler, Ben Scouling, Benoit Quesson, Peter Beerens, Jeroen van de Sande, Toon Beeks, Ad van Heijningen

TNO Innovation for life
IMARES Wageningen UR

Processing overview

TNO Innovation for life
IMARES Wageningen UR

Imaging: read and plot echograms

TNO Innovation for life
IMARES Wageningen UR

Pre-processing: clean echograms (WBT1 as example)

Original echogram - Bad ping detection & interpolation
 - Bottom detection & alignment

TNO Innovation for life
IMARES Wageningen UR

Pre-processing: normalization (WBT1 as example)

- Bad ping detection & interpolation
 - Bottom detection & alignment

- Echo normalization along depth

TNO Innovation for life
IMARES Wageningen UR

Detection: find the pixels corresponding to fish

WBT1 mask WBT2 mask WBT3 mask

TNO Innovation for life
IMARES Wageningen UR

Detection: find the pixels corresponding to fish

Input echograms detection mask Fish only!

Classification:
Frequency diversity and match with models

Classification:
Statistical classification

SOFC | **Classificatie (1/10)** | **TNO** innovation for life

Classificatie: Methode in 3 stappen

Stap 1: Scheiden van de input data in twee onafhankelijke sets: een training set en een test set
=> Elke dataset bevat tenminste een voorbeeld van de 4 vissoorten

SORC | **Classificatie (2/10)** | **TNO** innovation for life

Classificatie: Methode in 3 stappen

Stap 2: Training
=> Elke ping (bewerkt sonarbeeld) wordt aan de classifier aangeboden met een met de hand bepaalde vissoort (label)

SOFC | **Classificatie (3/10)** | **TNO** innovation for life

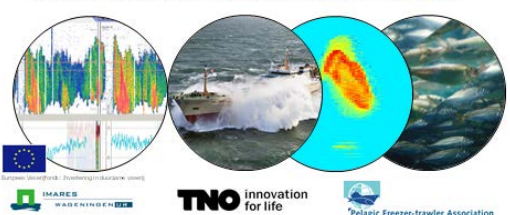
Classificatie: Methode in 3 stappen

Stap 3: Classificatie
=> Voor elke ping geeft de classifier de kans dat het beeld een van de getrainde soorten bevat

De onderzochte ping heeft:
75% kans op Haring
5% kans op Makreel
12% kans op Sprot
8% kans op Horsmakreel

Identification of commercially important species by wideband acoustic data collected on pelagic fishing vessels

Sascha M.M. Fässler, Peter Beerens, Martin Pastoors, Benoit Quesnon, Jeroen van de Sande, and Ben Scouling




IMARES WAGENINGEN, TNO innovation for life, Pelagic Freezer-trawler Association

Introduction

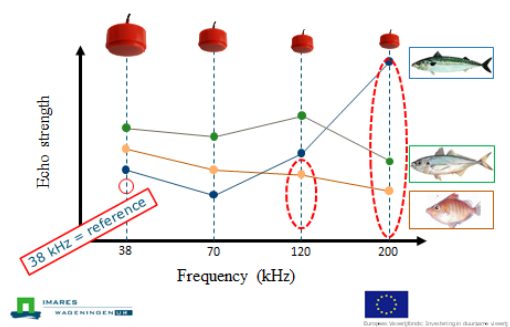
- Quota regulations under EU CFP
- seasonal fisheries & mixed catches
- Landing obligation under the new EU Common Fisheries Policy (pelagics: from 01.01.2015)

Need for better species selectivity!!!



IMARES WAGENINGEN, EU

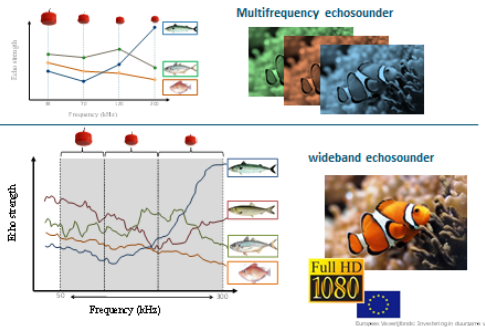
multifrequency ID



38 kHz = reference

IMARES WAGENINGEN, EU

multifrequency -> wideband

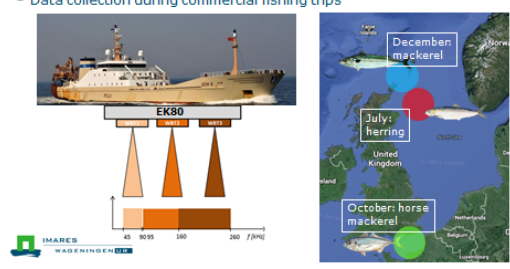


IMARES WAGENINGEN, EU

Project approach

Objective: to use wideband echosounders to improve species ID and thereby selectivity in pelagic fisheries

- Data collection during commercial fishing trips



IMARES WAGENINGEN, EU

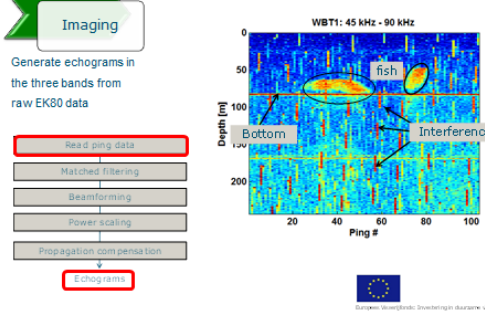
analysis chain

Imaging

Generate echograms in the three bands from raw EK80 data

- Read ping data
- Matched filtering
- Beamforming
- Power scaling
- Propagation compensation

Echograms



IMARES WAGENINGEN, EU

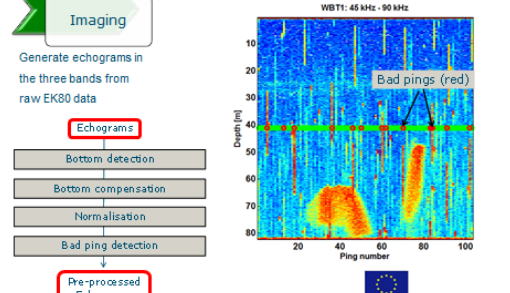
analysis chain

Imaging

Generate echograms in the three bands from raw EK80 data

- Echograms
- Bottom detection
- Bottom compensation
- Normalisation
- Bad ping detection

Pre-processed Echograms



IMARES WAGENINGEN, EU

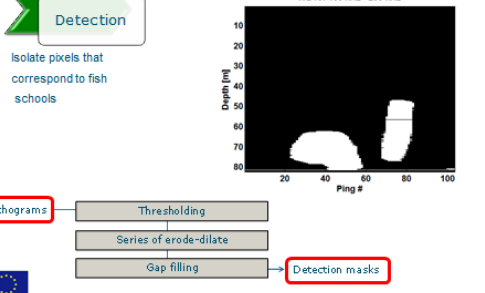
analysis chain

Detection

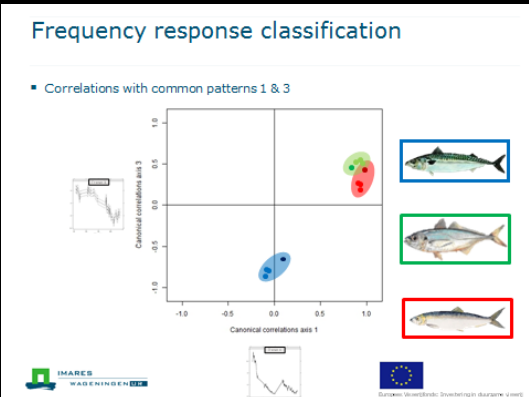
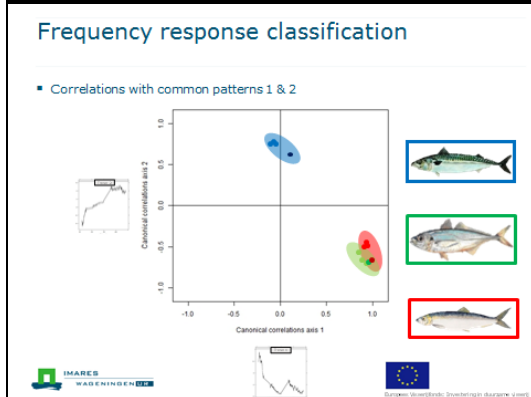
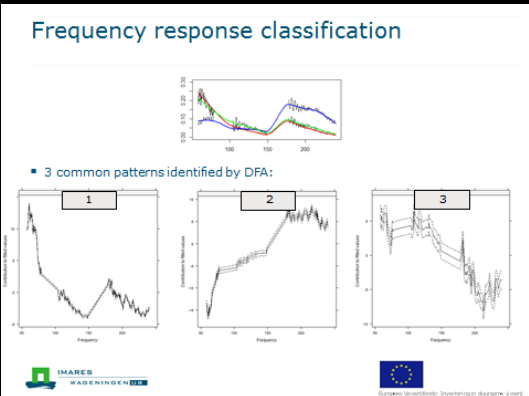
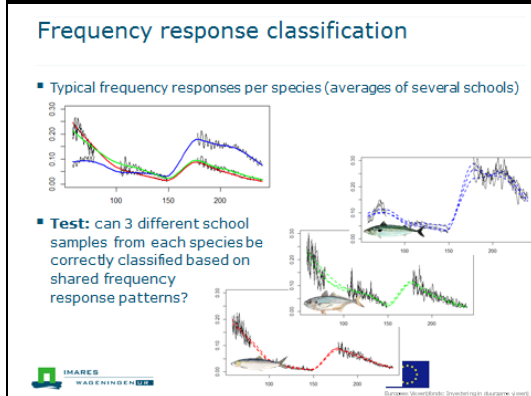
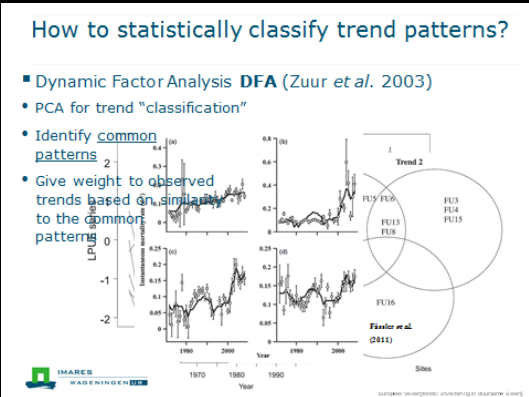
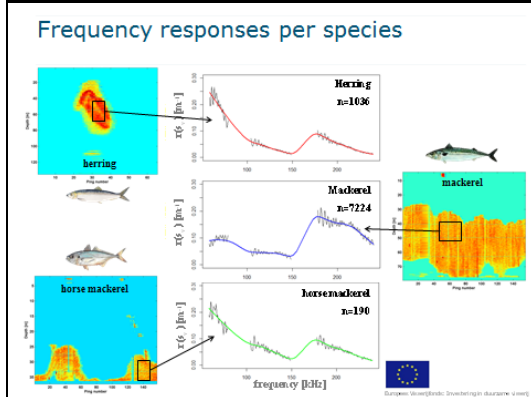
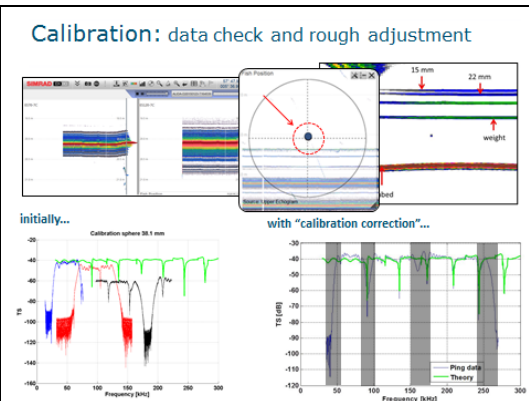
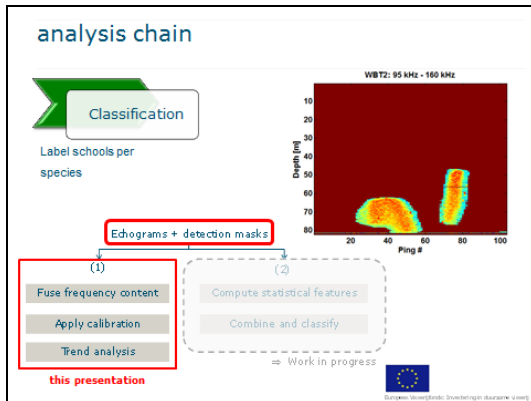
Isolate pixels that correspond to fish schools

- Echograms
- Thresholding
- Series of erode-dilate
- Gap filling

Detection masks

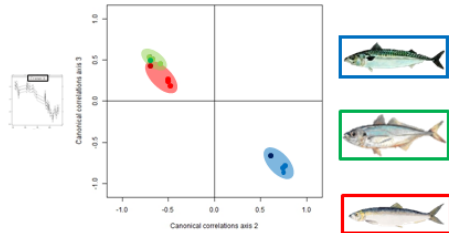


IMARES WAGENINGEN, EU



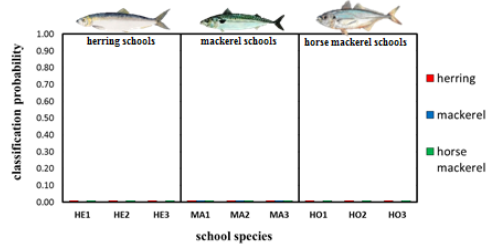
Frequency response classification

- Correlations with common patterns 2 & 3



Frequency response classification

- Classification result based on similarities of response patterns



Conclusions

- Wideband echosounders provide useful additional information to support species identification
- Early results show potential to distinguish HER, MAC, and HOM based on relative frequency response patterns from wideband data
- Further work:
 - test on more data (seasons, species, sizes, areas,...)
 - So far only 3 bands used, add more frequency channels!
 - Apply full volume backscatter calibration



Thanks!

Crew and skipper of the SCH6 'Alida' are acknowledged for their efforts in data collection



The project was selected for the Dutch Operational Programme "Perspectives for a Sustainable Fishery" and co-financed by the European Fisheries Fund



The European Fisheries Fund
Investing in Sustainable Fisheries



Netherlands Enterprise Agency



Broadband Identification of Fish Species

Alessandro Antona
Bioacoustics Day 2015
Friday, Nov 6th – IMARES IJmuiden

WAGeningen UR For quality of life

Introduction

- MSc student in Biosystems Engineering at WUR
 - Specialisation Biobased Chemistry and Technology (BCT)
- HERAS North Sea Herring Acoustic Survey 2015
 - Research vessel R/V "TRIDENS"
 - Aim: remote species identification using a novel broadband echosounder (16-470 kHz)

WAGeningen UR For quality of life

Species

- Atlantic herring (*Clupea harengus*)
- Sprat (*Sprattus sprattus*)
- Norway pout (*Trisopterus esmarkii*)

Previously undistinguished using narrowband multifrequency echosounders

- Fässler and Gorska (2009) – herring vs sprat
- Fässler et al. (2007) – herring vs pout

WAGeningen UR For quality of life

Methodology

- Clusterwise classification
 - Facilitate the statistical learning
 - Weighting different areas within a school
 - Identifying two species in the same aggregation

WAGeningen UR For quality of life

Supervised Machine Learning

How to recognise spectra automatically?

- Artificial Neural Networks (ANN)
- Discriminant analysis
- Classification trees and Random Forest
- Support Vector Machines (SVM)
- k-Nearest Neighbour (k-NN)

WAGeningen UR For quality of life

Supervised Machine Learning

Example applications

- Face recognition
- Character recognition
- QR code reading
- Time series, spectra

WAGeningen UR For quality of life

Supervised Machine Learning

Classification algorithms are relatively fruitful, accessible and easy to use, but...

- The more features (input variables) in use, the more data is required for training
 - Surveys are expensive, time demanding and dependent on uncontrollable conditions and natural cycles
- Incorrect learning can occur if the training dataset is incomplete or unrepresentative
- Identification is purely based on empirical observations, no physical explanation is given

Alternatives? Modelling...

WAGeningen UR For quality of life

Physical Modelling

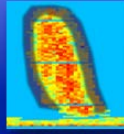
Frequency-dependent TS modelling with COMSOL® Multiphysics

- Pressure acoustics study
- Finite Element Model (FEM)
- 2D and 3D models
- Fish body elements (swimbladder, flesh, backbone) modelled from Computed Tomography (CT) images of fish
- Output: species- and size-specific TS spectra of fish

WAGeningen UR For quality of life

A Grey-box Algorithm

- Model-based recognition never described in literature so far
- Single fish model can be applied to isolated individuals at the edge of the school, but not where targets interactions are predominant (inner portion of the school)

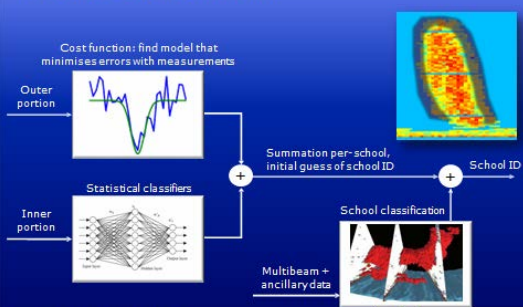


→ Create a synergy between model-based descriptors and information learnt from the data

WAGeningen UR
For quality of life



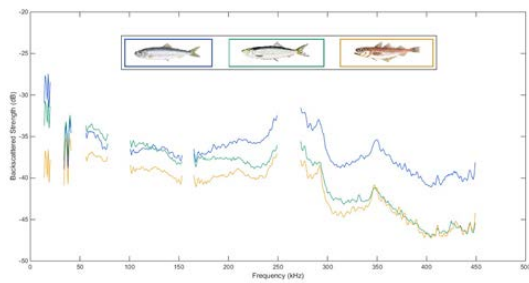
A Grey-box Algorithm



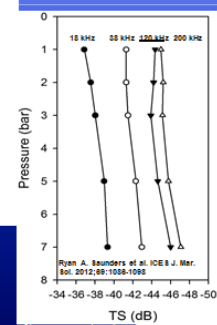
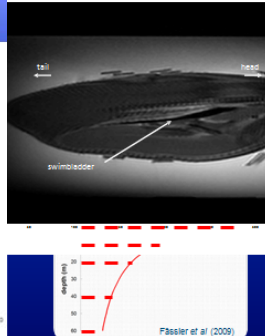
WAGeningen UR
For quality of life



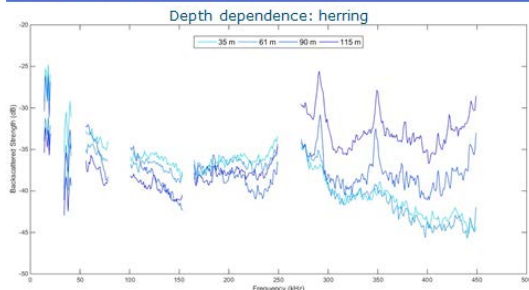
Preliminary Results



WAGeningen UR
For quality of life



Preliminary Results



WAGeningen UR
For quality of life



Preliminary Results

- Classification results: 29 schools, including depth as input

Classifier	Overall Success Rate (%)
Classification Tree	Not applicable
Linear Discriminant Analysis	45.4
Quadratic Discriminant Analysis	45.1
Linear SVM	68.8
Quadratic SVM	73
Cubic SVM	72.9
Gaussian SVM	75.6
k-NN	71.3
Cubic k-NN	71.1
Weighted k-NN	72
Subspace k-NN	69.9
Random Forest	80.4
ANN single hidden layer	73.7
ANN 2 hidden layers	74.6
ANN 3 hidden layers	76.8

WAGeningen UR
For quality of life



What's next

- Assess the capability of a model-based algorithm
 - Does it equal or enhance the performance of machine learning techniques?
- Assess the contribution of 3D school descriptors and ancillary information in the identification process
- Cope with the so called "Big Data":
 - Too big: Memory required for modelling at high frequencies
 - Too fast: Order of GB/min data to be processed on-line
 - Too complex: Simultaneous data from different sources
- Assess the suitability for real-time applications (computational analysis)

WAGeningen UR
For quality of life



Thank you for your attention

Questions?

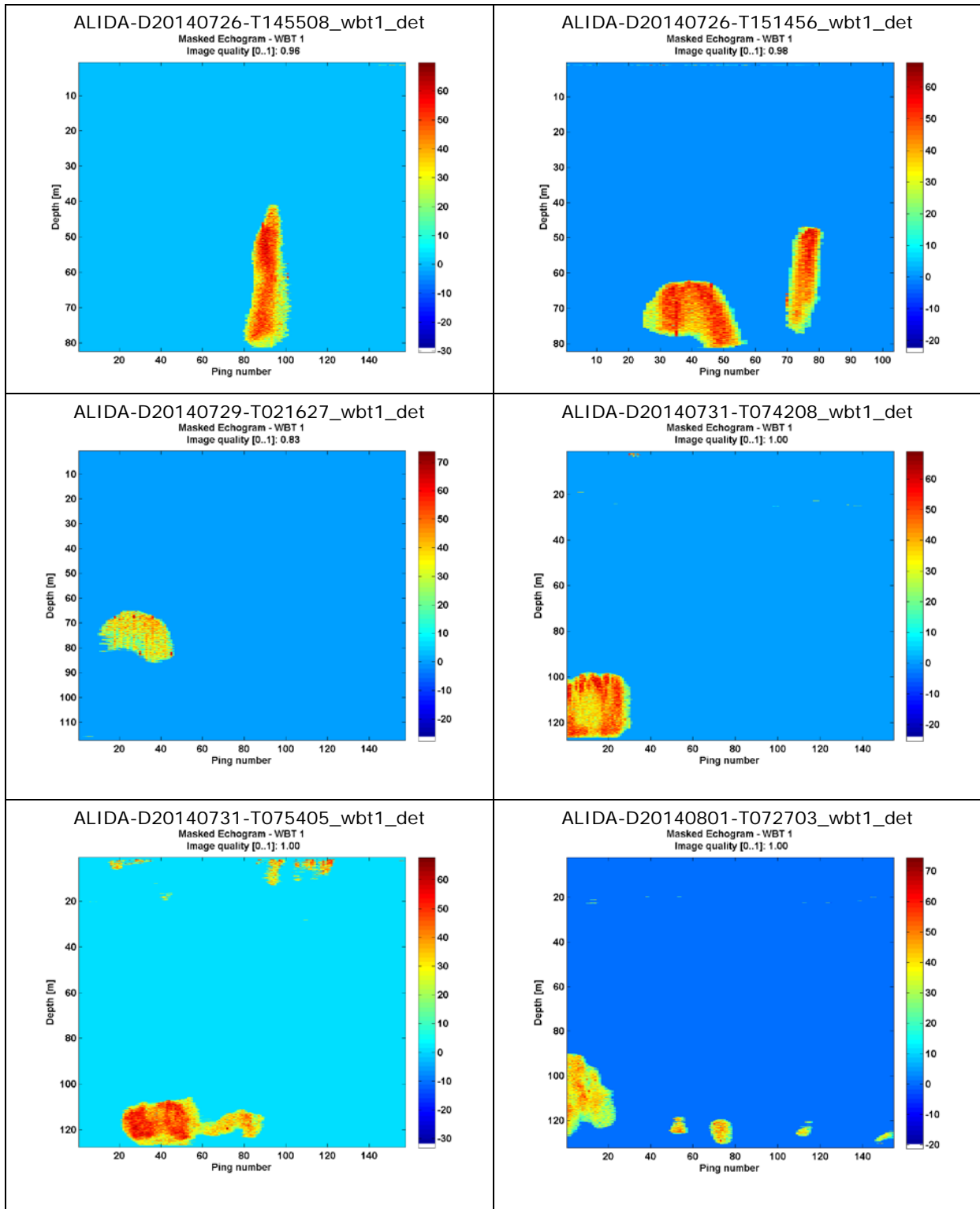


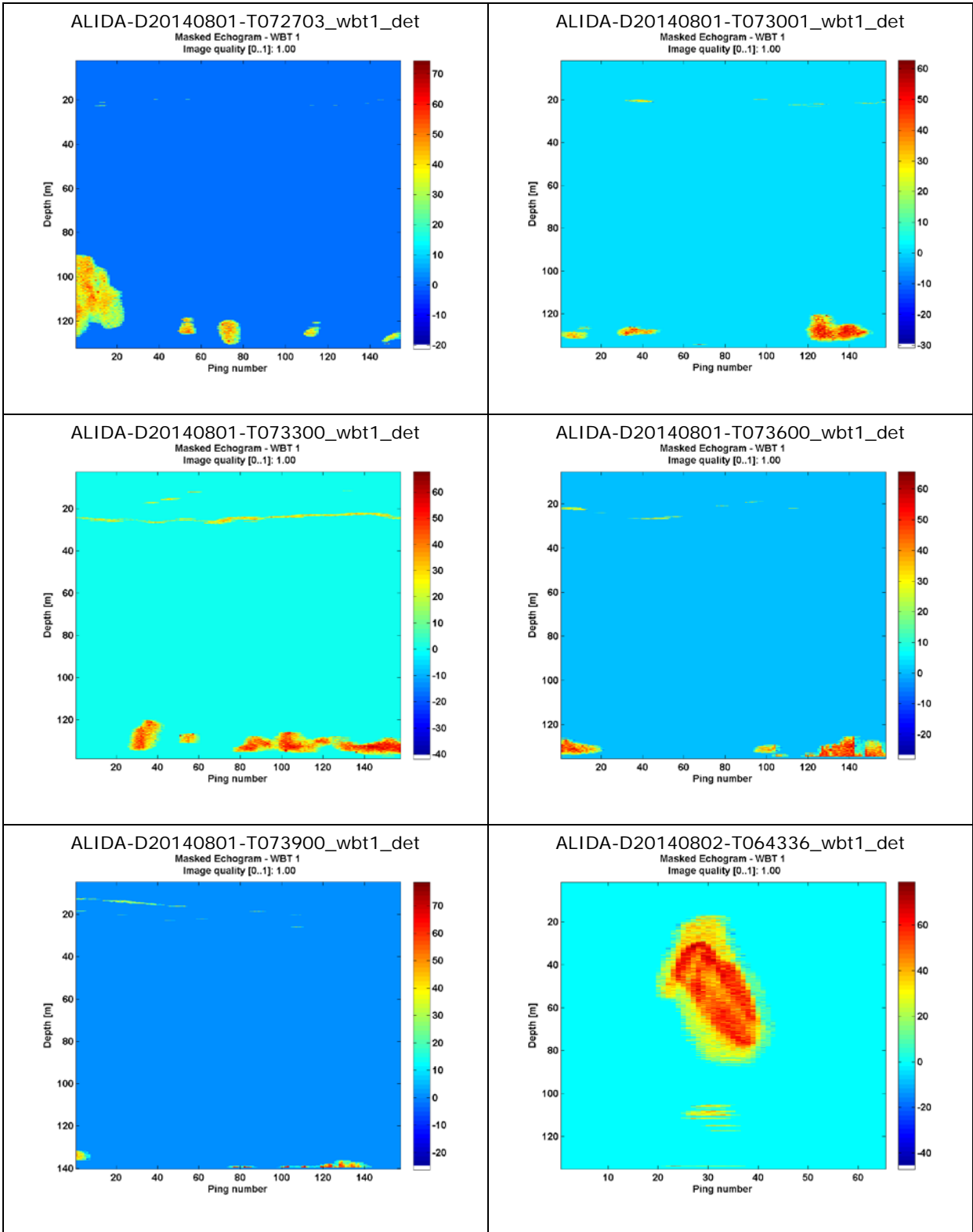
WAGeningen UR
For quality of life

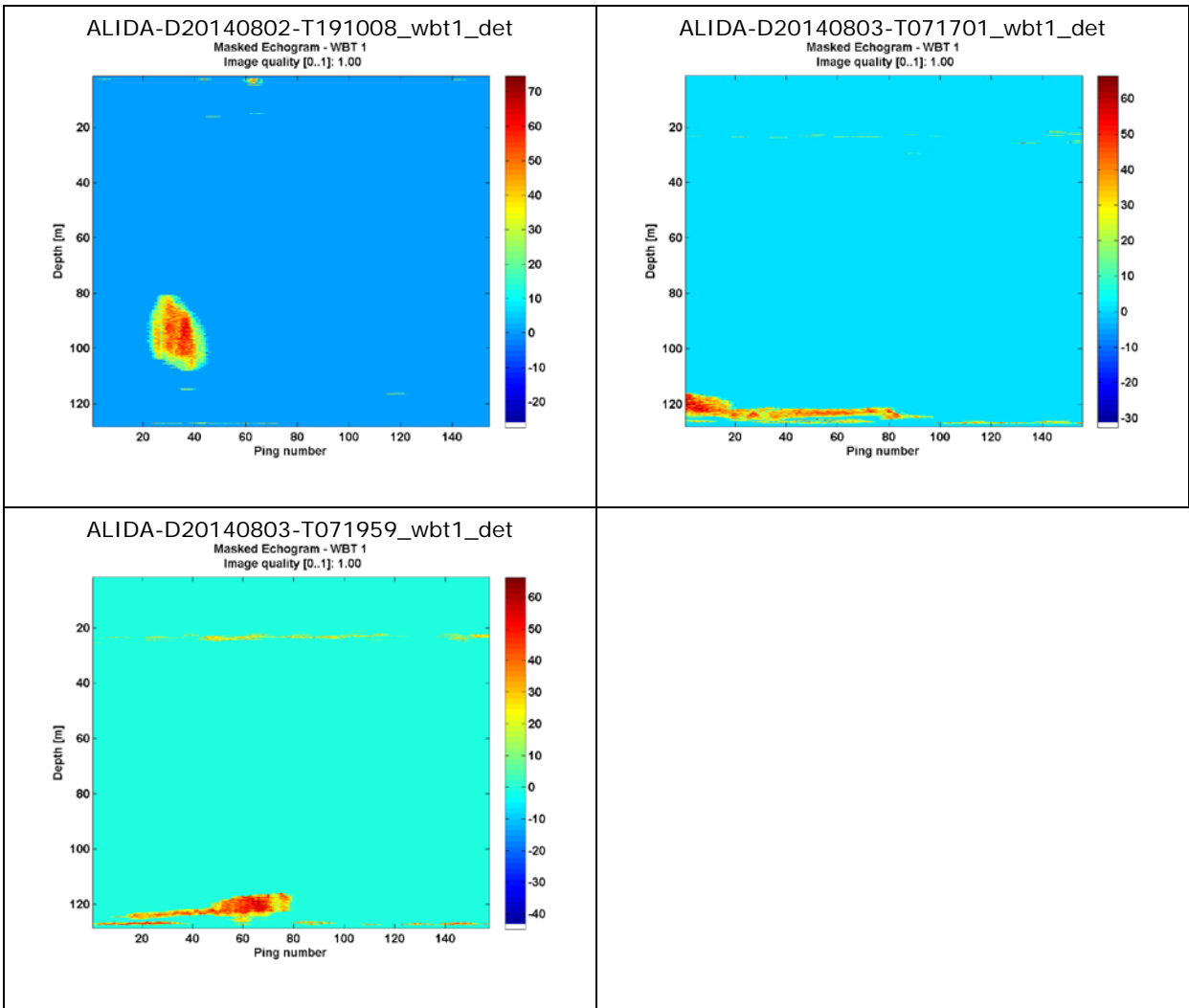


Appendix C: echograms of school data (by species and file)

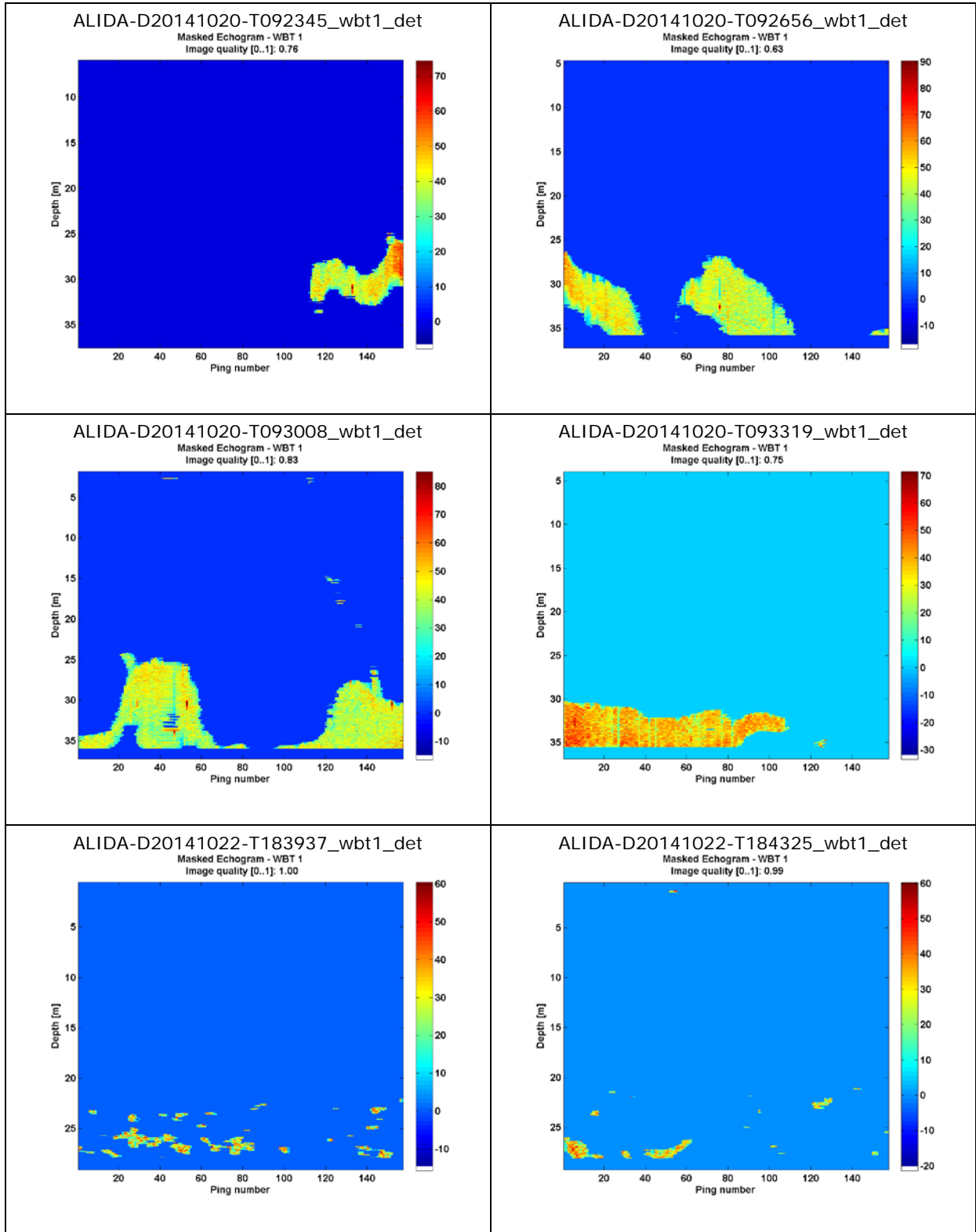
Herring

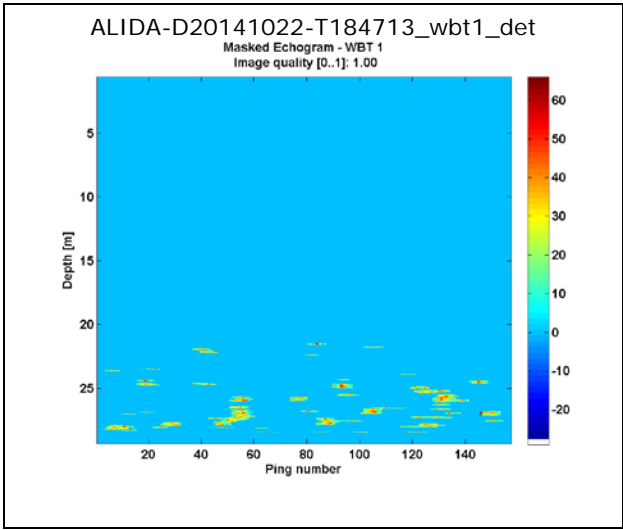






Horse mackerel





Mackerel

